**TELEDYNE
ENGINEERING SERVICES**

TECHNICAL REPORT

TECHNICAL REPORT TR-5310-1

MARK I CONTAINMENT PROGRAM

PLANT-UNIQUE ANALYSIS REPORT
OF THE
TORUS SUPPRESSION CHAMBER
FOR
PILGRIM STATION - UNIT 1

OCTOBER 27, 1982

BOSTON EDISON COMPANY
800 BOYLSTON STREET
BOSTON, MA 02199

TECHNICAL REPORT TR-5310-1

MARK 1 CONTAINMENT PROGRAM

PLANT-UNIQUE ANALYSIS REPORT
OF THE
TORUS SUPPRESSION CHAMBER
FOR
PILGRIM STATION - UNIT 1

OCTOBER 27, 1982

**◥◤ TELEDYNE
ENGINEERING SERVICES**

ABSTRACT

The work summarized in this report was undertaken as a part of the Mark 1 Containment Long-Term Program. It includes a summary of the analysis that was performed, the results of the analysis and a description of 19 significant modifications that were made to the structure and internals to increase safety margins.

In all cases, the stresses reported in this document meet the allowable levels as defined in the structural acceptance criteria (Reference 3). The methods and assumptions used in this analysis are in accordance with USNRC NUREG 0661 (Reference 2), except as noted in the text. The modifications described in this report are also in compliance with NUREG 0661, unless otherwise noted.

TELEDYNE
ENGINEERING SERVICES

TABLE OF CONTENTS

TABLE OF CONTENTS (CONTINUED)

TELEDYNE
ENGINEERING SERVICES

TABLE OF CONTENTS (CONTINUED)

**TELEDYNE
ENGINEERING SERVICES**

TABLE OF CONTENTS (CONTINUED)

**TELEDYNE
ENGINEERING SERVICES**

FIGURES AND TABLES

FIGURES AND TABLES (CONTINUED)

◀▶ TELEDYNE
ENGINEERING SERVICES

FIGURES AND TABLES (CONTINUED)

TELEDYNE
ENGINEERING SERVICES

1.0   GENERAL INFORMATION

The purpose of the Mark 1 Torus Program is to evaluate the effects of hydrodynamic loads resulting from a loss of coolant accident and/or an SRV discharge to the torus structure. This report summarizes the results of extensive analysis on the Pilgrim torus structure and reports safety margins against established criteria. The content of this report deals with the torus shell, external support system, vent header system and internal structures. Analysis and results for piping attached to the torus (including shell penetrations and internal piping), for the SRV line (except the submerged portion and Tee-Quencher), and for the SRV line vent pipe penetration will be presented in a separate piping report, TR-5310-2.

The criteria used to evaluate the torus structure is the ASME Boiler & Pressure Vessel Code, Section III, Division 1, with addenda through Summer 1977 (Reference 11) and Code Case N-197. Modifications were done under Section XI of the ASME Code and meet the Summer 1978 edition of Section III for design, materials and fabrication.

A great many technical reports have been written and issued as a part of this program. These reports provide detailed descriptions of the phenomena, the physics controlling the phenomena, calculational methods and detailed procedures for plant unique load calculations. Several of these documents are listed as references in this report. The approach of this report will be to reference these documents, wherever possible, and to avoid a re-statement of the same information.

A major part of this program has dealt with providing plant-unique load calculation procedures (References 9, Volume 1-10 are examples of this). In most cases, the loads used to support the analysis were calculated in strict accordance with those procedures, as amended by NUREG 0661 (Reference 2). In some cases, optional methods have been used; these methods are specifically referenced in Program documentation. Examples of these are the use of plant-

**TELEDYNE
ENGINEERING SERVICES**

unique SRV test data to calibrate SRV analysis, and use of plant unique quarter scale pool swell movies to refine certain water impact and froth loads. In a few cases, analysis assumptions have been made that do not appear in Program documentation; these are identified in the text.

Extensive structural analysis was performed as a part of this evaluation. The major analysis was for dynamic response to time-varying loads. Analysis for static and thermal conditions was also done. The computer code used to perform almost all of this analysis was the STARDYNE code, as marketed by Control Data Corporation. STARDYNE is a fully qualified and accepted code in this industry; details of the code are available through CDC. Cases where a computer code other than STARDYNE is used will be identified in the text. All dynamic analysis used damping equal to 2% of critical, unless stated otherwise.

As an aid in processing the large amounts of calculated data, post-processors for the STARDYNE program were written and used. These programs were limited in function to data format manipulations and simple combinations of load or stress data; no difficult computational methods were included.

The loads and load combinations considered in this program required special consideration to determine the appropriate levels of ASME Code application. Reference 3 was developed to provide this standard. Table 5-1 of Reference 3 is the basis for all the evaluation work in this report; it is reproduced in this report as Table 1 and shows 27 load combinations that must be considered for each structure. The number actually becomes several times that when we consider the many different values associated with various SRV discharge conditions. The approach used in the final evaluation of structures is to reduce this large number to a smaller number of cases by conservative bounding. For example, load combinations including SSE seismic, have a higher allowable than the same combination with OBE seismic. For these cases, our first evaluation attempt is to consider the SSE combination against the OBE allowables. If this produces an acceptable result, those numbers are reported as final. This procedure results in many cases where safety margins are understated; this is the case for most of the results.

As an aid in correlating discussion of particular load analyses to detailed program documentation, most analysis described in this report has been referenced directly to a paragraph in the Load Definition Report (Reference 1). This has been done by identifying the applicable LDR paragraph in parenthesis immediately following the title of the load. This referencing directs the reader to a more detailed description of the load than can be included in this report.

🔻 TELEDYNE
ENGINEERING SERVICES

2.0 PLANT DESCRIPTION

2.1 General Arrangement

The configuration of the Pilgrim torus structure is shown in Figures 2-1 and 2-2.

Figure 2-1 shows a plan view of the torus. It is made up of the sixteen (16) mitred sections, connected to the drywell by eight (8) equally spaced vent pipes. It is supported by two external columns and an intermediate saddle at each of sixteen places, as shown. The saddles and columns are connected to the basemat with eight anchor bolts per saddle. Four earthquake restraints, spaced equally around the torus, connect the belly of the torus to the basemat (Figure 3-10).

Figure 2-2 shows some of the inside arrangement. Ring girders reenforce the outer shell at each of the sixteen planes defined by the external support system. The vent header system is supported off of the ring girders and is directly connected to the drywell via the vent pipes. Openings where the vent pipes penetrate the torus shell are sealed by bellows. The ring girder also supports the catwalk, spray header and SRV tee-quenchers. Figures 2-3 to 2-21 show several details of the torus structure. Table 2.0 lists several of the plant specific dimensions.

2.2 Recent Modifications

Over the period of the past few years, many modifications have been made to the Pilgrim torus, both to increase its strength and also to mitigate the hydrodynamic loads. The modifications are illustrated and listed in the composite sections of Figures 2-3 and 2-4, along with their installation dates. A description and illustration of each individual modification follows:

2.2.1 Modifications to Reduce Hydrodynamic Loads

Drywell Pressurization System ($\triangle$P System)

Installation of a system to maintain a pressure differential between torus and drywell was the first modification of this Program. The system is illustrated in Figure 2-5. It is designed to maintain a minimum positive pressure difference of 1.17 psi between the vent system (drywell) and the airspace inside the torus. The result of this pressure difference ($\triangle$P) is to depress the water leg in the downcomers and reduce the water slug that must be cleared, if rapid pressurization of the drywell occurs. Early generic testing in the Program demonstrated that this was an effective means to reduce shell pressures related to DBA pool swell. The 1.17 psi pressure difference was selected as the basis for the Pilgrim plant unique quarter-scale pool swell tests and is intended to be the normal operating condition of the plant. The system complies with NUREG 0661, which requires two narrow range instrument channels with less than $\pm$ 0.1 psid error. Pilgrim Station uses a narrow range instrument for drywell-to-wetwell $\triangle$P and backup instruments to measure drywell and wetwell pressures separately. The maximum error for the above instruments is $\pm$ .08 psid.

Downcomer Shortening

Downcomer shortening is an additional means of reducing the water slug that must be cleared from the downcomers during rapid drywell pressurization. Its primary advantage is to reduce pool swell loads during those periods of time when the $\triangle$P system may be inoperative. It also allows for a very small water leg during normal operation, without the problems associated with higher drywell pressures. The downcomers at Pilgrim were cut to provide a minimum submergence of 3.0 feet (distance from bottom of downcomer to minimum torus water level).

Vent Header Deflector

The vent header deflector at Pilgrim is illustrated in Figures 2-6 and 2-7. It is a 16-inch schedule 120 pipe with ½-inch plate welded to the sides.

The deflector extends under the belly of the vent header to protect the vent header from direct water impact during pool swell. It shields the most sensitive part of the vent header by separating and diverting the rising pool before it can reach the vent header. This deflector was included in the plant unique pool swell tests for Pilgrim to provide accurate vent header loading for detailed analysis.

SRV Tee-Quencher

A tee-quencher has been installed at the discharge end of each main steam relief line to replace the existing ramsheads. A typical quencher and its support are illustrated in Figure 2-8. The quencher serves to divide the SRV discharge bubble into hundreds of smaller bubbles and to distribute them over an entire bay. This division and distribution of SRV discharge has been shown in generic testing to reduce torus shell pressure by factors of two or more when compared to ramshead pressures. The plant-unique characteristics of these devices at Pilgrim were determined by in-plant testing after their installation. End cap holes in the tee-quencher were also provided to promote suppression pool mixing and minimize temperature gradients.

The quencher support is also illustrated in Figure 2-8. It is a 20-inch schedule 120 pipe welded to the ring girder, as shown.

Temperature Monitoring System & RHR Return Lines

The addition of a pool temperature monitoring system and an elbow to the discharge end of the RHR return lines are both intended to assure proper operation of the SRV quencher. These modifications are illustrated in Figures 2-9, 2-10, 2-17 and 2-20.

The temperature monitoring system senses pool temperature through a set of 26 sensors set in thermowells around the torus shell (Figures 2-17 and 2-20). Of these 26, 12 are mounted in redundant pairs (6 locations)

to sense local pool temperature*. The remaining 14 are mounted in seven redundant pairs and are used along with the local sensors to determine bulk pool temperature. The system is hard wired to a console in the control room.

The elbows on the RHR return lines were added to improve pool circulation during periods of extended SRV blowdown. Circulation of the pool with these lines assures that local-to-bulk temperature differences will be minimized and that SRV quencher performance will be maintained for the maximum possible time during extended discharge. These two RHR return lines were further modified by re-routing them to the ring girders. The ring girders react drag loads on these lines and also provide for reactions due to elbow discharge loads (see Figure 2-10).

Additional SRV Vacuum Breakers

Each of the four SRV discharge lines at Pilgrim has been fitted with two, ten-inch vacuum breakers, in addition to the original one-inch vacuum breakers. This modification minimizes the temporary formation of the high water leg in the SRV line which could occur due to steam condensation oscillation after an initial actuation; and thereby prevents the high clearing loads which could occur if a second actuation occurred at that time. The location of these devices is different on each SRV line due to space constraints, and is not illustrated.

Removal of Submerged Piping

Some of the piping inside the torus extended to greater depths than was necessary for its proper functioning. This additional submergence resulted in drag loads on the piping that was unnecessary. In order to reduce the loads, these piping systems were cut off to provide a three-foot

*The six local pairs are located in the six SRV tee-quencher bays. Only four of these quenchers are operative; the other two are not connected to the steam relief lines and have been installed for possible future use.

submergence at minimum torus water level. The five lines affected were the
HPCI exhaust, RCIC exhaust, HPCI drain, RCIC drain and a 18-inch diameter
spare line.

In addition, the eight vent drain lines (one-inch diameter)
were cut off and capped above the pool. In the future, any condensation in
the vent system will be manually drained, as required.

Removal of Monorail

The monorail originally installed at Pilgrim was a low capa-
city unit of relatively light design. Modification of the unit to withstand
worst-case froth loads was judged impractical. The monorail was removed, and
not replaced.

2.2.2 Modifications to Strengthen the Structure

Torus Support Saddles and Anchor Bolts

Support saddles were added under each ring girder as shown
in Figure 2-11. The saddles, support columns and ring girder all lie in the
same plane and react all vertical loads on the torus - most of the load is
reacted by the saddle.

Each saddle is constructed of $1\frac{1}{2}$-inch type SA 516 GR 70 steel
web plates, which are welded to the torus shell at the top, and to a clevis/
sole plate assembly on the bottom. Anchor bolt attachments are welded to the
web plates and clevis sole plates, and eight anchor bolts per saddle restrain
upward motion. A total of 128, two-inch diameter Williams Rock Bolts were
installed, with a 24-inch minimum embedment into the basemat.

The anchor bolt restraints are set with a small clearance,
and the sole plates rest on lubrite plates, to allow for normal radial growth
of the torus due to temperature changes. The lubrite plates rest on a bed
plate which is grouted to the basemat.

**᠁ TELEDYNE
ENGINEERING SERVICES**

Installation of the saddles required relocation of the 18-inch core spray lines, to eliminate interference problems.

Torus Support Columns and Bases

The torus columns were welded to the saddle webs and the bases will be held down by using the existing "J" bolts (two per column). Figure 2-12 shows one of the two beams that bridge the base holding down the column. There is a gap between the beam and base that will allow for thermal growth, radial movement of the column sliding on the lubrite plate.

Downcomer Tie-Rods and Vent Header Gussets

The downcomer tie-rods and vent header gussets are illustrated in Figure 2-13.

The tie-rods are constructed from $2\frac{1}{2}$-inch schedule 40 pipe and provide greatly increased capacity to downcomer lateral loads than the original tie bars. They are attached to the downcomers with specially fabricated 24-inch pipe clamps, constructed from 3/4-inch steel. The clamps are prevented from sliding on the downcomers by welded steel clips both above and below the clamp.

The gussets between the downcomers and vent header are to reduce local intersection stresses due to chugging lateral loads on the downcomers. They are constructed from $\frac{1}{2}$-inch thick SA 516 GR 70 steel plate, and are welded to the vent header and downcomers.

Ring Girder Weld Modifcation

The weld between the ring girder and the torus shell will be increased in the area of the tee-quencher as illustrated in Figure 2-21. The existing 5/16-inch fillet weld was increased to $\frac{1}{2}$-inch, as shown, to help react and distribute the lateral tee-quencher reaction loads due to SRV discharge.

Catwalk and Handrail

The catwalk and handrail at Pilgrim required substantial modification, as illustrated in Figures 2-14 and 2-15. The planned or completed modifications included the following:

- Replacement of original catwalk extension support columns with four-inch diameter pipe columns.

- Addition of bracing between catwalk channels.

- Addition of lateral supports.

- Addition of grating restraints.

- Replacment of handrails.

Electrical Junction Box Modification

There are two large, barrel-shaped, electrical junction boxes inside the Pilgrim torus. These boxes are mounted at the top of the torus, in the path of both froth 1 and froth 2 impingement loads. They are constructed with sheet metal covers which could deform under these loads.

The junction box covers were strengthened by the addition of external reenforcement as shown in Figure 2-19. The reenforcement consists of three longitudinal struts connected to two rings which encircle the box and prevent buckling from occurring.

Drywell-Wetwell Vacuum Breaker Support

The attachment between the wetwell vacuum breaker mounting stub and the end cap of the vent pipe was strengthened by the addition of three gussets as illustrated in Figure 2-18. This modification assures

acceptable stress levels in the intersection, during postulated pool swell impact. There are ten vacuum breakers at the Pilgrim Plant.

Spray Header Support Modification

The spray header piping inside the torus is hung from the ring girder at the top of the torus, as illustrated in Figure 2-3. The original supports for this line was a "U" shaped rest support which could not react upward loads. These were modified as shown in Figure 2-16 to react the upward loads associated with pool swell and froth.

**TELEDYNE
ENGINEERING SERVICES**

EXTERNAL SUPPORT
COLUMNS

29'-6"

SADDLES   51'-0"

VENT PIPE
PENETRATION

FIG. 2-1
TORUS PLAN VIEW

TELEDYNE
ENGINEERING SERVICES

VACUUM BREAKER LINE

VENT
HEADER

CAT WALK

DEFLECTOR

DRYWELL

DOWNCOMER

VENT

BELLOWS

RING GIRDER
SRV LINE

QUENCHER

SUPPORT
COLUMN
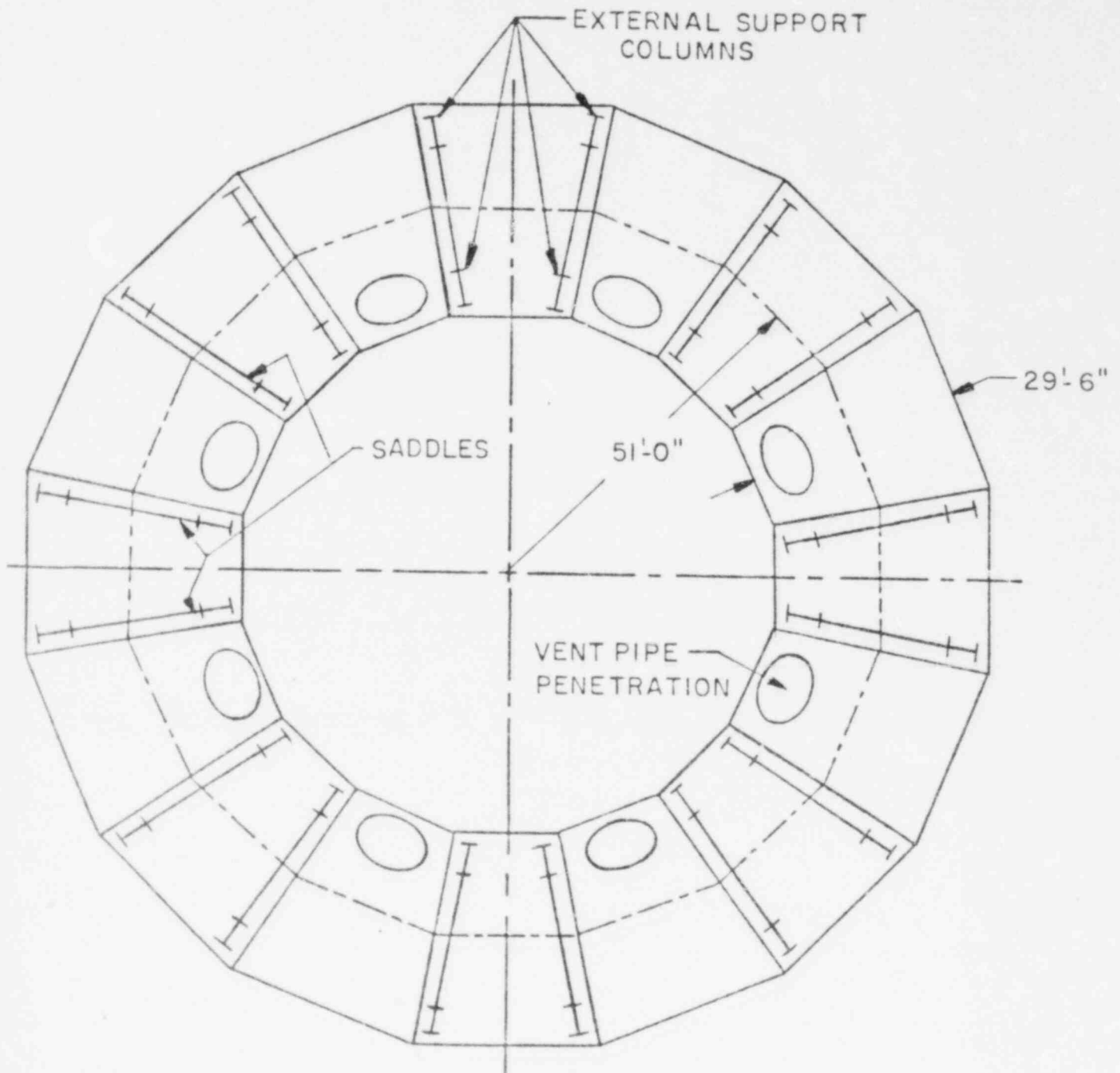
SUPPORT
SADDLE
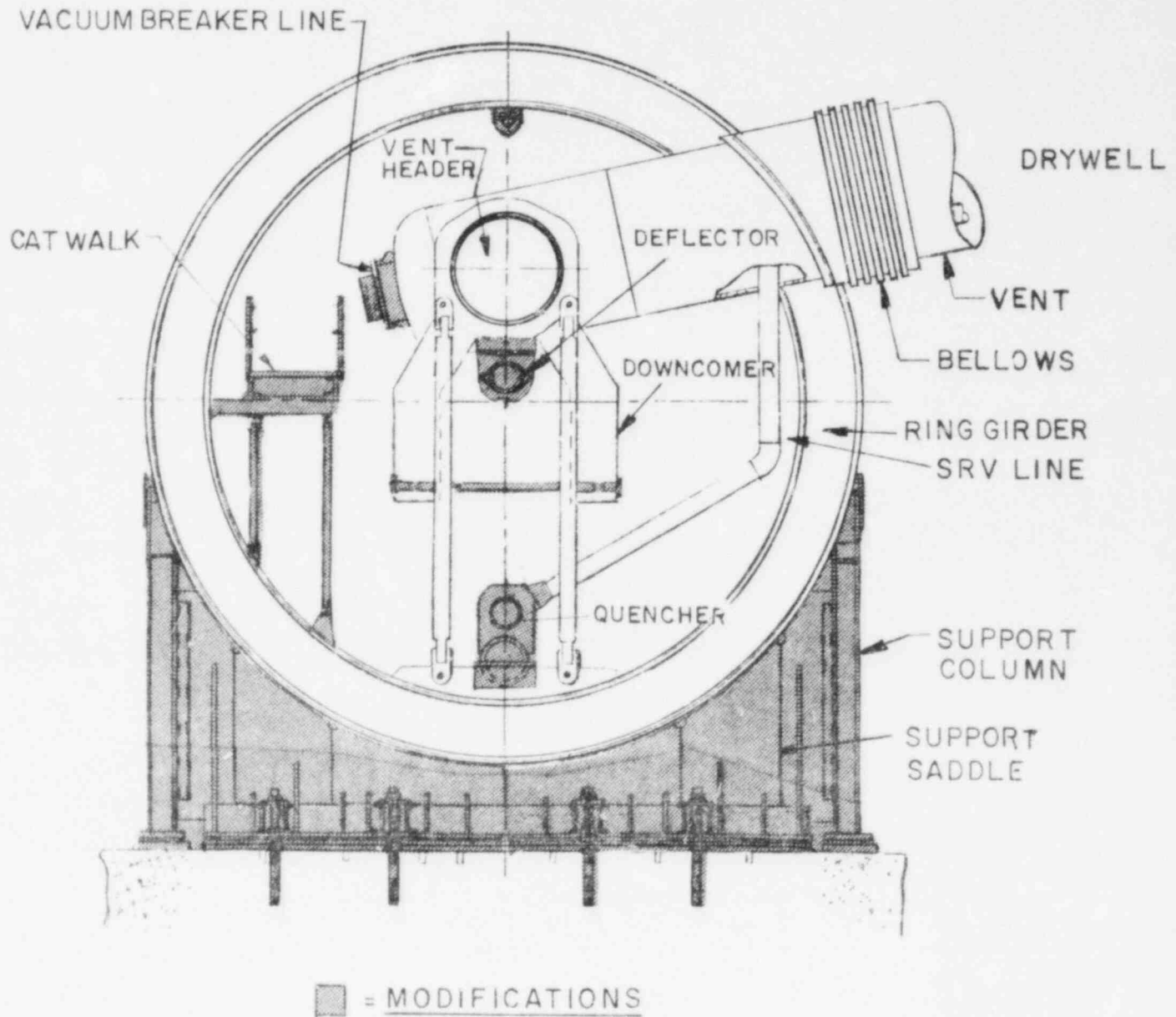
☐ = MODIFICATIONS

FIG. 2-2

TORUS COMPOSITE CROSS SECTION-PILGRIM

**TELEDYNE
ENGINEERING SERVICES**

KEY FOR FIGURES 2-3 AND 2-4

	Modification	Completion Date
1.	Reenforce Supports on 4" Spray Header	12/81
2.	RHR Elbow Return	5/80
3.	Strengthen Electrical Penetrations	12/81
4.	Shorten HPCI Exhaust Line	12/81
5.	Shorten RCIC Exhaust Line	12/81
6.	Shorten HPCI & RCIC Drain Lines	12/81
7.	Shorten 18" Spare Line	12/81
8.	Mitred Joint Saddle	5/80
9.	Saddle Anchor Bolts	4/82
10.	Shorten Downcomers	12/81
11.	Downcomer Ties	5/80
12.	Vent Header Deflector	5/80
13.	Vent Header Downcomer Stiffening	12/81
14.	Vent and Drain Cut and Cap	12/81
15.	Monorail - Remove	12/81
16.	Drywell to Wetwell P Control	1976
17.	Add Temperature Monitoring System (Except Thermowell)	Prior to fuel cycle #7
18.	Thermowells	5/80
19.	Add Larger Vacuum Breakers to the SRV Line in Drywell and Support Lines	5/80 & 12/81
20.	Add Tee-Quenchers	5/80
21.	Tee-Quencher Supports	5/80 & 12/81
22.	Wetwell Vacuum Breaker Penetration Modification	12/81
23.	Catwalk Modifications	12/81 & prior to fuel cycle #7
24.	Increase Ring Girder Weld	Prior to fuel cycle #7
25.	Column Base Holddown	Prior to fuel cycle #7

**TELEDYNE
ENGINEERING SERVICES**
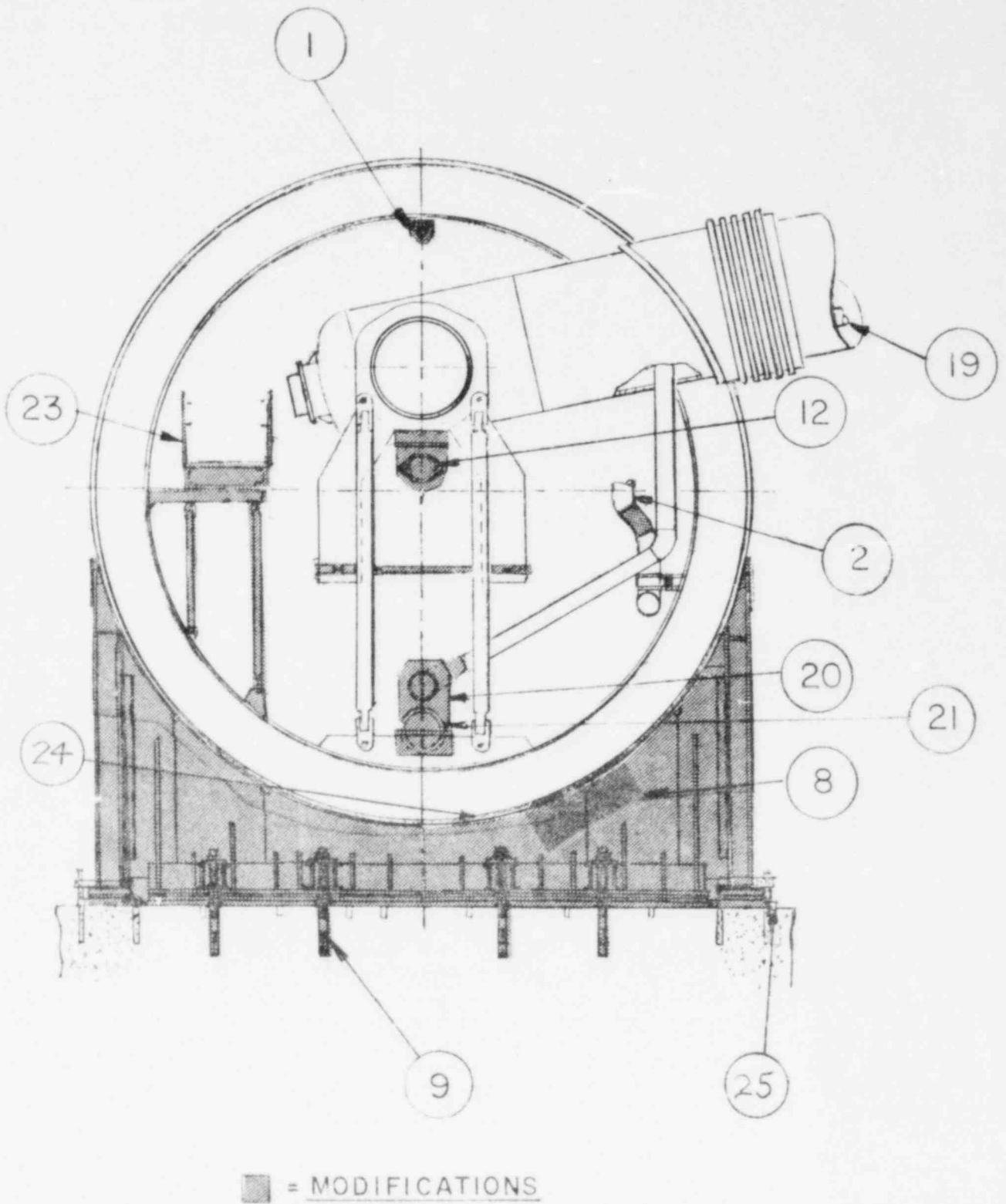
= MODIFICATIONS

FIG. 2-3

TORUS MODIFICATIONS - CROSS SECTION AT RING GIRDER
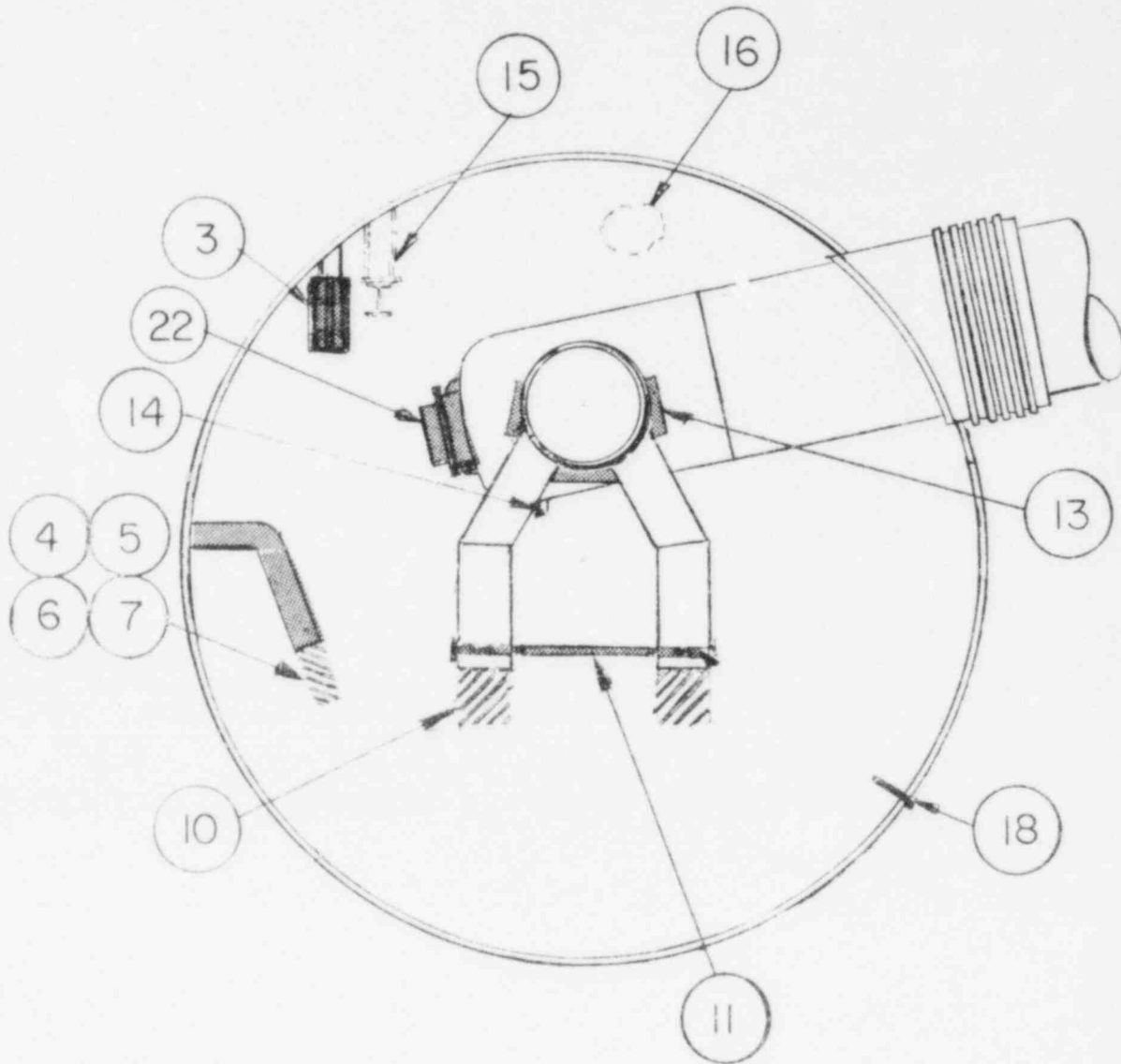
= MODIFICATIONS

FIG. 2-4

TORUS MODIFICATIONS–CROSS SECTION AT MID BAY

TELEDYNE
ENGINEERING SERVICES

1.17 PSIG - PRESSURE MAINTAINED BY N$_2$
INERTING SYSTEM

0 PSIG

WATER
LEVEL
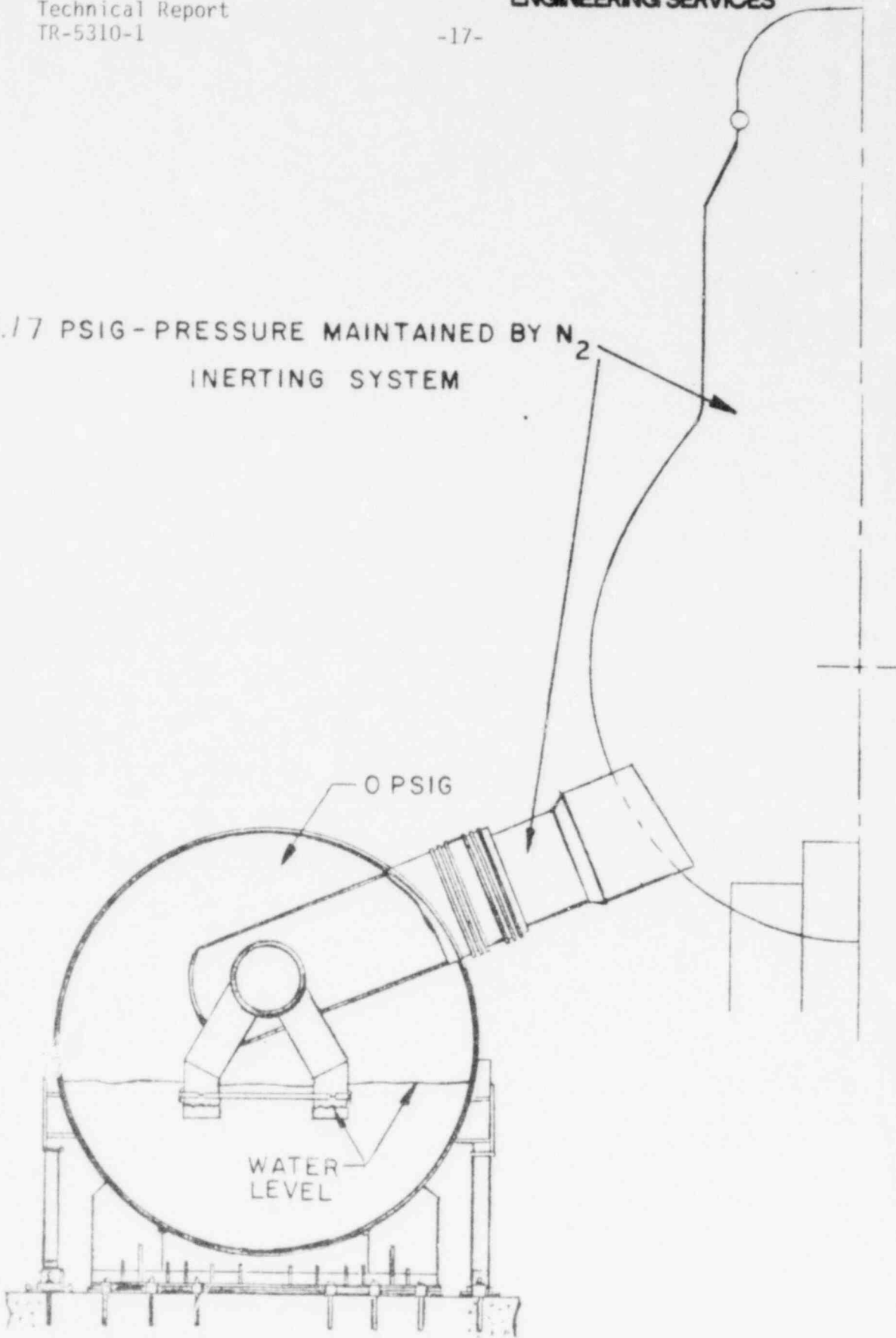
FIG. 2-5
ΔP PRESSURIZATION SYSTEM

FIG. 2-6

VENT HEADER DEFLECTOR

**TELEDYNE
ENGINEERING SERVICES**

VENT HEADER
RE-INFORCING COLLAR

MT

3/8

16" SCH 120 PIPE

ROTATIONAL
STOP

$\frac{1}{2}$" PLATES
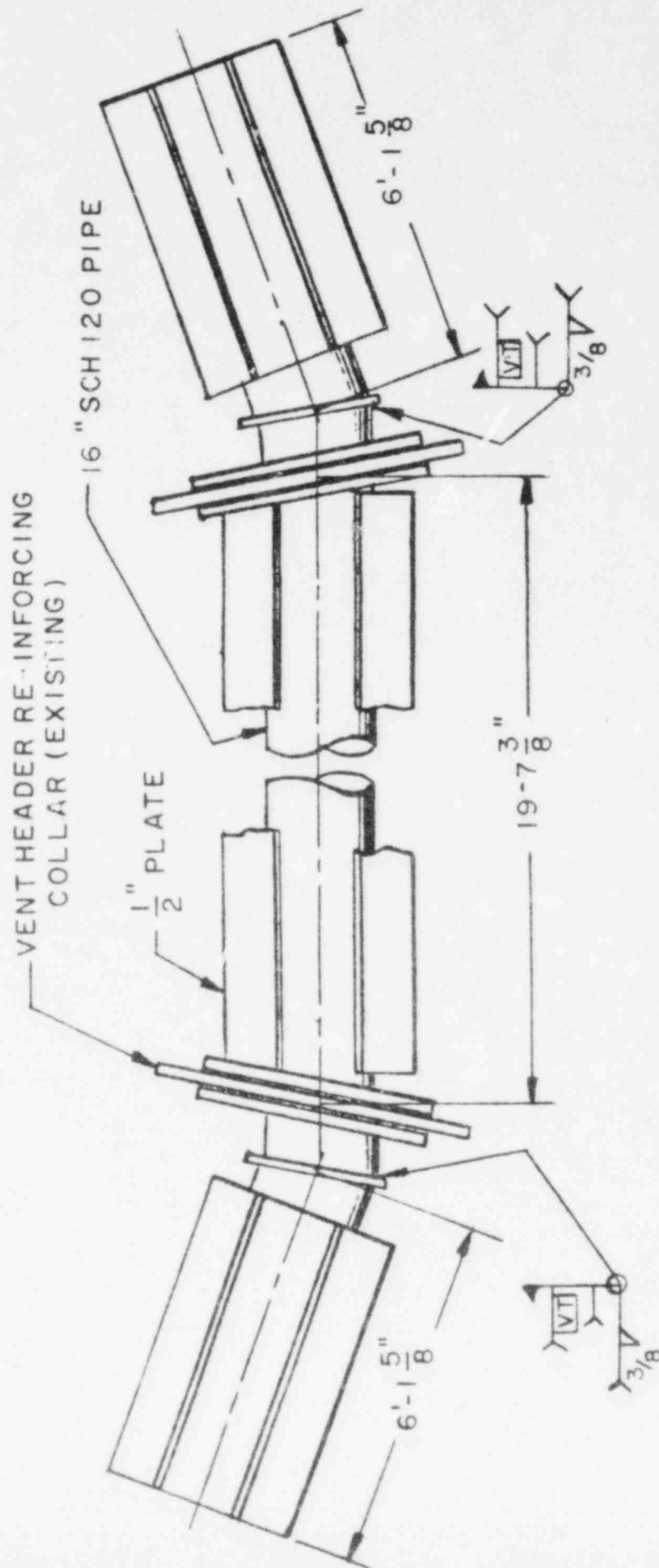
DEFLECTOR SUPPORT
PLATE
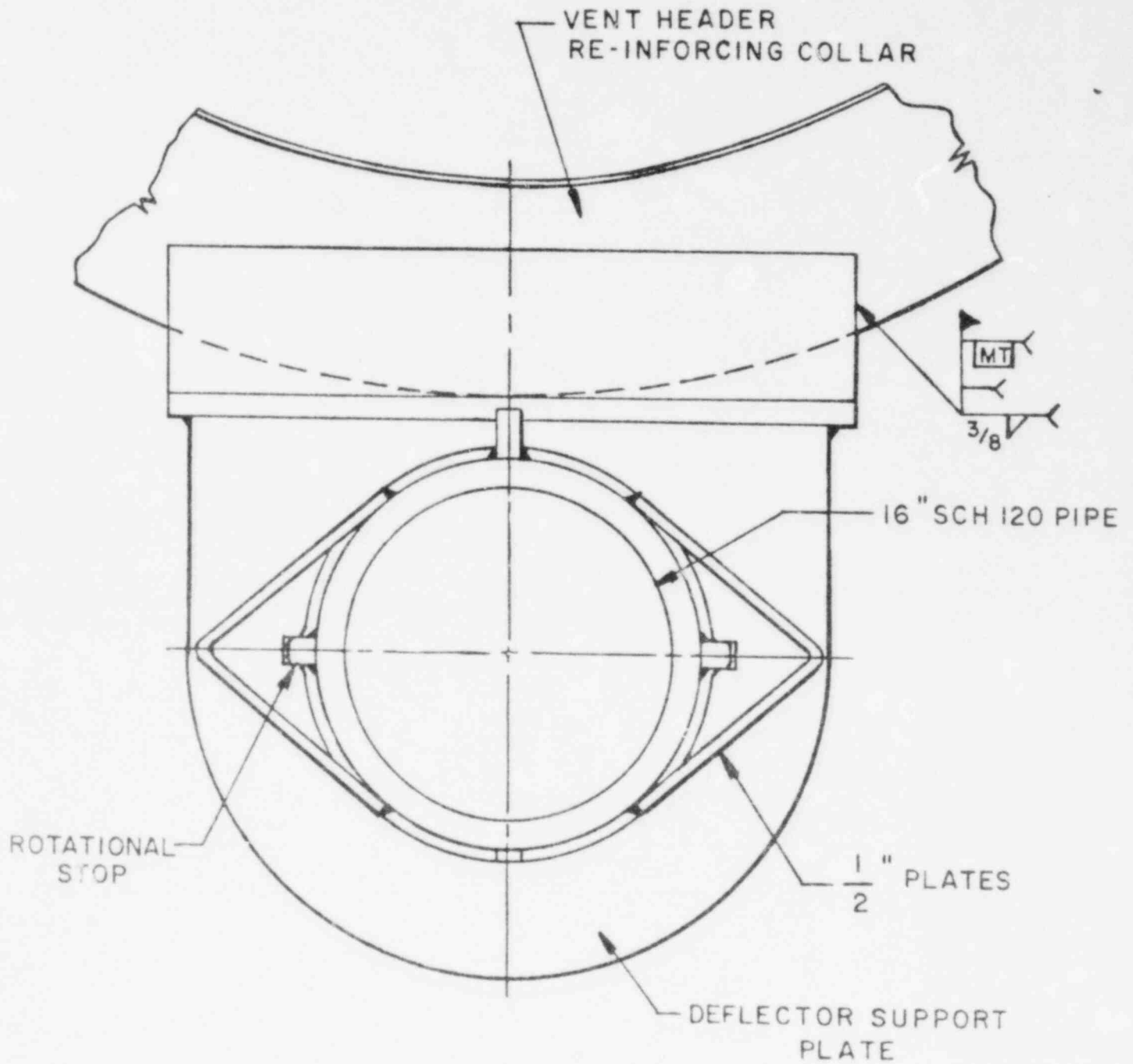
FIG. 2-7

VENT HEADER DEFLECTOR ATTACHMENT

**TELEDYNE
ENGINEERING SERVICES**

QUENCHER

20°

VT
VT

5/16
5/16

SUPPORT
BEAM

SUPPORT
BEAM

VT

3/8

VT

37½°

12" QUENCHER

NOTE

SUPPORT BEAM 20" SCH 120

SUPPORT BRACE

RING GIRDER

TORUS SHELL

NOTE: QUENCHER IS CENTERED ON
SUPPORT BEAM FOR PILGRIM
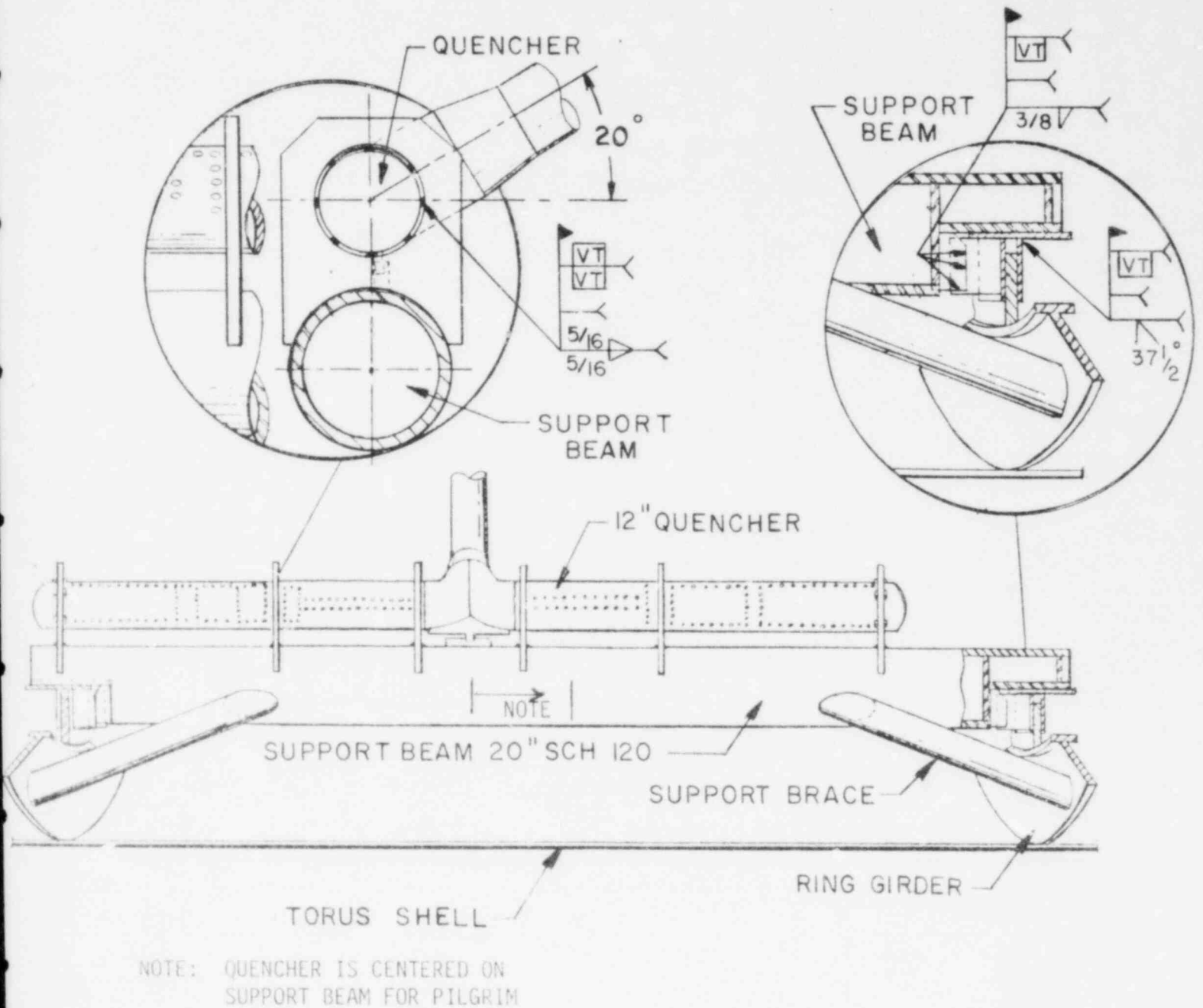
FIG. 2-8
SRV TEE-QUENCHER & SUPPORT
PILGRIM
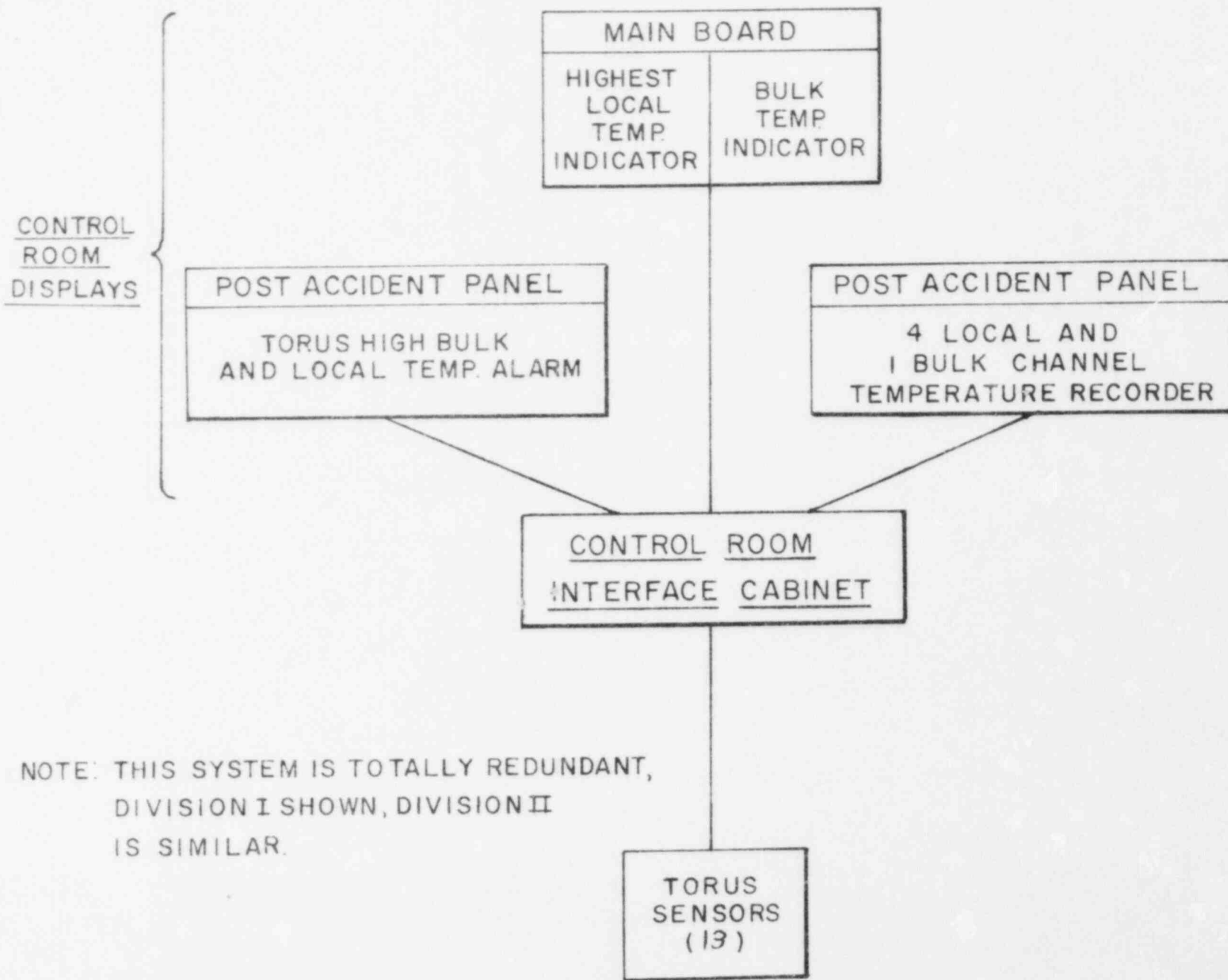
NOTE: THIS SYSTEM IS TOTALLY REDUNDANT, DIVISION I SHOWN, DIVISION II IS SIMILAR.

FIG. 2-9
POOL TEMPERATURE MONITORING SYSTEM

**TELEDYNE
ENGINEERING SERVICES**

ELBOW

EXISTED

NEW PIPE

WATER LINE

TORUS

RING GIRDER
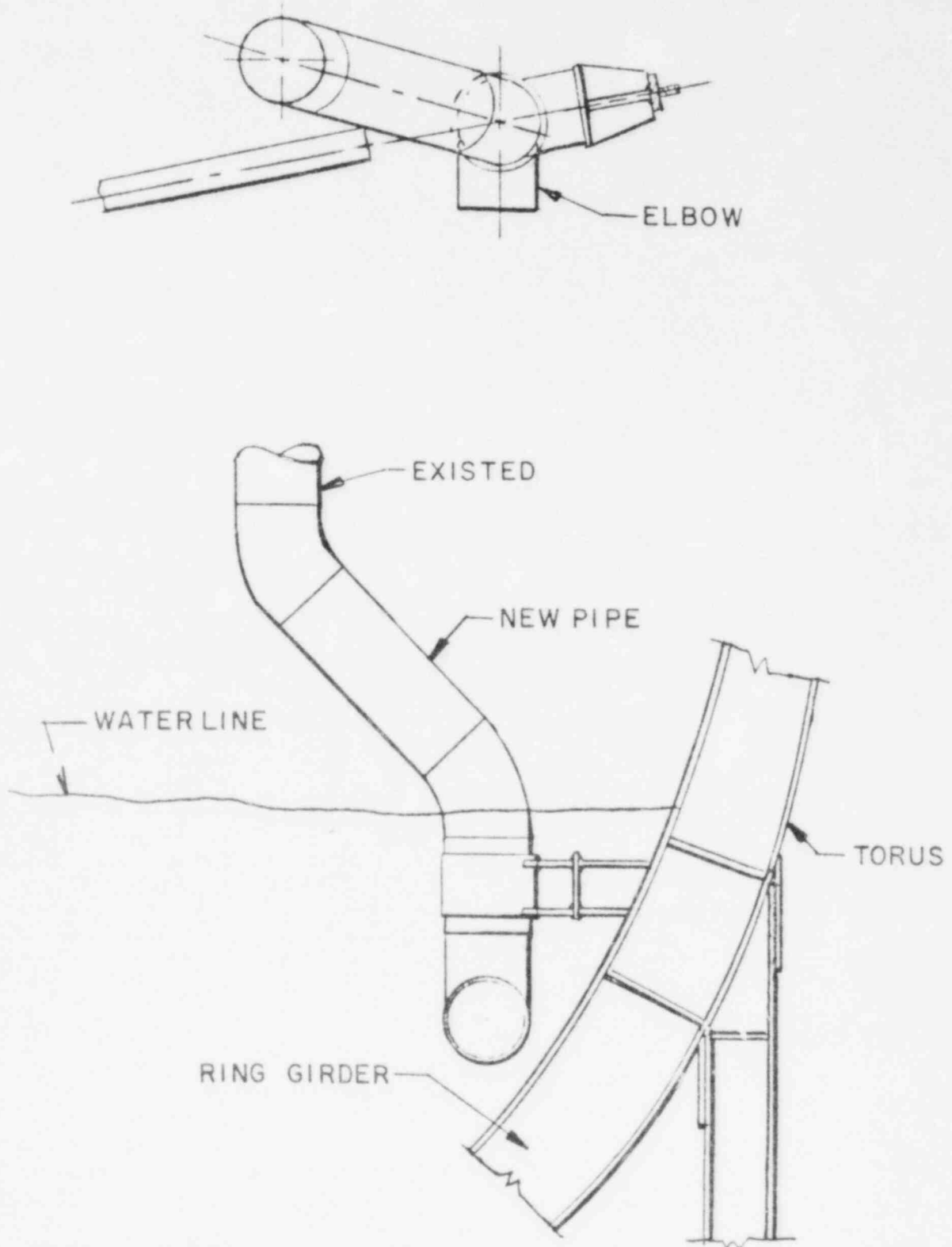
FIG. 2-10

RHR RETURN LINE ELBOW & SUPPORT

TELEDYNE
ENGINEERING SERVICES

CLEARANCE
TO ALLOW
SLIDING

LUBRITE
SURFACE (SLIDES)

SECTION A-A

TORUS

RING GIRDER

CLEVIS-SOLE PLATE

1 1/2" PLATE

GUSSET
STIFFENERS

8 - 24" LONG 2" DIA. ANCHOR
BOLTS PER SADDLE
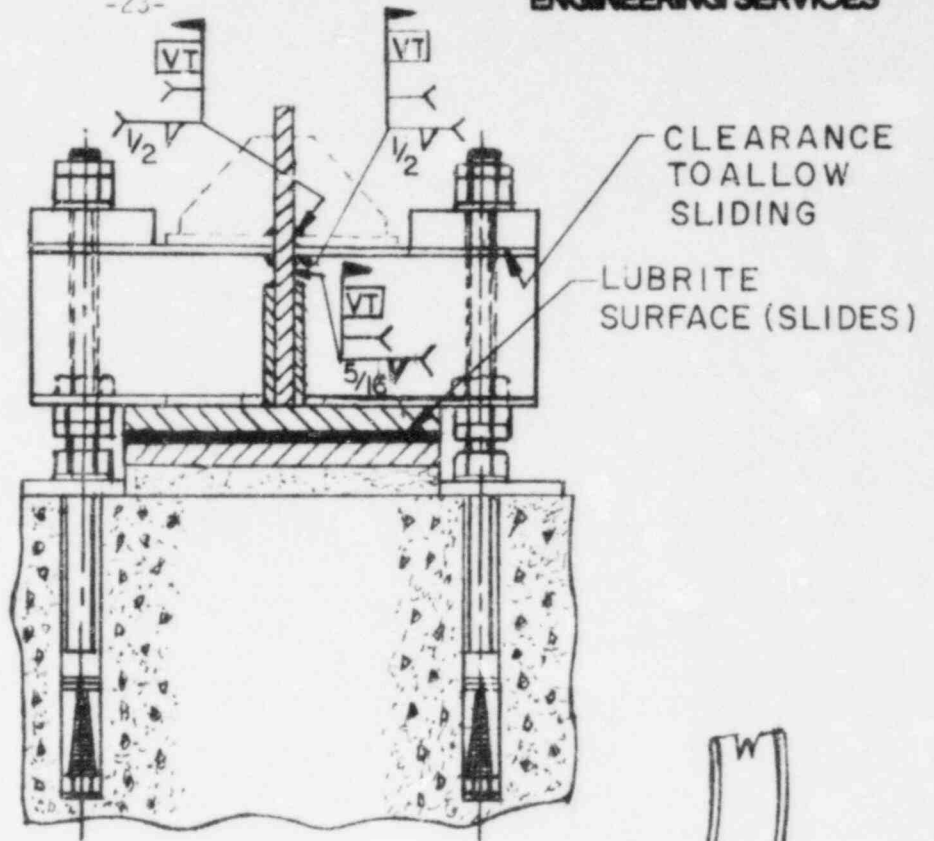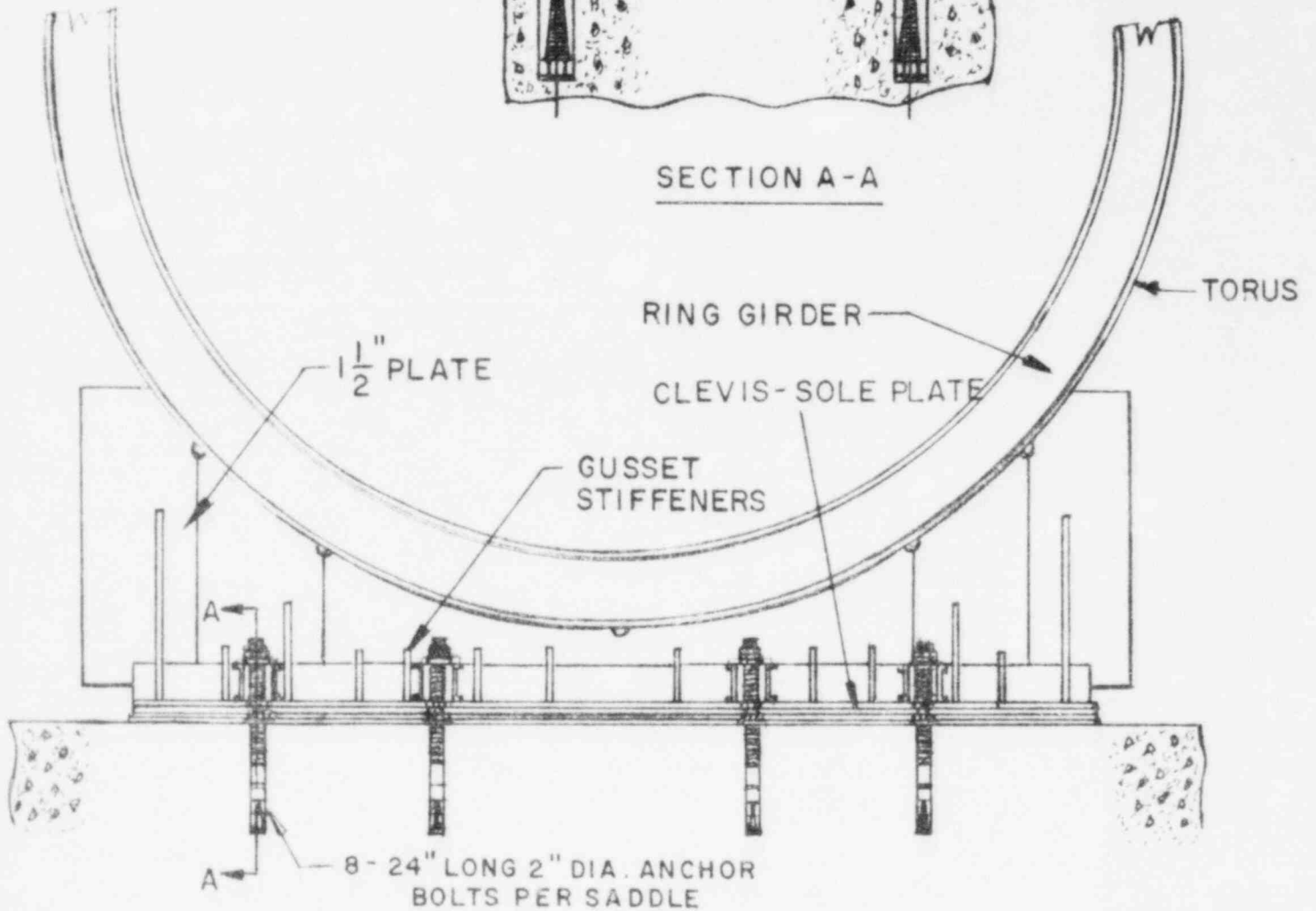
FIG. 2-11

TORUS SUPPORT SADDLES & SADDLE ANCHORS

**TELEDYNE
ENGINEERING SERVICES**

RING GIRDER

MT

3/8

SUPPORT COLUMN

MT

3/8

SUPPORT SADDLE

LUBRITE PLATE
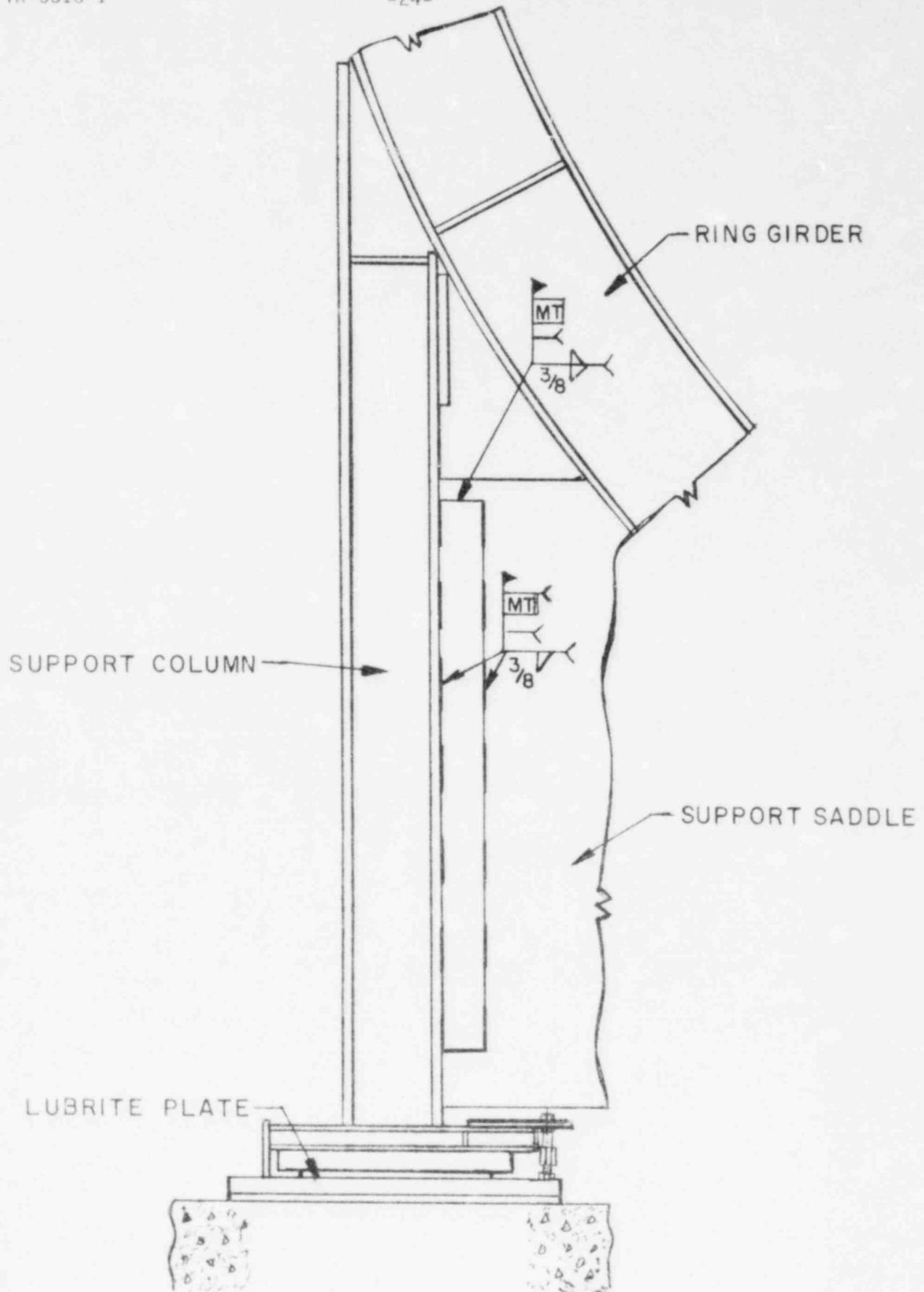
FIG. 2-12
TORUS SUPPORT COLUMNS
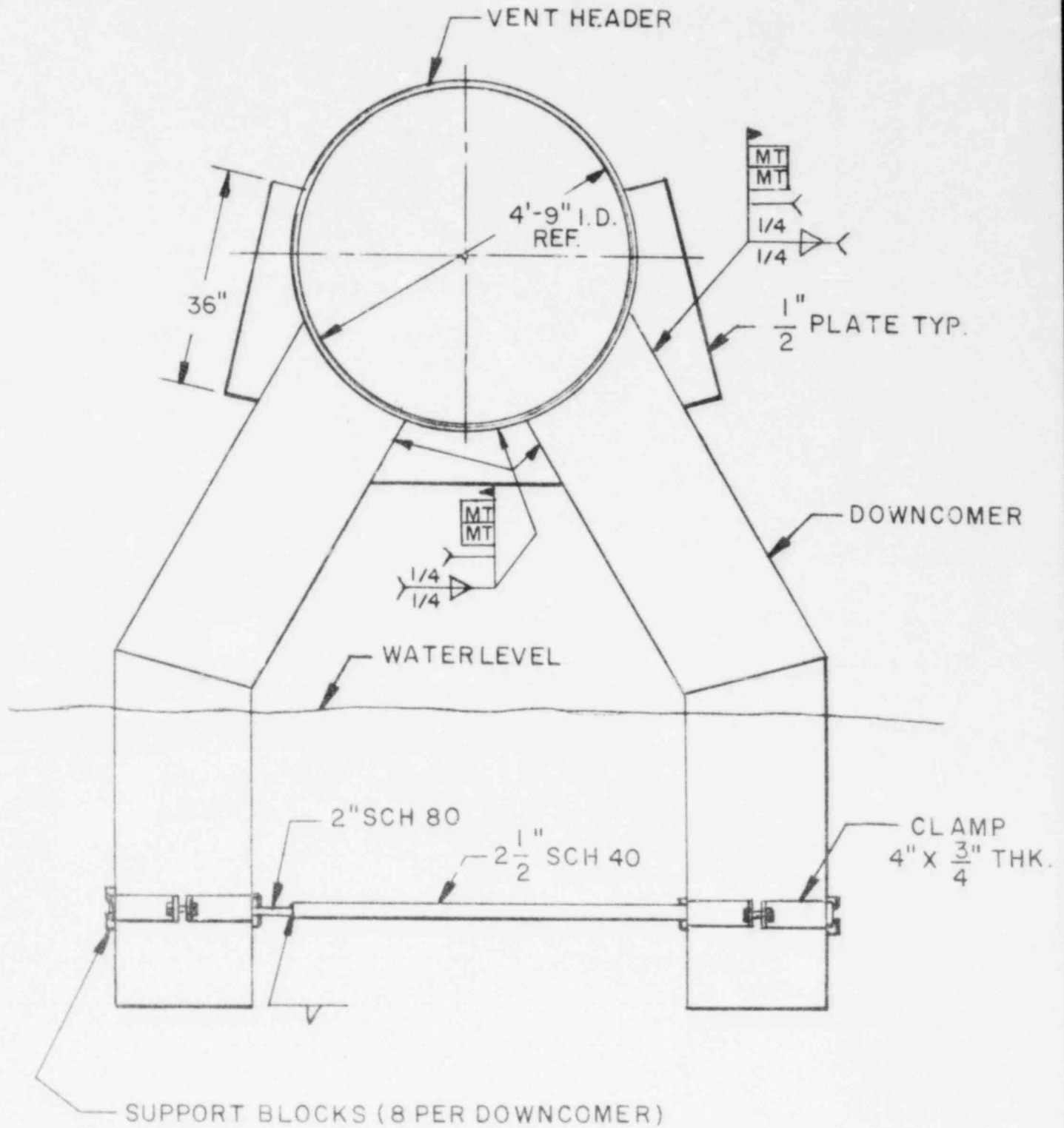
FIG. 2-13

DOWNCOMER TIE-ROD & GUSSET MODIFICATION

EXISTING RING GIRDER
& FLANGE

A

A

4" SCH 80 PIPE

RING GIRDER

EXISTING WALKWAY

EXISTING
LEG 4 X 4
ANGLE

4" SCH 80 PIPE

EXISTING RING GIRDER

ELEV. A-A
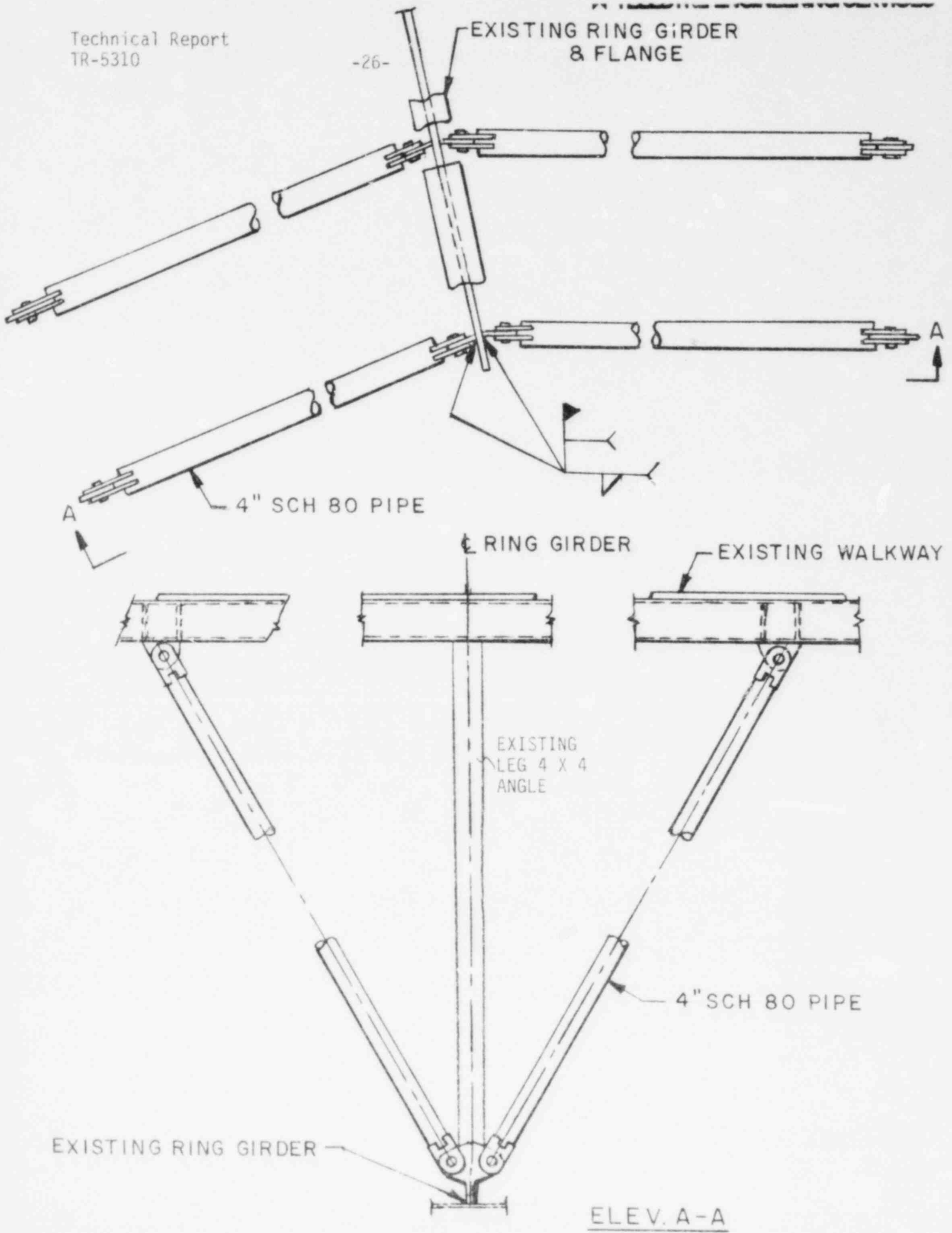
FIG. 2-14

CATWALK & HANDRAIL MODIFICATION

GRATING
RESTRAINT BAR

$\frac{3}{4}$" WIRE ROPE

TUBING 3" X 3" X
5/16 WALL MAT'L:
ASTM A500,
GRADE B

EXISTING
LEG 4 X 4
ANGLE

RING GIRDER

WALKWAY
EXTENSION
3 VENT BAYS
ONLY

4" SCH 80 PIPE

4" SCH 160 PIPE
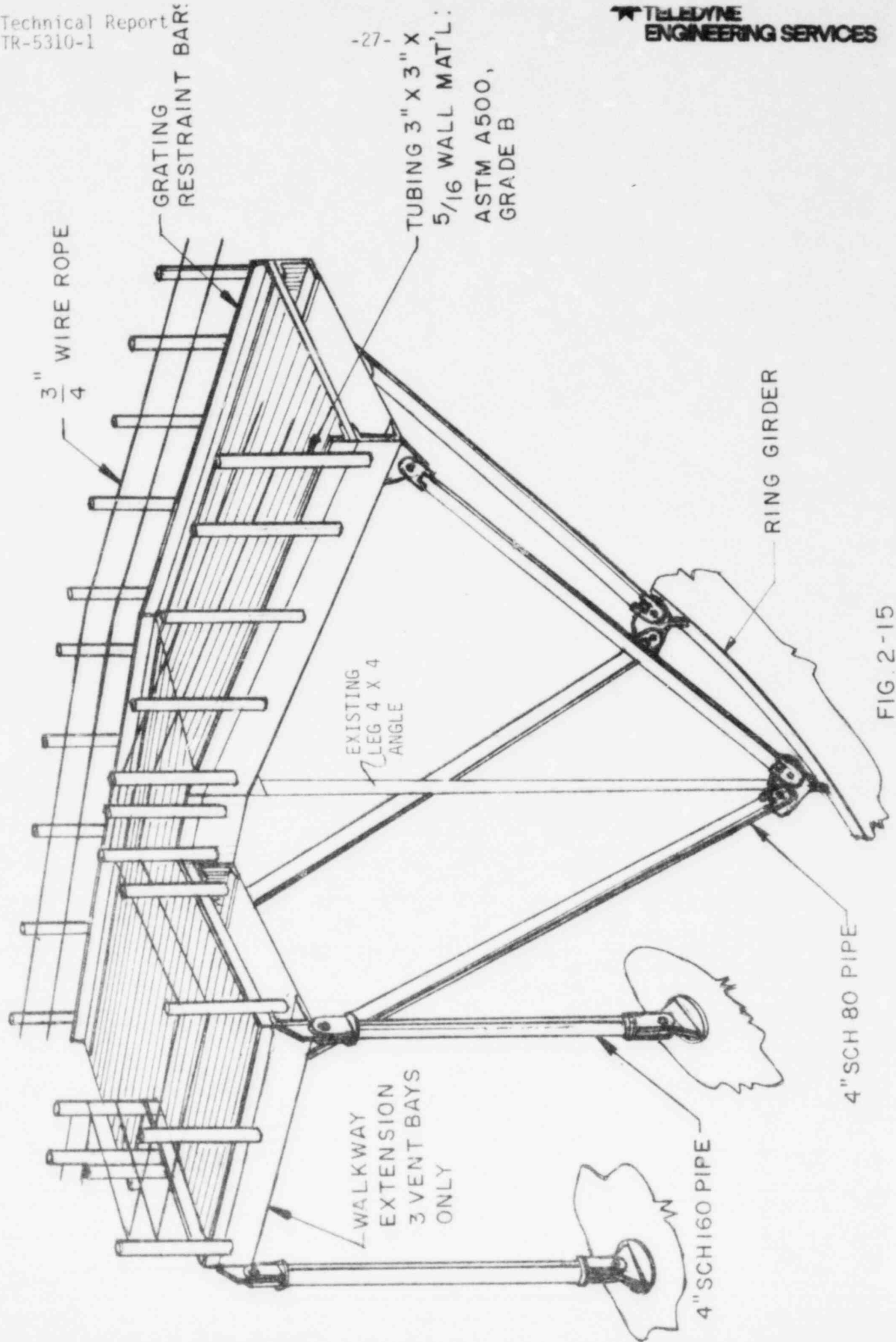
FIG. 2-15

CATWALK & HANDRAIL MODIFICATION

$6\frac{1}{2}"$ X 2" RESTRAINT ADDED

VT

$\frac{3}{16}$

EXISTING
RING GIRDER

EXISTING HEADER
SUPPORT

RING GIRDERS

SPRAY HEADER
ALL TORUS BAYS
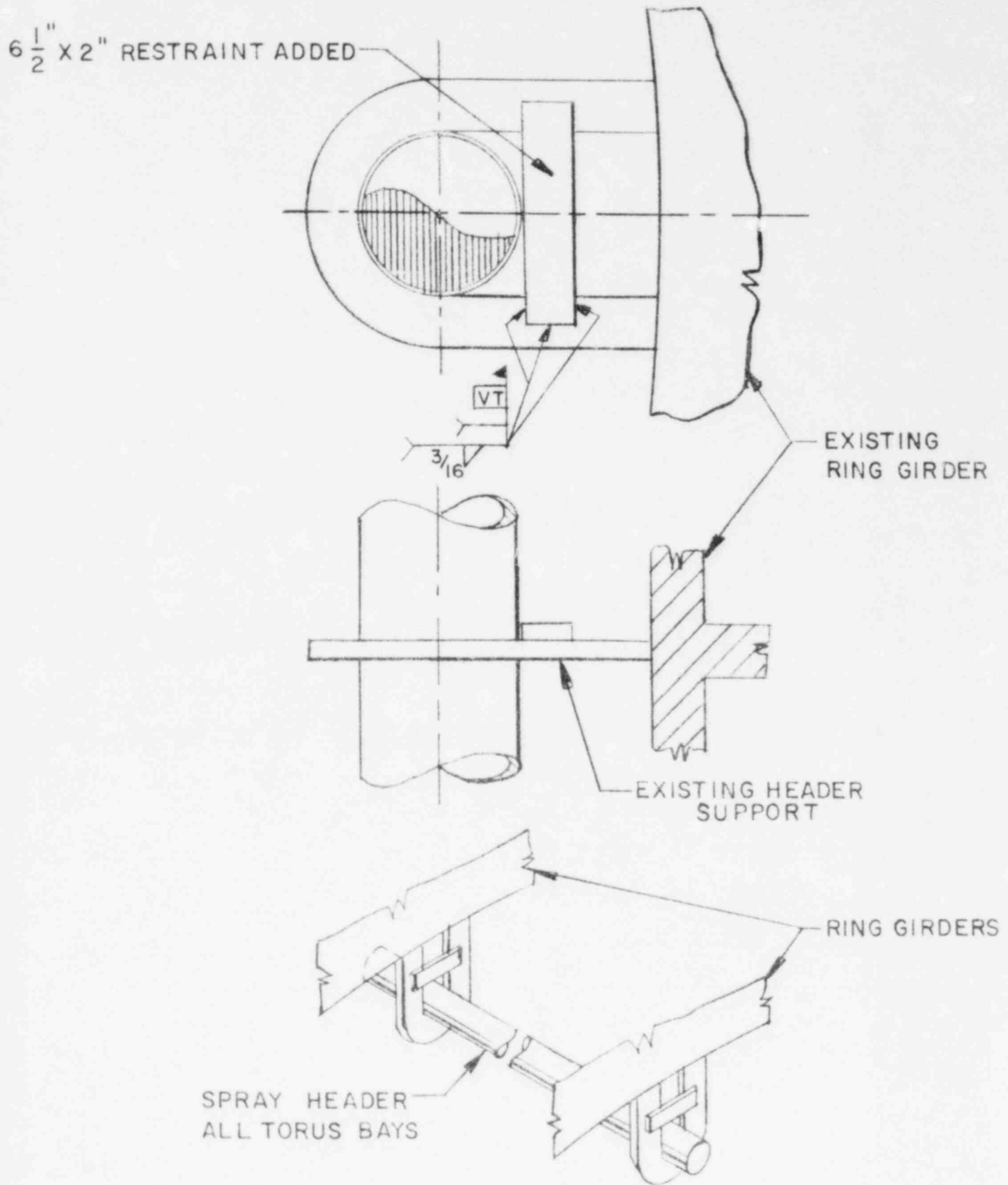
FIG. 2-16

TORUS SPRAY HEADER SUPPORT MODIFICATIONS

TELEDYNE
ENGINEERING SERVICES

$13\frac{1}{2}"$

TORUS SHELL

LP

$3/8$

$1\frac{3}{4}"$
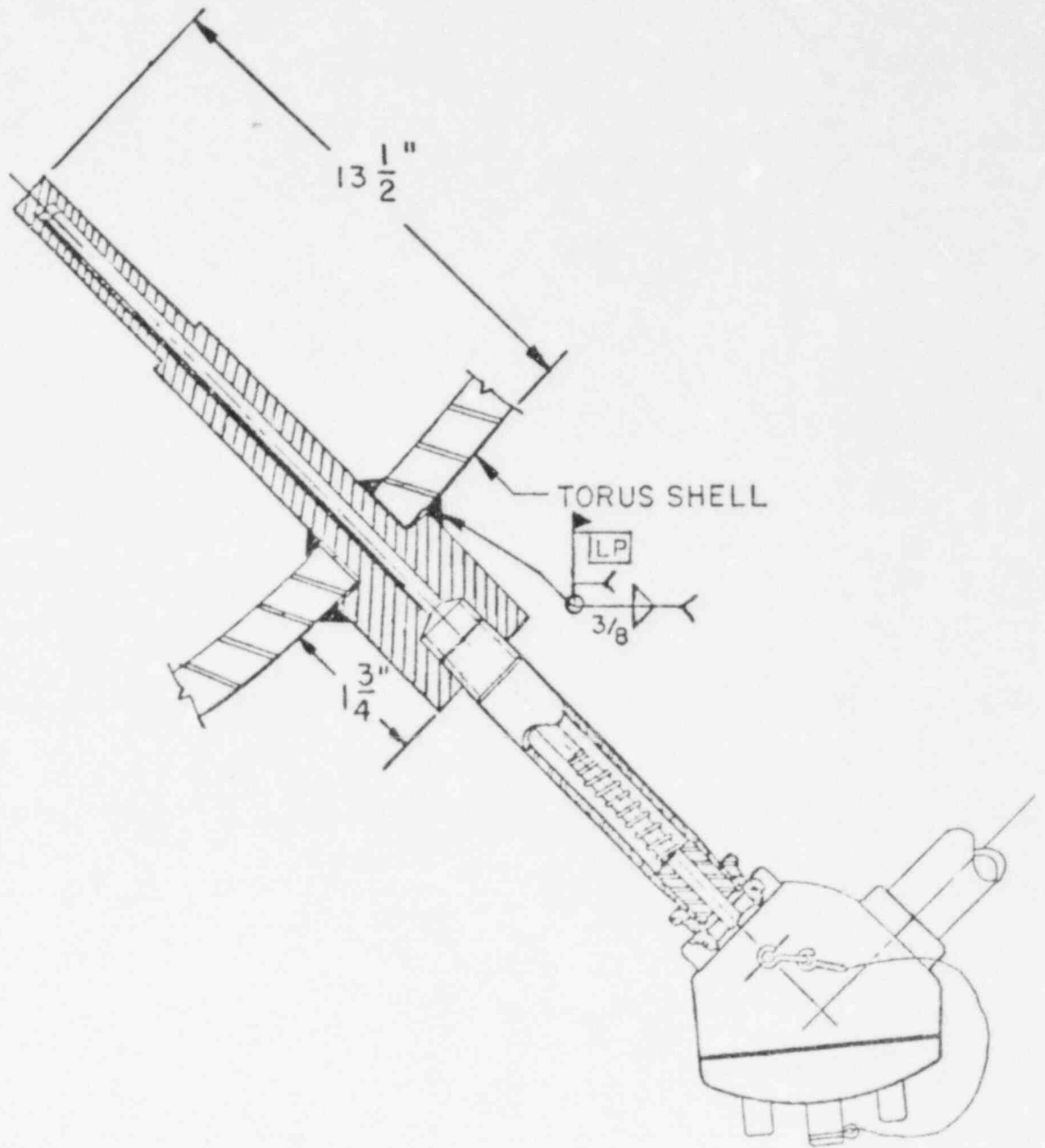
FIG. 2-17
THERMOWELL DETAIL

-30-
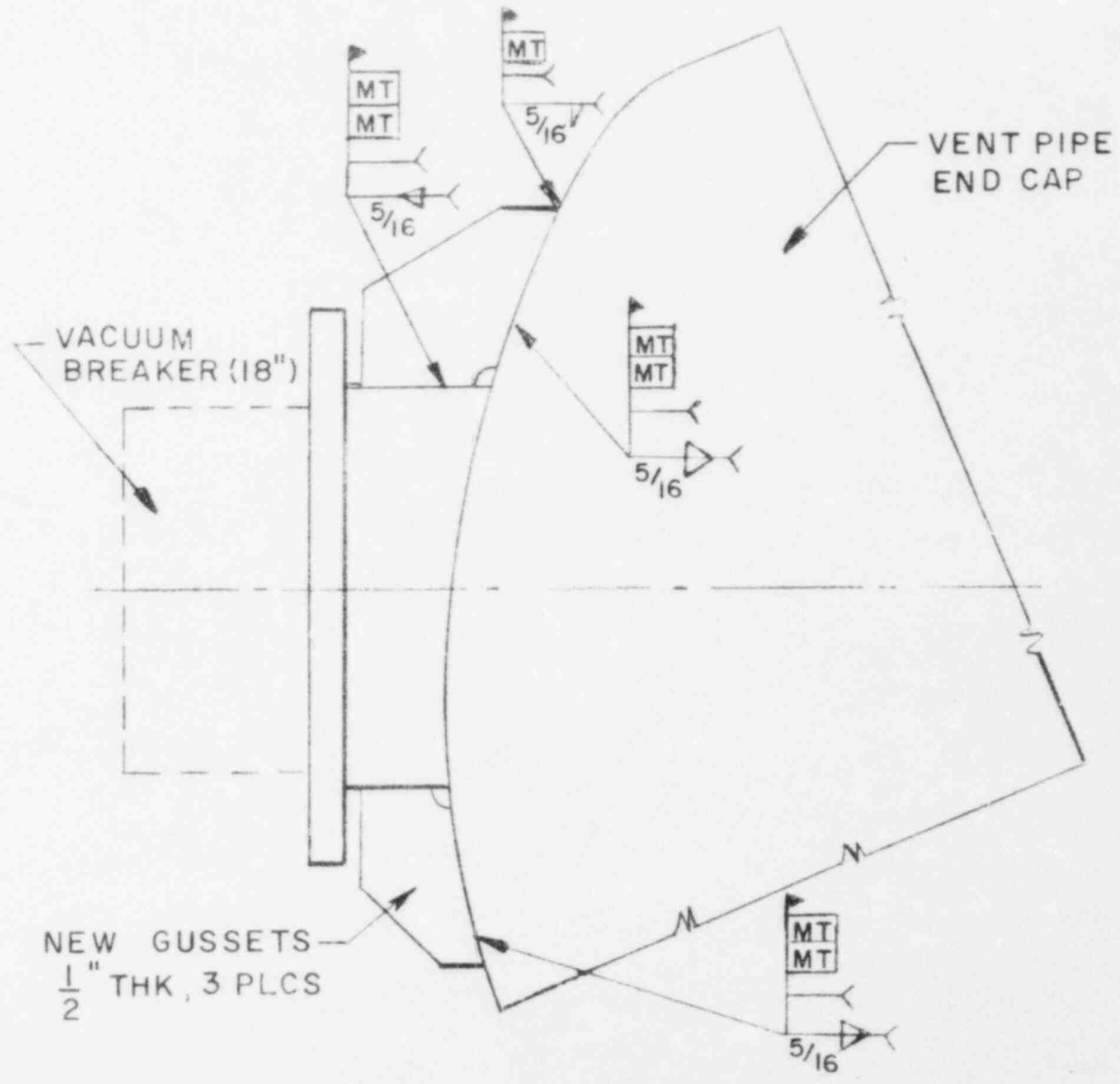
FIG 2-18

VACUUM BREAKER-VENT INTERSECTION MODIFICATION

EXISTING
LINER PLATE

LONGITUDINAL
STRUTS (NEW)

VT

1/4

JUNCTION
BOX

VT

1/4

MT

3/8

TORUS SHELL

SUPPORT
RINGS (NEW)

EXISTING
PENETRATION

-31-
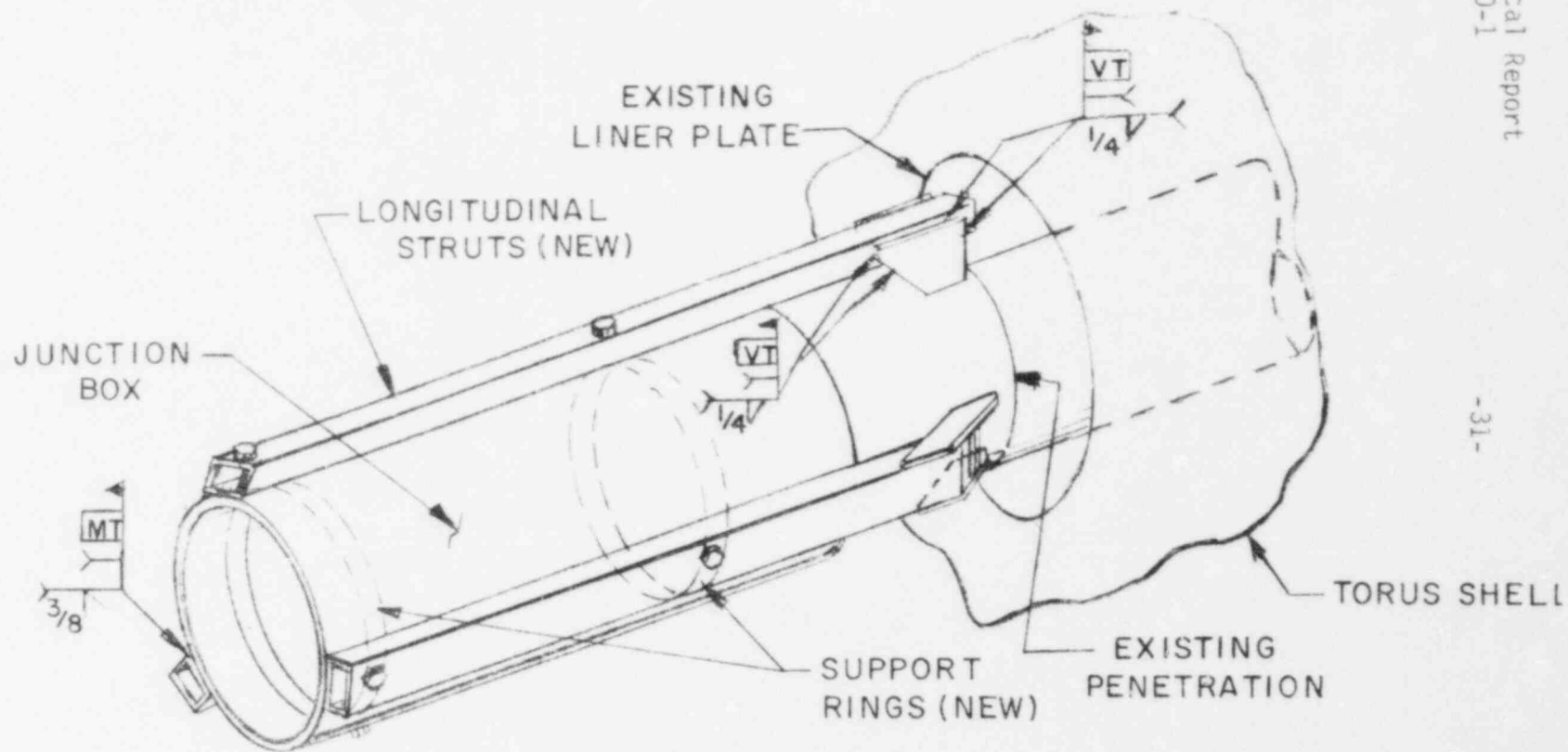
FIG. 2-19

ELECTRICAL JUNCTION BOX MODIFICATION
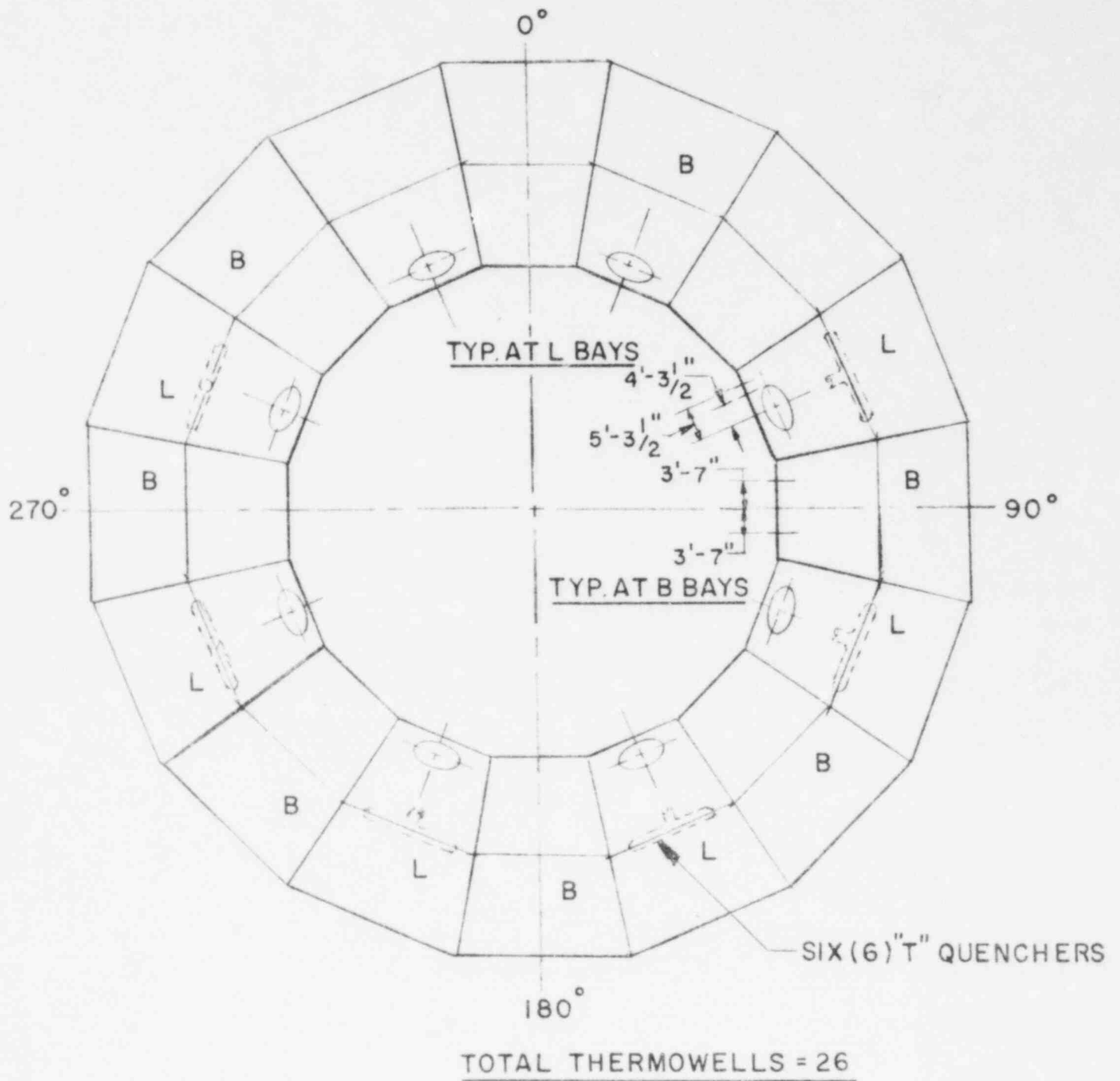
FIG. 2-20
THEROMOWELL LOCATIONS - PILGRIM

**TELEDYNE
ENGINEERING SERVICES**
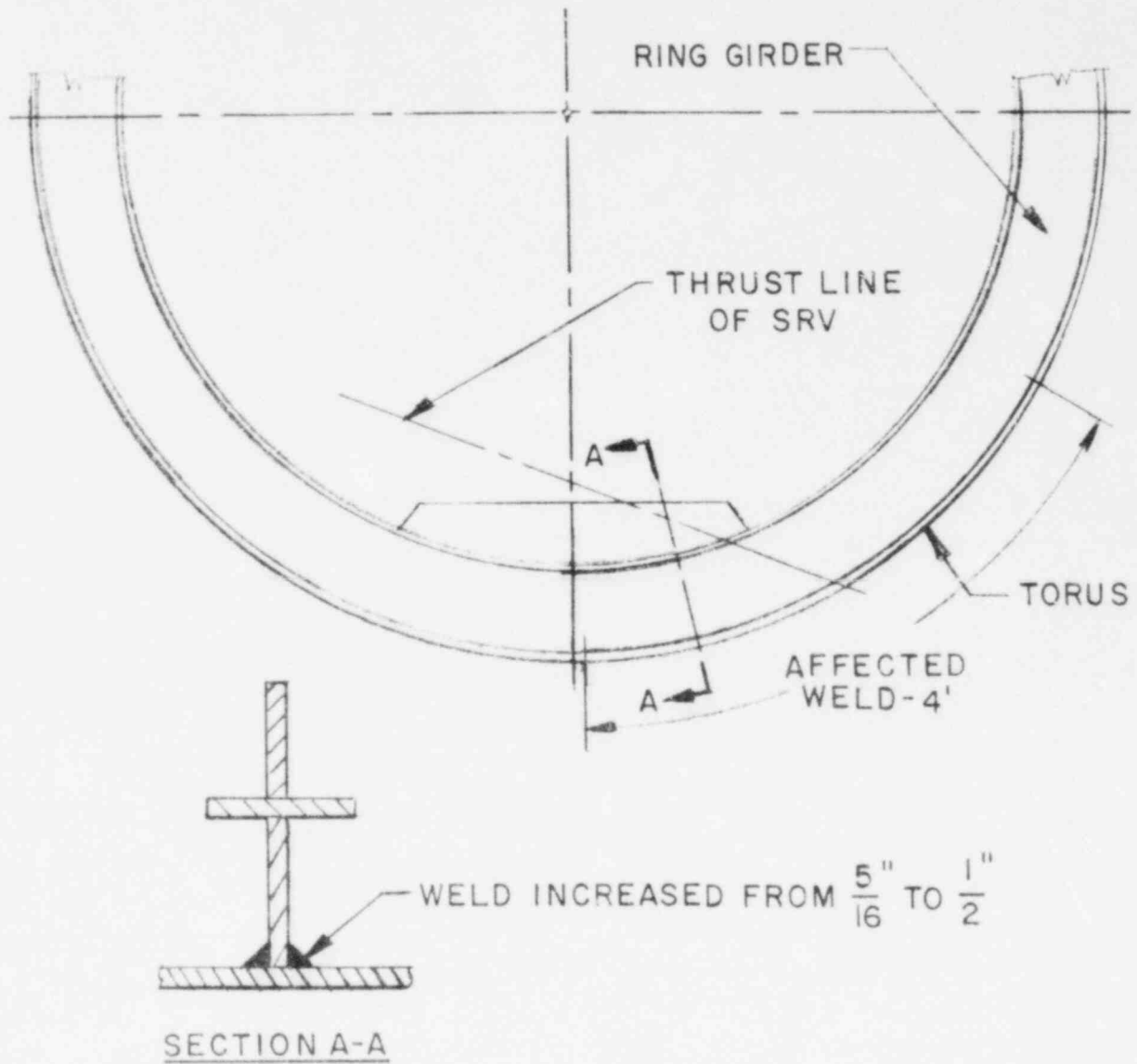
FIG. 2-21

RING GIRDER WELD MODIFICATION

**^T TELEDYNE
ENGINEERING SERVICES**

3.0 CONTAINMENT STRUCTURE ANALYSIS - OUTER SHELL & EXTERNAL SUPPORT SYSTEM
     (INCUDING ANCHORS)

The containment structure section of this report includes the analysis
and evaluation of the following structures:

> Torus Shell
> Support Columns
> Column-To-Torus Weld
> Support Saddles
> Saddle-to-Torus Weld
> Earthquake Restraints & Attachment
> Anchor (Tie-Down) System

3.1 Computer Models

Analysis of the containment structures was accomplished using the
computer models shown in Figure 3-1 to Figure 3-4. The detailed shell model
shown in Figure 3-1 was used to calculate the effects of all loads on shell
stress, as well as all symmetric loads on the support and anchor system. The
beam model shown in Figure 3-4 was used to determine the effects of asymmetric
loads on the support system. Asymmetric loads on the torus structure are
horizontal earthquake, SRV and chugging. Evaluation of the support system
considered the combined effect of symmetric and asymmetric loads in accord-
ance with the load combination table (Table 1).

The detailed finite element model shown in Figure 3-1 simulates
one-half of the non-vent bay. It is bounded by the ring girder on one end and
the mid-bay point on the other. The vent header system is assumed to be
dynamically uncoupled from the shell by the support saddles and is not
included in this model. This model was constructed with the assumption that
the small offset that exists between the ring girder and mitre joint will not
affect results; accordingly, the offset is not included in the model.

**TELEDYNE
ENGINEERING SERVICES**

This model includes 513 structural nodes, 518 plate elements, 2242 static degrees and 364 dynamic degrees of freedom. Symmetric boundary conditions were used at both ends of the model.

The model was modified for various load calculations to account for differences in the percent of the water mass that is effective for that load event. In all cases, modeling of the water mass was accomplished using a 3-D virtual mass simulation as an integral part of the structural analysis. The percent of water mass used is identified in the discussion of each load calculation that follows.

The 360° beam model of the torus is shown in Figure 3-4. This model was used to evaluate the effects of lateral loads on the support system and earthquake restraint system. The beam element properties were selected to simulate combined bending and shear stiffness of the sections. Water mass was lumped with the structure weight on the wetted nodes.

3.2 Loads Analysis

3.2.1 Pool Swell Loads (4.3.1 & 4.3.2)

Analysis for pool swell loads was done using the finite element model shown in Figure 3-1. This was a dynamic analysis performed in the time domain by applying a force time history, to simulate the pressure-time histories of the pool swell event to each node on the computer model. Input pressure-time histories were varied in both the longitudinal and radial directions in accordance with the information in References 1, 2, 9 and 10. Typical pressure-time history curves are shown in Figures 3-5 through 3-7. (These pressure-time histories are taken directly from Reference 10, before adjustment, as required by Reference 2. Therefore, the amplitudes shown are slightly different than the loads used in the analysis).

The computer analysis was run for two different pool swell conditions, full $\triangle$P and zero $\triangle$P. Figures 3-5 through 3-7 show comparative values and time histories for the two cases. The only difference between the analyses was the input loads; the models were identical. Details of the full load distribution can be found in References 1, 9 and 10.

Plant-unique quarter scale pool swell tests showed that the effective water mass was less than 100% after bubble breakthrough and was different for both zero and full $\triangle$P conditions (Reference 4). The water mass used in the computer simulation was constant throughout the analysis and was set at the average of the two reduced masses identified in the quarter scale tests. The reduced and average mass values are given in Table 3. This simplification in water mass analysis is consistent with the relatively slow (pseudo-static) nature of the pool swell load. This simplification only affects the inertial (frequency) calculation; the effects of weight are accurately calculated for each load and time in the deadweight analysis.

3.2.2 Condensation Oscillation - DBA (4.4.1)

Analysis for condensation oscillation (CO) was also done with the structural model shown in Figure 3-1.

The condensation oscillation shell load is specified as a spectrum of pressures in 1 Hz bands (Reference 1). The analysis for this load was performed by considering the effects of unit loads at each load frequency (harmonic analysis) and then scaling and combining the individual frequency effects to determine total stress at selected elements. The three variations in the CO spectrum (Reference 1) were evaluated by re-scaling the results of the unit load analysis. 100% of the water mass was used for all CO analysis. A plant-unique factor was applied to the nominal condensation oscillation pressures as discussed in Reference 1; the factor is listed in Table 3.

The combination of individual harmonic stresses into total element stress was done by considering frequency contributions at 31 Hz and

**✦ TELEDYNE
ENGINEERING SERVICES**

below. The actual combination was done by adding the absolute value of the four highest harmonic contributors to the SRSS combination of the others for shell stress. Loads on the support and anchor system were determined by adding the absolute value of the three highest harmonic contributors to the SRSS of the others. These combination methods and use of the 31 Hz cutoff are the result of extensive numerical evaluation of full scale test data, which is reported and discussed in References 6 and 14, and in Appendix 2 of this report.

3.2.3 Chugging

3.2.3.1 Pre-Chugging & IBA/CO (4.5.1.2 & 4.4.1)

The pre-chug load was evaluated for both the symmetric and asymmetric distribution described in Reference 1. Results for the symmetric pre-chug analysis were also used for IBA/CO as described in paragraph 4.4 of Reference 1.

Results for symmetric pre-chug were developed directly from the unit-load harmonic analysis done for CO. The results of that analysis were scaled to two psi (the pre-chug pressure) and all frequencies in the pre-chug range were scanned to determine the highest possible stresses.

Analysis for asymmetric pre-chug was performed using the beam model in Figure 3-4 by applying the unbalanced lateral load through the prescribed frequency range.

3.2.3.2 Post Chugging (4.5.1.2)

Post chugging is defined as a spectral load across a wide band, similar in nature to the CO, but much lower in amplitude. Analysis done on one of the TES plants produced very low stresses and loads that were bounded by pre-chug values. The analyses for pre- and post chug produced these results for maximum shell stress:

7 TELEDYNE
ENGINEERING SERVICES

Maximum Shell Stress

Shell Membrane Stress

Pre-Chug   1284 psi

Post Chug   774 psi[1]

1.   Based on frequencies to 30 Hz - sum of 4 maximum +
      SRSS of others.

Additional work published in Reference 12 showed that pre-chug bounded post chug (to 50 Hz) for column and saddle loads (Table 5-1, Ref. 12). It also showed that $P_L + P_b$ stress due to post chug exceeded pre-chug by 53%.

TES analysis for post chug used the pre-chug stress values. The pre-chug stress may be increased by 53% to account for the 30 to 50 Hz contribution and they will still meet allowable stress.

No further post chug analysis was done for the shell. This position was also influenced by the fact that post chug stresses were very small.

3.2.4 SRV Discharge

Calculation of stresses due to SRV line discharge pressures, were also done using the finite element model in Figure 3-1. The loading function used for this analysis was based on data collected from in-plant SRV testing in this facility. Testing was done in general accordance with the guidelines given in Reference 2. In these tests, pressure amplitude and frequency were recorded and compared to calculated values for the test conditions. Factors were developed that related test to calculated values for both amplitude and frequency (see Appendix 1). These factors were then applied to calculated load values for other SRV conditions; the structural analyses were

TELEDYNE
ENGINEERING SERVICES

performed using these adjusted values. Appendix 1 discusses the in-plant test and analysis in more detail. A typical set of SRV shell pressures is shown in Figure 3-8.

The method of modeling the water mass in the SRV computer model was the subject of extensive study in this program. Initial attempts to reproduce measured stresses by applying measured pressures to the computer models failed badly. After considerable study of the nature of the SRV phenomena itself, and the differences between it, and the pool swell related loads, it appeared that a dry structure analysis should produce acceptable correlation. The method was tested and correlation of calculated-to-measured shell stress was excellent. The dry structure analysis method was subsequently used as a basis for all SRV analysis.

3.2.5 Deadweight, Thermal & Internal Pressure

Deadweight, thermal and internal pressure analyses were done using the computer model shown in Figure 3-1. Resulting stresses were calculated and considered for all elements on the model.

For the thermal analysis, conduction into the columns and saddles from the torus was considered. Convection from the columns and saddles to ambient produced a calculated temperature gradient in these elements. The torus water, internals and shell were all assumed at the same temperature.

3.2.6 Seismic

Seismic analysis for shell stress was done by applying static G levels to the model in Figure 3-1. Load orientation and values were adjusted for vertical and horizontal earthquakes in accordance with Table 3.

The effects of lateral seismic loads on the support system were determined using the model in Figure 3-4. The effective water mass used in this (lateral) analysis was adjusted in line with test results which showed

that net dynamic reaction loads due to the water mass were substantially less than those obtained from static application of the seismic acceleration. A discussion of this fact can be found in Reference 7; the effective water mass used can be found in Table 3 of this report.

3.2.7 Fatigue Analysis

Fatigue analysis of the torus shell and external support system is described here. Analysis of the shell at piping penetrations will be described in TES report TR-5310-2, when the piping analysis is complete.

The fatigue analysis of the shell and support system was a conservative one, which was based on applying a stress concentration factor of 4.0 on the most highly stressed elements for each load case. In the case of the support system, only the column-to-torus and saddle web-to-torus welds were considered, since they have higher stresses then the rest of the support system. The process is conservative because:

- It applies the maximum stress concentration (4.0), recognized by Section III of the ASME Code to all elements (Reference 11).
  and
- It adds the maximum absolute stress for each load case even though they do not usually occur at the same element.

The procedure used in this analysis consists of the following steps.

1. For a given load, locate the maximum component-level stresses (S_x, S_y, S_{xy}) for the free shell, local shell, and the supports.

2. For these locations, establish the stress intensity ranges and the approximate number of cycles.

3.   Repeat the process for all other loads in the load
combination.

4.   Add the stress ranges for all loads, independent of
sign.

5.   Multiply these total stress ranges by 4.0 (the
SIF).

6.   Calculate the alternating stress intensity and com-
plete the fatigue analysis in compliance with Ref-
erence 11.

Fatigue analysis resulting from chugging was done assuming
that the operator would depressurize the system within 15 minutes after chugg-
ing begins. Plant procedures are presently under study to provide for this
action.

3.3 Results and Evaluation

Results are reported for each structural component of the containment
system for the controlling load combination. Controlling load combinations
are the ones that produce the smallest margins against the allowable stress -
not necessarily the highest stress.

All load combinations listed in Table 1 have been considered. As
stated previously, most results include some level of bounding analysis and,
therefore, understate the margins which actually exist.

3.3.1 Torus Shell

Results of shell stress due to individually applied loads
were calculated and maintained on a component stress level until all the load
combinations were formed. Stress intensities were then calculated from these
total component-level values.

The controlling load combinations for the shell at Pilgrim are cases 14 and 20 in Table 1; these are:

Case 14 - IBA.CO + SRV + Seismic (SSE Used) + Pressure + Weight

Case 20 - DBA.CO + Seismic (SSE) + Pressure + Weight

These load combinations control all categories of shell stress, although the location of the elements is different for the different types of stress. The following table summarizes the controlling stresses. Approximate locations of the controlling stresses are shown in Figure 3-9.

CONTROLLING SHELL STRESSES - PILGRIM

TYPE OF STRESS & LOAD CASE	LOCATION	ACTUAL STRESS (psi)	ALLOWABLE STRESS (psi)
Membrane (Pm) (Case 14)	Free Shell Element 17	13,324	19,300
Local (Pl) (Case 14)	Local Shell Element 125	8,365	28,950
Membrane + Bending (Case 20)	Free Shell Element 19	17,258	28,950
Stress Range (Case 14)	Local Shell Element 147	26,399	69,900

Compressive Buckling - Acceptable (see below)

Compressive Buckling Reference 13 discusses the results of analytical studies and tests on Mark 1 torus structures to determine their compressive buckling capabilities. The report concludes that SRV is the dynamic load which presents the maximum chance of com-

Technical Report
TR-5310-1   -43-

**TELEDYNE
ENGINEERING SERVICES**

pressive buckling failure; but, that a safety factor of 7 still exists for an applied SRV pressure of +29.3/-22.6 psi. The maximum worst-case SRV shell pressures for Pilgrim are +12.6 psi and -9.6 psi, which are lower than those used in the referenced study. Based on this, compressive buckling stresses are considered to be acceptable for the Pilgrim torus.

FATIGUE EVALUATION - PILGRIM

CUMULATIVE USAGE FACTOR SUMMARY
STRESS INTENSIFICATION FACTOR = 4.0)

	NORMAL OPERATION	EVENT TYPE SBA/IBA	DBA
	.005	.001	.015
	.164	.003	.026

3.3.2 Support Column & Attachments

The controlling load case for the support column and attachment weld to the torus shell is load case 16 in Table 1. Controlling stresses are associated with the downward loads. Case 16 includes:

Pool Swell (0△P) + Pressure + Weight

For this load case, the following controlling stresses were identified:

SUPPORT COLUMN - CONTROLLING AXIAL CONDITION

COLUMN	LOAD DIRECTION	CONTROLLING STRESS	ACTUAL FACTOR	ALLOWABLE FACTOR
Inner	Down	Axial + Bending	.307	1.0
Outer	Down	Axial + Bending	.352	1.0

COLUMN-TO-SHELL WELD

LOCATION	LOAD DIRECTION	CONTROLLING STRESS	ACTUAL STRESS	ALLOWABLE STRESS
Inner	Down	Shear	12.32 K/in	28.9 K/in
Outer	Down	Shear	10.99 K/in	28.9 K/in

3.3.3 Support Saddles & Shell Weld

The controlling load case for the weld between the saddle and the torus shell, and for down loads on the saddle is load case 16 in Table 1. This case includes:

Pool Swell ($0\triangle P$) + Weight

The resulting stresses are:

SADDLE STRESSES

LOCATION	LOAD DIRECTION	TYPE STRESS	ACTUAL STRESS	ALLOWABLE STRESS
Sole Plate	Down	Bending	19.65 K/in	28.5 K/in

SADDLE-TO-SHELL WELD

LOCATION	LOAD DIRECTION	TYPE STRESS	ACTUAL STRESS	ALLOWABLE STRESS
Outside End	Down	Shear	11.93 K/in	13.64 K/in

The controlling case for the saddle associated with up load is case 21, which includes:

DBA.CO + Seismic (SSE) + Weight

Loads for this case are:

LOCATION	LOAD DIRECTION	TYPE STRESS	ACTUAL LOAD	ALLOWABLE LOAD
Clamping Plate	Up	Bending	95 kips	103.2 kips

3.3.4 Earthquake Restraints & Attachments

The earthquake restraint system is illustrated in Figure 3-10. The controlling load case for this system is the one that produces the largest lateral load. This is case 15 which includes:

Chugging + SRV + SSE

All three of these loads have been selected to produce the highest lateral load on one earthquake restraint; contributions from the individual loads were added directly.

The controlling stress results follow:

EARTHQUAKE RESTRAINT

STRESS LOCATION	STRESS TYPE	ACTUAL STRESS	ALLOWABLE STRESS
Tie Plate at Slot	Pin Bearing	4,879 psi	27,000 psi

**TELEDYNE
ENGINEERING SERVICES**

ATTACHMENT WELD

STRESS LOCATION	STRESS TYPE	ACTUAL STRESS	ALLOWABLE STRESS
Weld at Tie Plate - Base Plate Connection	Shear	3,668 psi	21,000 psi

3.3.5 Anchor System

The torus at Pilgrim is restrained against upward loads by two-inch diameter anchor bolts in the support saddle and 1½-inch anchor bolts in the column bases that were part of the original plant design.

The original 1½-inch column base bolts did not restrain upward movement because they were used only to hold a base plate which was not attached to the column. The tiedown fix will use the original bolts with clamping plates to tie down the torus columns.

The controlling load case for these anchor bolts is case 21 in Table 1. This case includes:

DBA.CO + Seismic (SSE) + Weight

The loads are:

SADDLE ANCHOR BOLTS (PER SADDLE)

ACTUAL MAXIMUM LOAD	MAXIMUM CAPACITY	FACTOR OF SAFETY
76.6 K/bolt	264 K/bolt	3.45

**TELEDYNE
ENGINEERING SERVICES**

The original column anchor bolts are a "J" bolt embedded in the concrete and constucted from structural steel. The capacity of these bolts will be determined by the stresses in the steel bolt rather than concrete pull out capacity. Accordingly, they are evaluated against stress:

COLUMN ANCHOR BOLTS - ORIGNAL

COLUMN LOCATION	ACTUAL MAXIMUM LOAD	MAXIMUM CAPACITY	FACTOR OF SAFETY
Inner	47.5 kips	60 kips	1.26
Outer	40.3 kips	60 kips	1.49
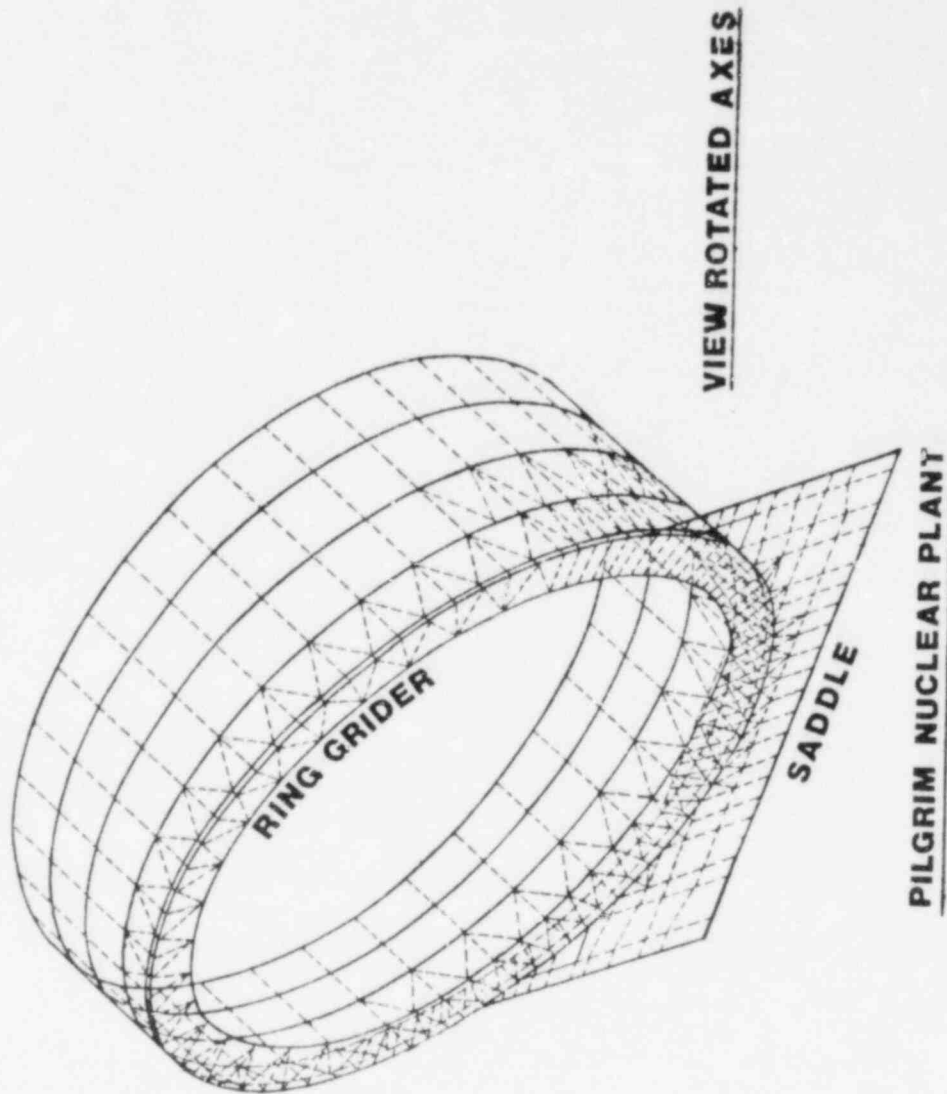
FIGURE 3.1 DETAILED SHELL MODEL
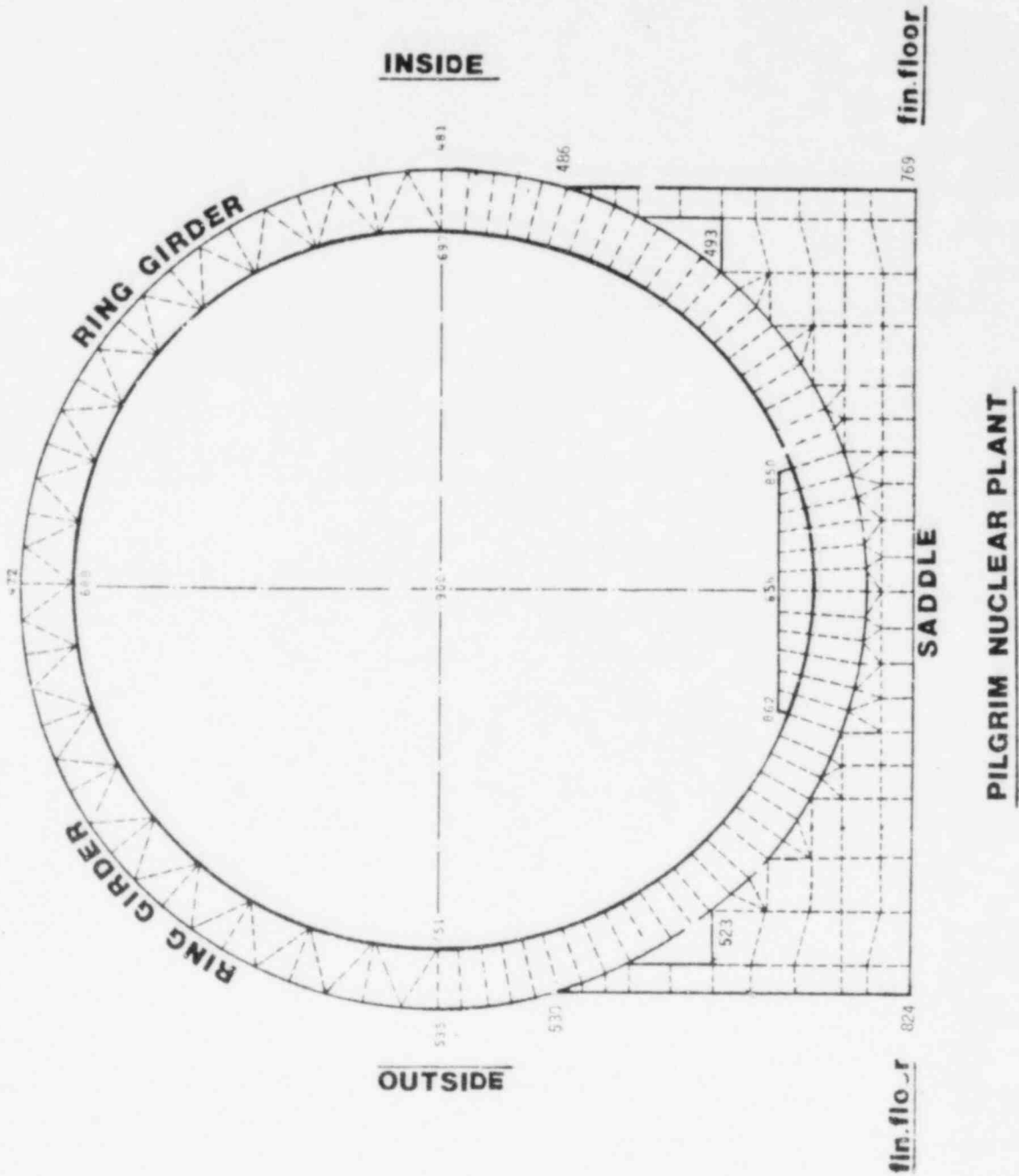
FIGURE 3.2 DETAILED SHELL MODEL

1/32nd
TORUS MODEL WITH
SADDLE

NOTE: all units in inches
unless otherwise
stated.

FIGURE 3.3 DETAILED SHELL MODEL

PILGRIM NUCLEAR PLANT
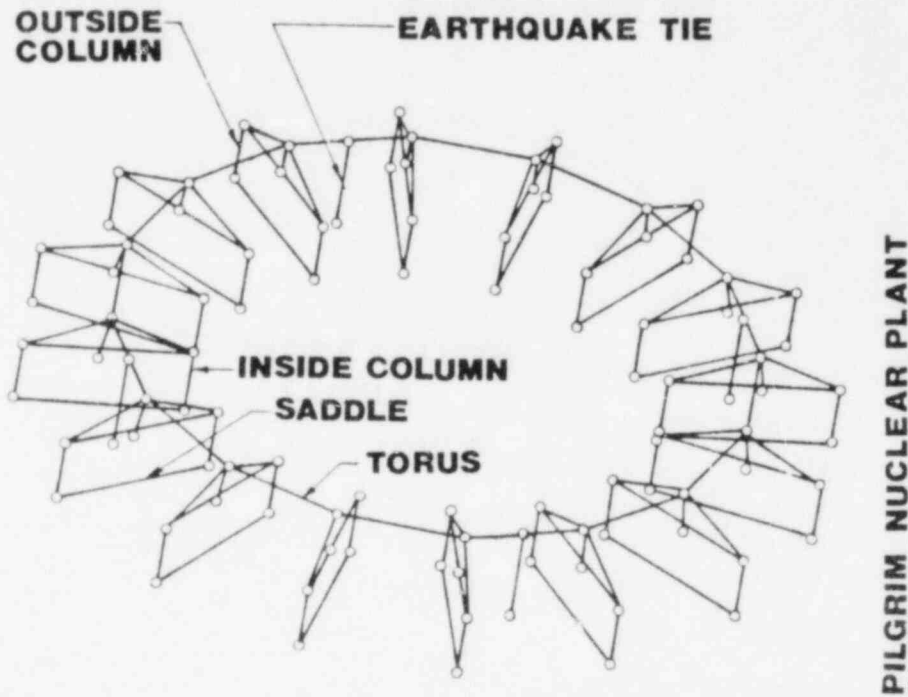
FIGURE 3.4 360° TORUS BEAM MODEL
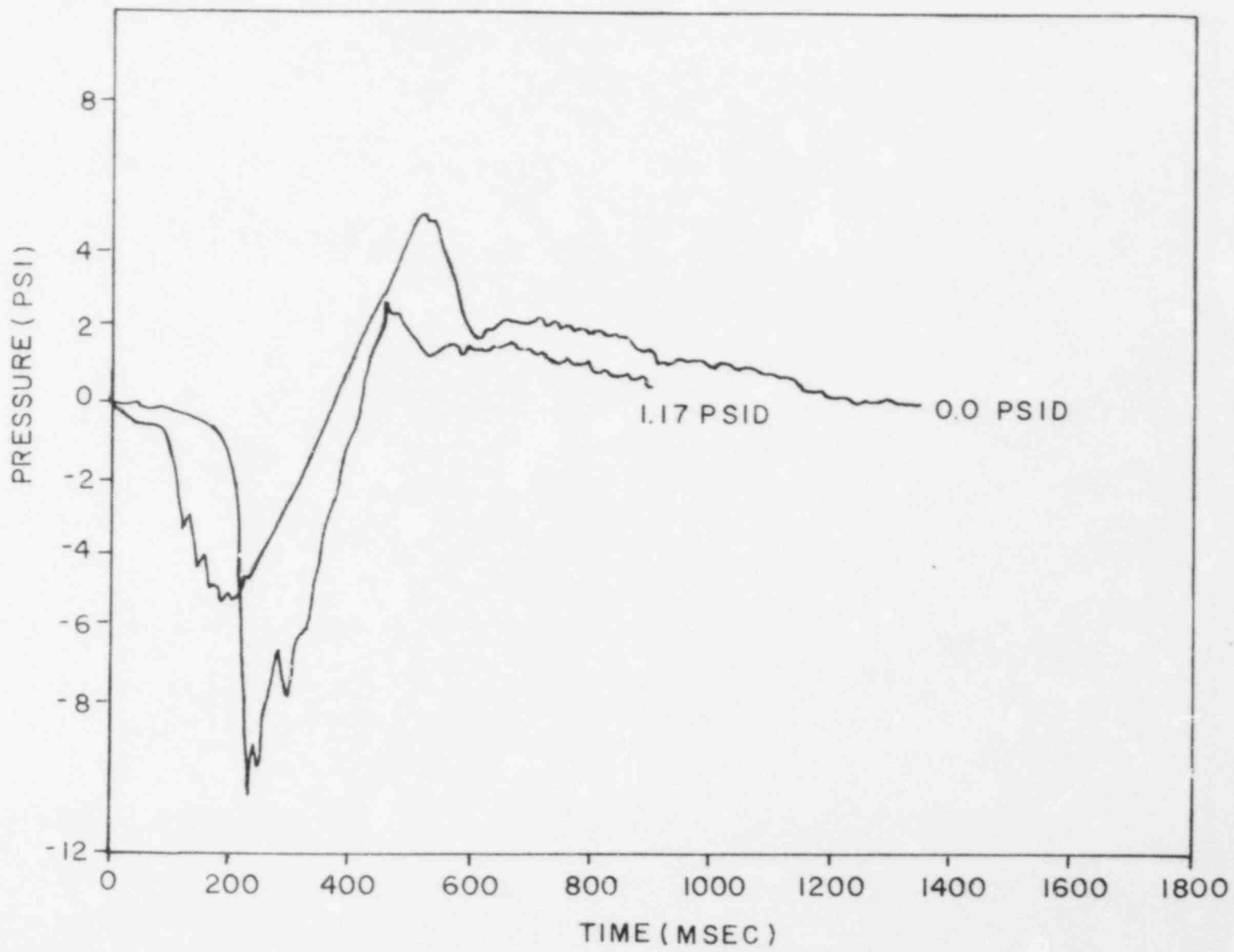
FIG. 3-5

POOL SWELL-NET VERTICAL LOAD

TELEDYNE
ENGINEERING SERVICES
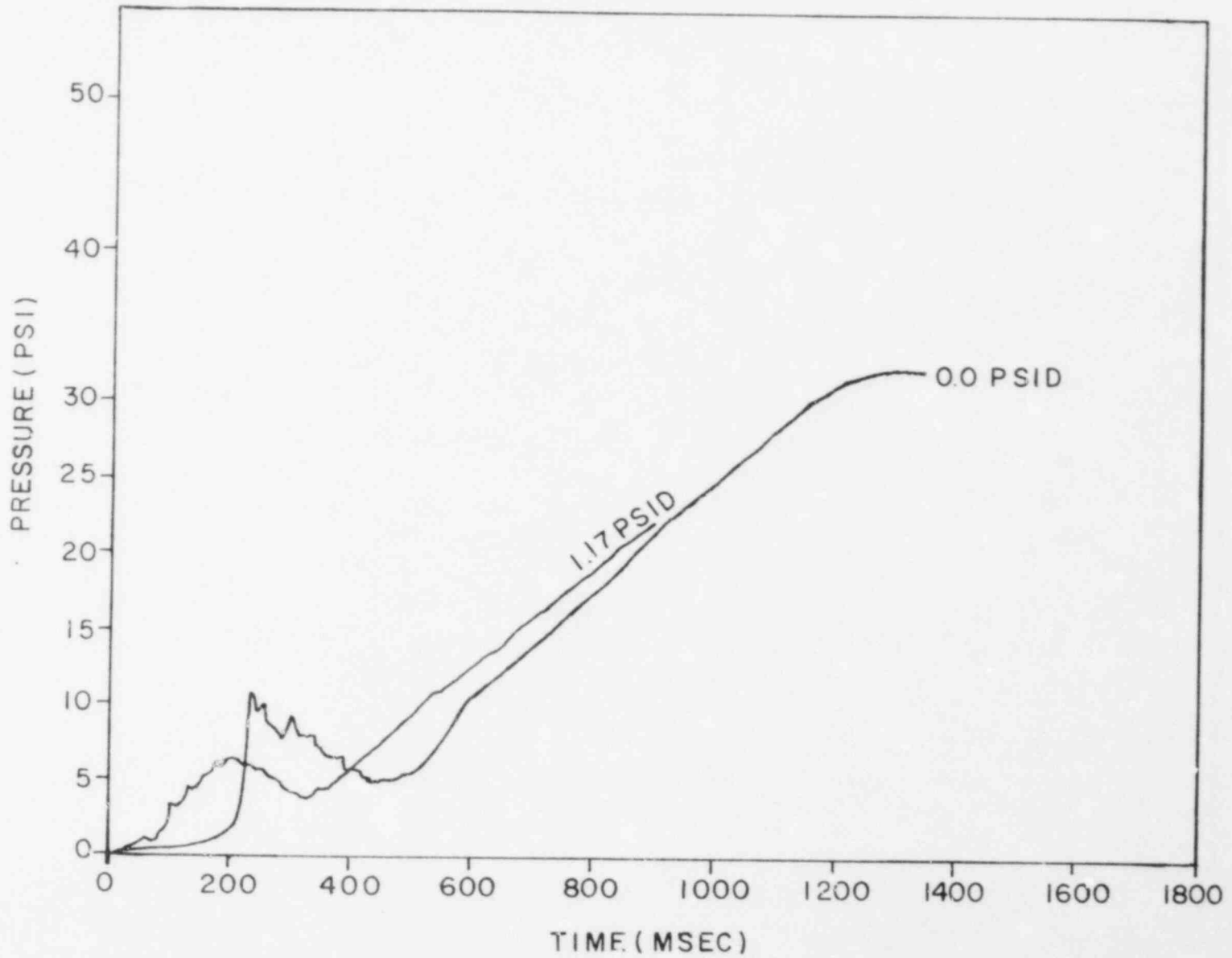
FIG. 3-6
POOL SWELL – AVERAGE SUBMERGED PRESSURE
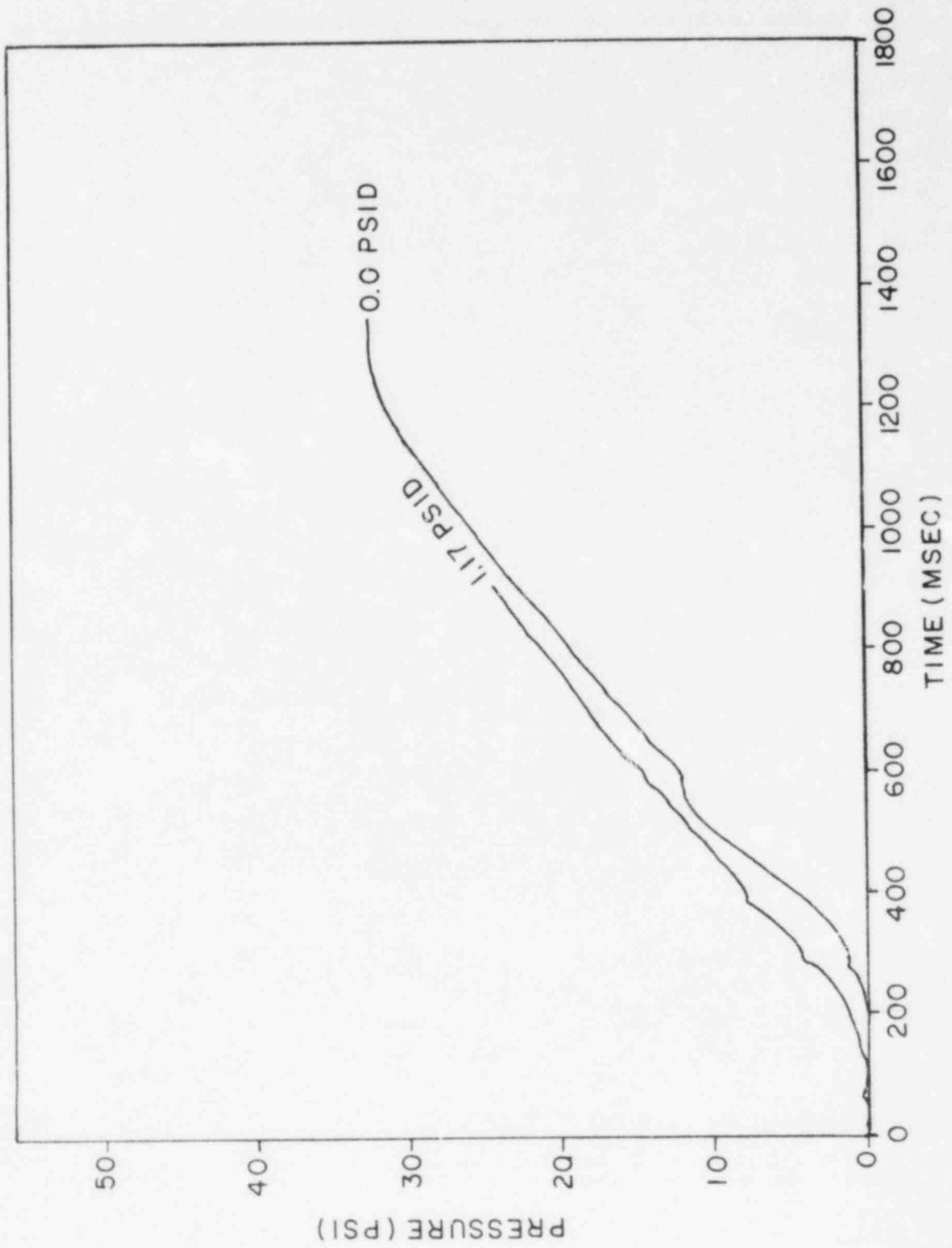
FIG. 3-7
POOL SWELL - TORUS AIR PRESSURE

-55-

BASED ON SRV TEST [#]1,
GAGE P3 - SCALED TO
WORST CASE
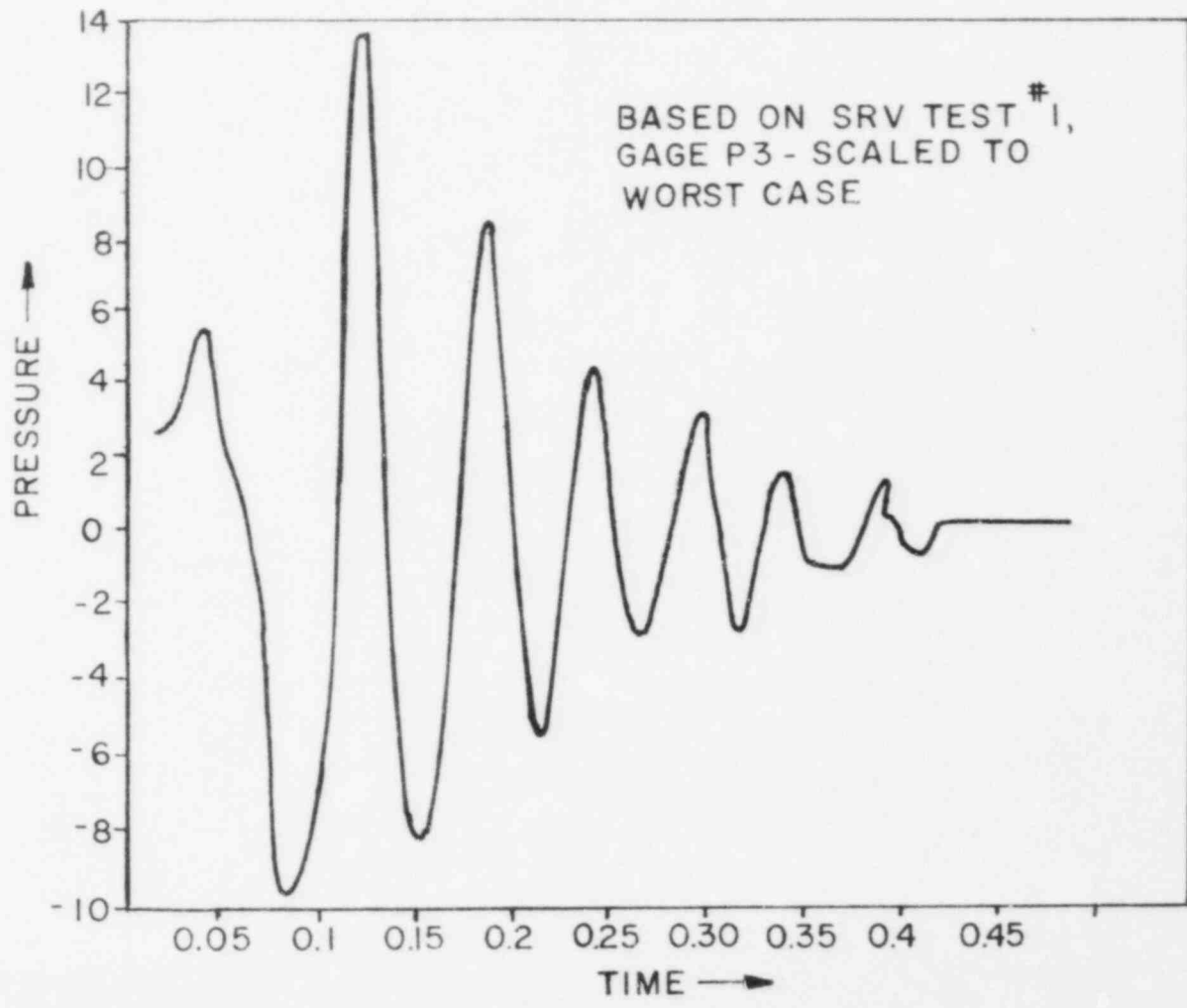
FIG. 3-8

TYPICAL SRV SHELL PRESSURE -PILGRIM

$\frac{1}{32}$ MODEL – LOWER
HALF OF SHELL
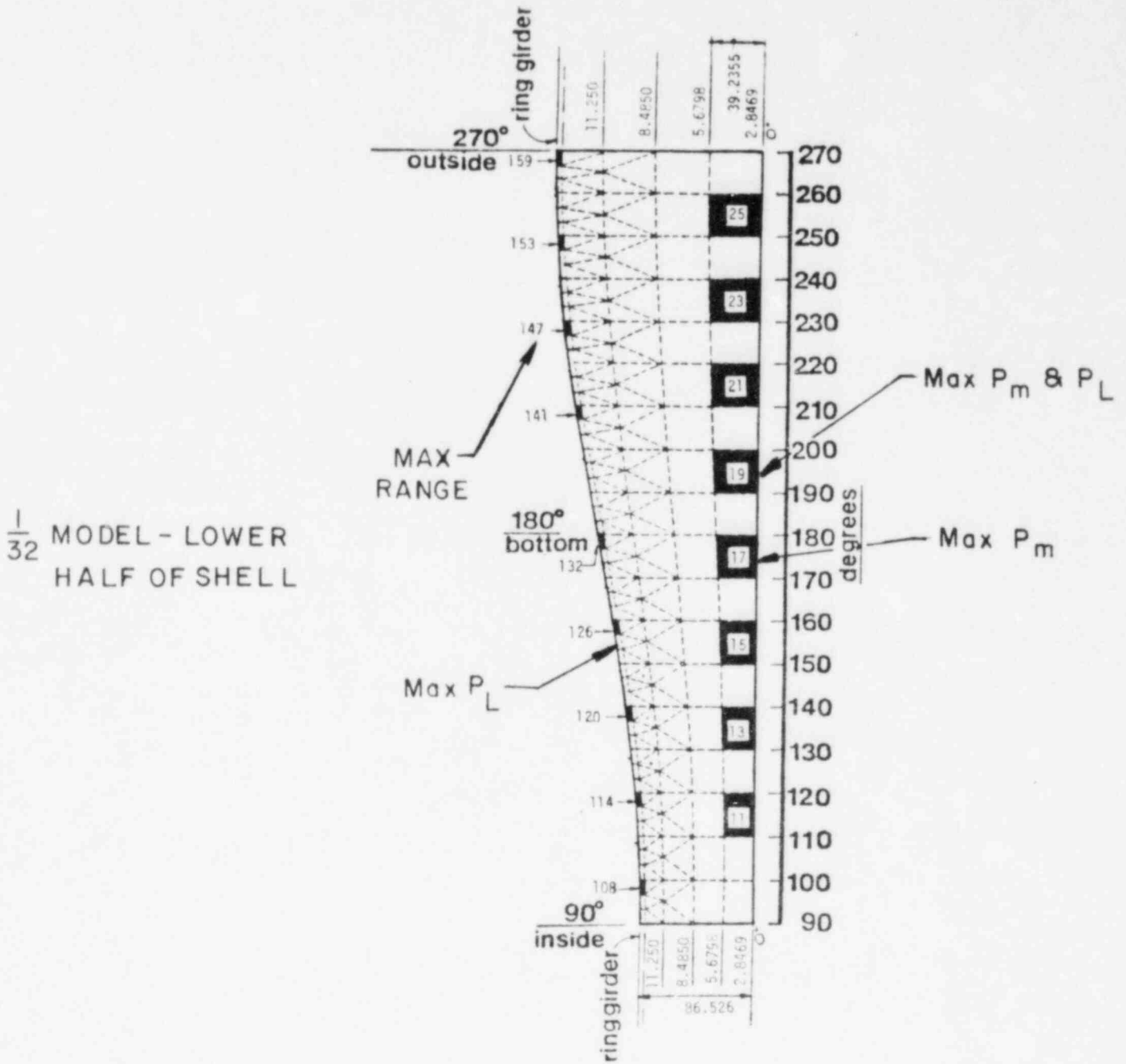
FIG. 3-9

MAXIMUM SHELL STRESS LOCATIONS – PILGRIM

TORUS SHELL

18'

2'-1"

$\frac{3}{8}$

$\frac{3}{8}$

$\frac{3}{8}$

A

A

TOTAL 4 RESTRAINTS
90° AROUND TORUS

5" DIA.

$\frac{3}{16}$

$\frac{3}{16}$

SECTION A-A

FIG. 3-10

EARTHQUAKE RESTRAINT SYSTEM

4.0 VENT HEADER SYSTEM

4.1 Structural Elements Considered

The vent header system, as defined in this section, includes the following structural components:

        a. Vent Header (V.H.)

        b. Main Vent Pipe (V.P.)

        c. Downcomers (D.C.)

        d. Downcomer Tie Bars

        e. Deflector

        f. Vent Header Support Columns & Attachments

        g. VH/DC Intersection

        h. VH/VP Intersection

        i. VP/Drywell Intersection

        j. Vent Header Mitre Joint

The main vent bellows are considered in Section 7.0.

4.2 Computer Models

Two computer models provided the means to analyze the vent header system, they are shown in Figures 4-1 through 4-4.

The first of these is a detailed shell model, (Figures 4-1 to 4-3), which includes a highly detailed representation of one-half of the header in a non vent bay, complete with four downcomers.

The model also includes an approximate representation of one-half of the vent bay; this was intended to provide the proper boundary conditions and stiffness transition near the non-vent bay. The vent bay half of the model was not used for stress determination. This large finite element model was used primarily to determine shell stresses in the non-vent bay; some other

uses are discussed in the following text. It was used for both static and dynamic analysis and provided detailed stress gradient information in the downcomer/vent header intersection region.

The second vent header model is the beam model shown in Figure 4-4. This model represents a full vent bay, complete with vent pipe and downcomers; as well as a half non-vent bay on either side. It was used to determine boundary loads on the vent system components to support a more detailed stress analysis of those components. This model was used to define loads on the following elements:

- Vent Header Support Columns
- Vent Pipe/Vent Header Intersection
- Vent Pipe/Drywell Intersection
- Vent Header Mitre Joint
- Main Vent Pipe

The loads and moments taken from the beam model were used in further analysis to determine stresses. The calculation methods used for these stresses are:

- VH support columns - hand analysis
- VP/VH intersection - applied stress multipliers (stress intensification factors) from Reference 7
- VP/drywell intersection - used stress multipliers from - Reference 16 (Bijlaard)
- Mitre joint - used stress multipliers from detailed shell model (Figure 4-1)
- Main vent pipe - hand analysis

The beam model used a stiffness representation of the VP/VH intersection taken from Reference 8. Attachment stiffness between the vent pipe and drywell was calculated using References 17 and 18.

Pool swell water impact on the vent header deflector was calculated with a hand analysis. The impact forces were applied statically to a beam model and a dynamic load factor was applied (see Figure 4-5).

4.3 Loads Analysis

4.3.1 Pool Swell Loads

4.3.1.1 Pool Swell Water Impact

Analysis for stresses due to pool impact and drag was done using both computer models.

Determination of shell stresses was done with the detailed model in Figure 4-1. For this analysis, force time histories based on QSTF test data were used (References 4, 9 and 10). These time histories were applied at 100 nodal points on the shell model and the dynamic response of the structure was calculated. Relative timing between loadings (Reference 1) was maintained to preserve accurate representation of longitudinal and circumferential wave sweep. Stresses in the vent header/downcomer intersection, as well as in the free shell areas, were taken directly from this model. Stresses in the downcomer tie bars were also taken from this model. Analysis was done for both full and zero ΔP impacts.

The beam model (Figure 4-4) was also used to determine stress from pool swell impact and drag. This was done with a time history dynamic analysis using loads developed by integrating the impact pressures over small areas and reducing them to nodal forces. Approximately 95 nodes along the length of the beam model were dynamically loaded in this analysis, including loads on the VP/VH intersection and vent pipe. The results of this analysis were used to define boundary loads on VP/VH intersection, mitre joint and other elements as listed in Section 4.2. Stress analysis for these elements was performed using the methods indicated in Section 4.2.

4.3.1.2 Pool Swell Thrust (4.2)

Pool swell thrust forces are defined as dynamic forces at each bend or mitre in the vent system, and are a consequence of the flowing internal fluids. Analysis for these loads was done using the beam model and applying the loads statically. This is consistent with the slow nature of the applied pressure forces.

The calculation was performed with the maximum value of all thrust forces applied simultaneously; this is a conservative condition.

4.3.1.3 Pool Swell Drag Loads (4.3.7 & 4.3.8)

The vent header support columns are loaded by forces from LOCA-jet and LOCA bubble drag. By inspection, it was concluded that LOCA-jet loads would not combine with water impact on the vent system due to differences in timing and, therefore, would not contribute to the maximum stress calculations - LOCA jet forces were not considered further.

LOCA bubble forces were calculated and the maximum normal components (radial and longitudinal) were applied simultaneously to conservatively bound the bending moments on the support column. These peak values were applied statically at the midpoint of the column. Stress calculations were done by hand.

4.3.2 Chugging Loads

4.3.2.1 Downcomer Lateral Loads (4.5.3)

Reference 1 identifies downcomer lateral loads as static equivalents with random orientation in the horizontal plane. The major consequence of this loading is to produce high local stress in the VH/

downcomer intersection. The detailed shell model (Figure 4-1) was used to identify stresses in the downcomer intersection due to static loads applied at the base of the downcomer. Frequencies of the first downcomer response mode were taken from a dynamic analysis on the same model (Figure 4-1) with the downcomers full of water to the operating level. This frequency was necessary to determine the proper dynamic scale factor to apply to the static load.

The stress results from the statically applied load were used as a basis for a fatigue evaluation of the intersection in accordance with Reference 9.

4.3.2.2 Chugging - Synchronized Lateral loads

The random nature of the downcomer lateral chugging load provides for all combinations of alternate force orientations on adjacent pairs of downcomers. Various load combinations were examined to determine stress levels in the vent header and mitre joint as a result of these loads. The cases considered are shown in Figure 4-6.

These cases were considered by applying static loads to the beam model (Figure 4-4) and determining final stresses as described in Section 4.2.

4.3.2.3 Internal Pressure (4.5.4)

Three vent system internal pressures exist during chugging. They are:

- Gross vent system pressure - a .7 Hz oscillating pressure with a maximum value of 5.0 psi. This pressure acts on the entire vent system.

- Acoustic vent system pressure - a sinusoidal pressure varying from 6.9 to 9.5 Hz at a maximum value of 3.5 psi. This pressure affects the entire vent system.

- Acoustic downcomer pressure oscillation - a 40-
  50 Hz pressure at 13 psi that produces only
  hoop stress in the downcomers.

Responses to these pressures were estimated using
hand analysis and were determined to be substantially less than those result-
ing from internal vent system pressures during pool swell. The values associ-
ated with pool swell pressures were used in all combined load cases involving
chugging pressures; this produces conservative results.

4.3.2.4 Submerged Structure Drag (Support Columns only)

Examination of the load combinations that include
chugging makes it clear that these cannot control maximum stress level in the
support columns; combinations that include vent header water impact will
produce much higher stresses. For this reason, stresses in the vent header
support columns were not calculated for chugging drag.

Drag forces on the downcomers and downcomer tie
bars are already included in the Downcomer Lateral Loads, which were based
directly on test data.

4.3.3 Condensation Oscillation - DBA

4.3.3.1 Downcomer Dynamic Load (4.4.3.2)

The downcomer dynamic load, due to condensation
oscillation, is a sinusoidal pressure variation that can be equal or unequal
in the two downcomers forming a pair.

The unequal pressure case produces a net lateral
load on the downcomer much like chugging. The major considerations for this
load are stresses in the downcomer intersection due to a net lateral load on

one pair of downcomers and a more general stress case where loads on adjacent downcomer pairs are phased to produce gross lateral loads on the vent system or torsion in the vent header.

The horizontal component of the CO downcomer load produces the same type of loading on the vent system as the CH lateral load, in terms of the stress analysis. A comparison of the magnitudes and frequencies of these two loads shows that stresses resulting from CH horizontal loads will bound CO horizontal loads.

The CO downcomer load also produces a vertical component of load, which is not present during CH. The effects of this load were evaluated by static analysis of the detailed vent header model (Figure 4-1) and consideration of dynamic amplification effects, using the beam model (Figure 4-4). This evaluation showed that the combined effects of the CO downcomer load (horizontal and vertical components) would still be bounded by CH lateral loads.

Based on this, CH lateral load results were conservatively used in all load cases in place of CO downcomer loads.

4.3.3.2 Vent System Loads (4.4.4)

Vent system loads consist of a sinusoidal pressure in the vent header and downcomers superimposed on a static pressure. The dynamic pressure in the downcomers is used to calculate hoop stress only.

Stresses for all pressure loads were based on hand analysis using static analysis. The static analysis assumption is consistent with the low frequency of the applied pressure and the fact that the ring modes of the structure are very high.

TELEDYNE
ENGINEERING SERVICES

4.3.3.3 Thrust Forces (4.2)

Stresses resulting from CO thrust forces were conservativel, taken from the pool swell thrust calculations and applied to all CO load cases (para. 4.3.1.2).

4.3.3.4 Drag Forces on Support Columns

Inspection of approximate total loads on support columns due to CO, CH, and pool swell showed that condensation oscillation would not contribute to the maximum column load, due to differences in timing. No detailed analysis was performed.

4.3.4 Condensation Oscillation - IBA

Stresses and loads resulting from IBA condensation oscillation are bounded in all cases by either DBA condensation oscillation or chugging. No detailed analysis was performed for IBA condensation oscillation.

4.3.5 SRV Loads

4.3.5.1 SRV Drag Loads

An SRV discharge produces drag loads which act on the vent header support columns, downcomers, and downcomer tie bars. Analysis for drag loads on these structures was based on data collected during in-plant SRV tests.

Data collected during these tests was scaled to correct it for the appropriate SRV conditions and then applied to the structural model to determine the resulting stress. A more detailed discussion of this procedure is provided in Appendix 1.

4.3.6 Other Loads

Deadweight and seismic stresses in the vent system were calculated using the beam model of Figure 4-4.

Seismic stresses were calculated by statically applying the acceleration values in Table 3.

Thermal stresses were determined for the steady state application of maximum vent system temperature, using hand analysis.

4.4 Results and Evaluation

Results are reported for each structural element of the vent system for the controlling load combination. Controlling load combinations are the ones that produce the smallest margins against the allowable stress - not necessarily the highest stress. All load combinations listed in Table 1 have been considered.

As stated previously, most results include some level of bounding analysis and, therefore, understate the margins which actually exist.

4.4.1 Vent Header - Downcomer Intersection

The controlling load on the vent header-downcomer intersection, both for maximum stress and fatigue, is the downcomer lateral load due to chugging. The worst load combination in which this load appears is case 27 of Table 1. This cases consists of:

Chugging (DBA) + Seismic (SSE) + Weight + Presssure + Thrust + SRV

For this case, the following stress occurs at a point 90° from the plane of a downcomer pair. It is primarily the result of a longitudinal chugging force on the downcomer.

**TELEDYNE
ENGINEERING SERVICES**

TYPE OF STRESS	ACTUAL STRESS	ALLOWABLE STRESS
Combined Maximum Stress	36, 719 psi	37,635 psi

4.4.2 Vent Header - Vent Pipe Intersection

The controlling load on the vent header/vent pipe inter-
section occurs as a result of pool swell water impact. The controlling load
condition is case 25 in Table 1 which includes:

Pool Swell (full$\triangle$P) + Thrust + Seismic (SSE) + Weight + SRV
Pressure

TYPE OF STRESS	ACTUAL STRESS	ALLOWABLE STRESS
Combined Maximum Stress	28,930 psi	28,950 psi

This load case was formed using a 0 P load, and was eval-
uated to a level A allowable. This conservative evaluation was performed to
eliminate the need to evaluate several other vent header load cases.

4.4.3 Vent Header Support Columns and Attachments

The controlling load combination for the vent header support
columns and the clevis joints at each end is case 25, Table 1. This case
includes:

Pool Swell (full$\triangle$P) + Seismic (SSE) + Weight + Thrust + SRV
Pressure

As before, the evaluation was conservatively performed using
0$\triangle$P loads and a level A allowable.

Controlling stress in the support column is:

TYPE OF STRESS	ACTUAL STRESS	ALLOWABLE STRESS
Axial in Column (tension)	17,420 psi	18,000 psi

Controlling stress in the clevis joint at the end of the support column is:

LOCATION	STRESS TYPE	ACTUAL STRESS	ALLOWABLE STRESS
Clevis Plate	Shear	13,015 psi	15,200 psi

4.4.4 Downcomer Tie-Bars and Attachments

The controlling load combination for stresses in the downcomer tie bar and attachments is case 25, in Table 1. The major load is associated with pool swell impact on the crotch region of the downcomers which produces tensile loads in the tie bar.

The controlling case includes:

Pool Swell Impact (fullΔP) + SSE Seismic + SRV + Weight + Pressure + Thrust

Zero ΔP pool swell loads and service level allowables were conservatively used in this analysis.

The controlling stress is:

LOCATION	STRESS TYPE	ACTUAL STRESS	ALLOWABLE STRESS
Tie Bar Clamp	Bending	16,800 psi	22,240 psi

◥◤TELEDYNE
ENGINEERING SERVICES

4.4.5 Vent Header Deflector and Attachments

The major load on the vent header deflector occurs as a result of pool swell water impact. The controlling load condition is case 19 in Table 1 which includes:

Pool Swell (fullΔP) + SSE Seismic + Weight + Thrust

The controlling stress in the deflector is:

LOCATION	STRESS TYPE	ACTUAL VALUE	ALLOWABLE VALUE
Center of the Long Span	Bending	21,000 psi	23,700 psi

The controlling stress for the attachments is:

LOCATION	STRESS TYPE	ACTUAL VALUE	ALLOWABLE VALUE
Fillet Weld	Shear	15,800 psi	17,100 psi

4.4.6 Main Vent/Drywell Intersection

The major load on the drywell penetration occurs as a result of chugging. The controlling load condition is case 21 in Table 1 which includes:

Chugging + Seismic (SSE) + Weight + Pressure (Drywell)

The controlling stress is:

TYPE OF STRESS	ACTUAL STRESS	ALLOWABLE STRESS
Primary and Secondary	39,970 psi	69,900 psi

The effects of all loads from the vent system, and the pressure load were considered using Reference 16. Information regarding stresses due to seismic and thermal response of the drywell is not available and therefore have not been included.

4.4.7 Vent Header, Main Vent & Downcomers - Free Shell Stresses

It was established by inspection of the computer results that large safety margins existed in free shell regions and that minimum safety margins would be controlled by local shell stresses. No further work was done for free shell stress in these structures.

4.4.8 Vent Header - Mitre Joint

The controlling load on the vent header mitre joint occurs as a result of pool swell water impact. The controlling load condition is case 25 in Table 1 which includes:

Pool Swell (full$\triangle$P) + Thrust + Seismic (SSE) + Weight + SRV + Pressure

TYPE OF STRESS	ACTUAL STRESS	ALLOWABLE STRESS
Combined Maximum Stress	27,137 psi	28,950 psi

4.4.9 Fatigue Evaluation

The fatigue analysis of the vent system is a conservative one which assumes that all maximum stresses occur simultaneously, and that all cycles reach these maximum values. The duration of the major loads in this analysis is 900 seconds, the length of chugging associated with an SBA/IBA event.

The procedure used in this analysis consists of the following steps:

TELEDYNE
ENGINEERING SERVICES

- For a given load and component, locate the highest stress.

- For this location, establish the stress range.

- Repeat this process for all other loads in the load combination.

- Add the stress ranges for all loads.

- Multiply this total stress range by the appropriate stress intensification factor.

- Calculate stress intensity and determine the allowable number of stress cycles.

- Determine the usage factor, using the methods of Reference 11.

The fatigue evaluation was performed for all high stress areas in the vent system. The major load, contributing to the fatigue evaluation, is chugging following a DBA. The controlling load case is case 21 in Table 1, which includes:

Chugging (DBA) + Seismic (SSE) + Weight

The controlling usage factor for the vent system is:

VENT SYSTEM FATIGUE RESULTS

LOCATION	ACTUAL USAGE FACTOR	ALLOWABLE USAGE FACTOR
VH Support	.76	1.0

TELEDYNE
ENGINEERING SERVICES

END NODES FIXED

SUPPORT COLUMNS

SYMMETRY
BOUNDARY
CONDITIONS
THIS END

TIE BARS

FIG. 4-1

VENT HEADER MODEL

DOWNCOMERS

SUPPORT COLLAR

THIS SECTION
FOR BOUNDARY
SIMULATION
ONLY

FIG. 4-2

DETAILED VENT HEADER MODEL

TELEDYNE
ENGINEERING SERVICES

GUSSET
RE-ENFORCEMENT

SECTION THROUGH
DOWNCOMER PAIR-
TIE BAR NOT SHOWN

FIG. 4-3

DETAILED VENT HEADER MODEL

-75-

II NODES/
SPAN(TYP)

RING HEADER

DOWNCOMER

VENT HEADER
SUPPORT
COLUMN

VENT PIPE

A   B

VENT HEADER INTERSECTION
(STIFFNESS MATRIX INPUT)

C

SYMMETRY BOUNDARY
CONDITIONS

FIG. 4-4
VENT SYSTEM BEAM MODEL

TELEDYNE
ENGINEERING SERVICES

ANALYSIS BEAM MODEL

APPLIED STATIC LOADING
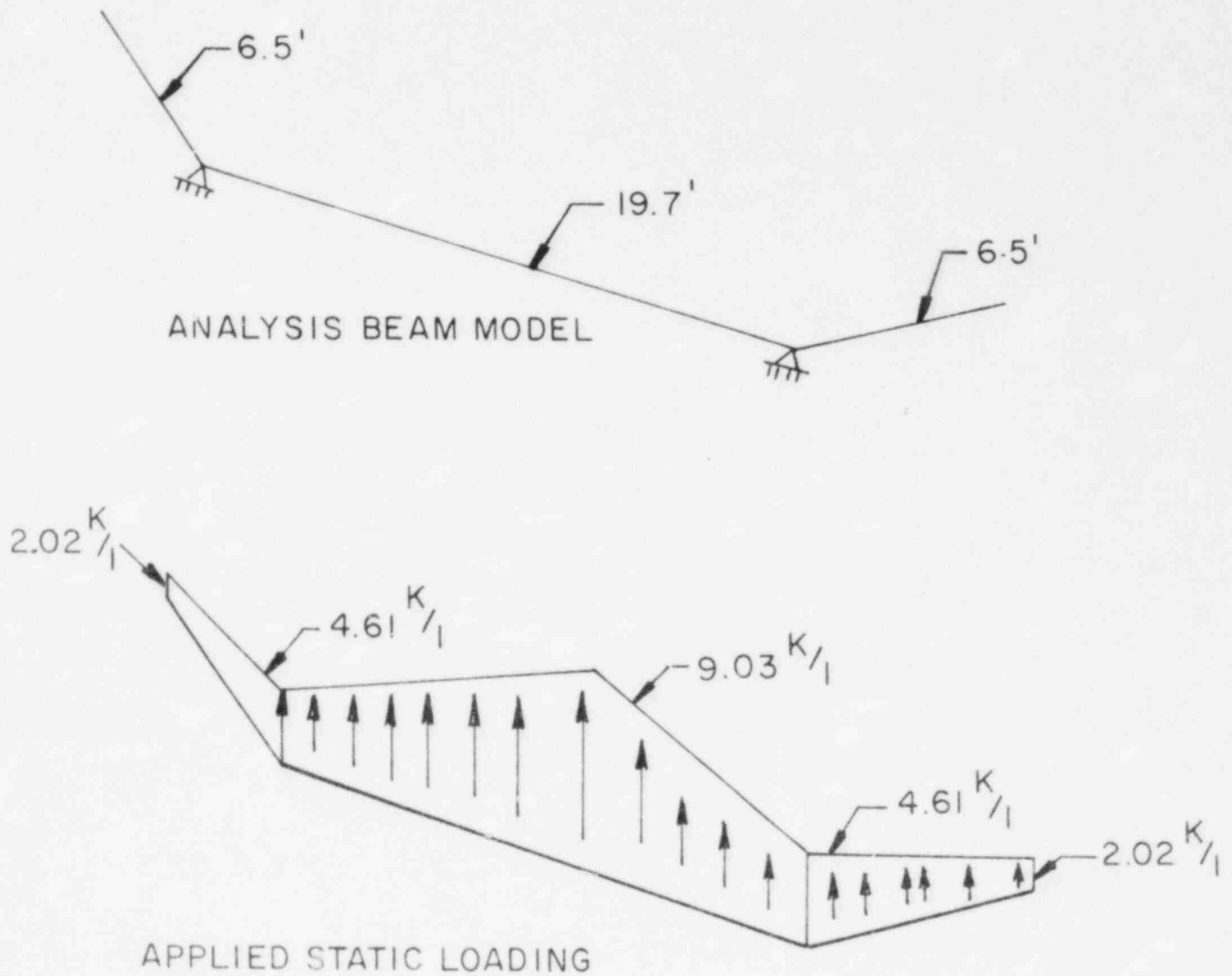
FIG. 4-5

VENT HEADER DEFLECTOR ANALYSIS - PILGRIM

**TELEDYNE
ENGINEERING SERVICES**

CASE 1

CASE 2

$3142^{\#}$ - TYP.

$-9176^{\#}$ - TYP.
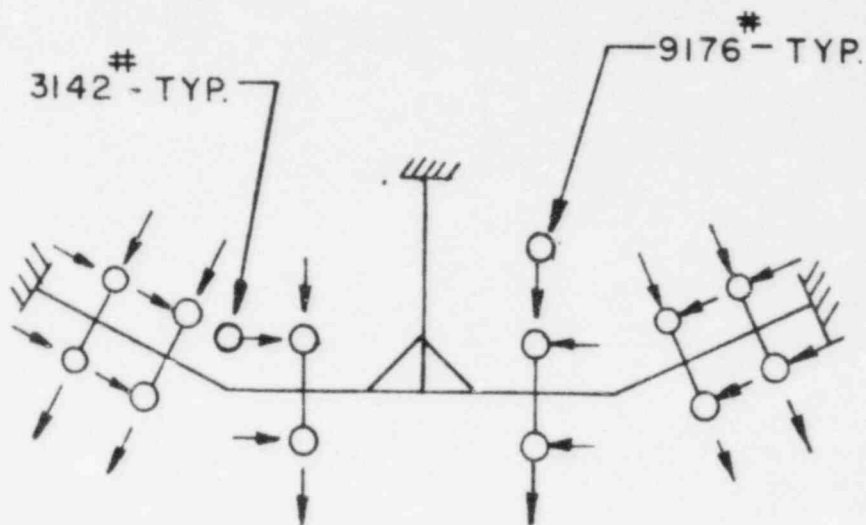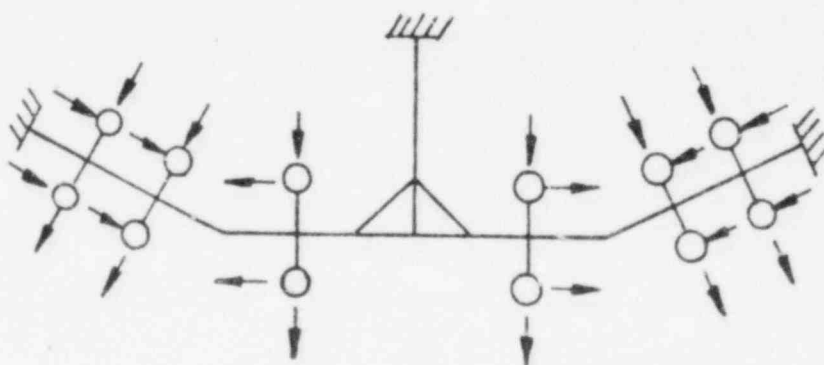
ANALYSIS CASES FOR SYNCHRONIZED LATERAL CHUGGING

FIG 4-6

5.0 <u>RING GIRDER ANALYSIS</u>

The ring girder for Pilgrim is shown in Figure 5-1. It is mounted in a vertical plane that passes through the support saddles and the support columns. Because all major internal structures are supported by the ring girders, the ring girders that must react to the largest number of individual loads.

5.1 <u>Structural Elements Considered</u>

Elements considered in this section are:

(a)   The ring girder web and flange
(b)   The attachment weld to the shell

Local stresses at attachments have also been considered and added, i.e., vent header support columns, catwalk, etc.

5.2 <u>Computer Models</u>

Two computer models were used as a part of the ring girder analyses; both are detailed models which also include the shell and external supports.

The first model is shown in Figure 5-2. This is a detailed model, which represents one-sixteenth of the torus structure; one half bay on each side of the mitre joint. It accurately simulates the ring girder offset (four-inches from the mitre joint) as well as structural differences between the vent and non-vent bays. Because the ring girder is not at the boundary of this model, out-of-plane motion of the ring girder can be accurately determined. This model was used to evaluate all direct loads on the ring girder; these include loads from attached structures such as the tee-quencher supports, catwalk and vent header system, as well as all drag loads. The one-

sixteenth model used for the Pilgrim ring girder analysis was one that had been constructed for one of the other Mark 1 plants analyzed by TES. The dimensions of this other plant are very similar to Pilgrim; the diameter of the torus, shell thickness and distance between the ring girder and mitre joint are all similar. The ring girder flange in this model is slightly smaller than Pilgrim and, therefore, produces conservative results since lateral loads control ring girder stresses. The comparison is:

Ring Girder Flange Dimensions (inches)

Pilgrim: 1.5 x 7
Model Used: 1.5 x 6

The second model used to determine ring girder loads is the Pilgrim 1/32 finite element model shown in Figure 3-1. This model was used previously to evaluate shell stresses of all symmetric loads that act on the shell. These same computer analyses produce information on ring girder stress for symmetric loads. Loads evaluated with this model include weight, internal pressure and all shell dynamic loads. The boundary conditions on this model restrict the ring girder to in-plane motion.

5.3 Loads Analysis

5.3.1 Loads Applied to Shell

As stated, the ring girder stresses for all symmetric loads applied to the shell were taken from the appropriate analyses described in Section 3.0; these include:

(a)   Pool Swell Shell Load (Paragraph 3.2.1)
(b)   Condensation Oscillation (3.2.2)
(c)   Chugging (3.2.3)

(d)   SRV Discharge*

(e)   Seismic

(f)   Deadweight, Thermal and Pressure

*SRV discharge is conservatively assumed to be a symmetrically applied load for shell analysis.

5.3.2 Drag Loads

The ring girder is subject to drag loads from each of the dynamic shell loads as well as Fluid Structure Interaction (FSI) effects from CO and CH. All these loads were evaluated by using the 1/16 model and applying static loads on the wetted nodes of the ring girder. The use of static analysis was based on the assumption that the stiffening effect of the saddle, columns and column gussets would make the ring girder very stiff and would prevent frequency interaction with the dynamic loads. Because of this, no dynamic amplification was applied to the static analysis results (DLF = 1.0). Drag loads considered were:

(a)   Pool Swell Bubble

(b)   Pool Swell Jet (bounded by a)

(c)   SRV Jet

(d)   SRV Bubble

(e)   CO including FSI (bounded by g)

(f)   Pre-chug including FSI (bounded by g)

(g)   Post Chug including FSI

The effects of SRV jet (c) and SRV drag (d) were evaluated based on data collected from in-plant tests. A discussion of the in-plant tests and the use of drag data from these tests is given in Appendix 1.

Calculation of ring girder drag loads due to condendation oscillation and post chug FSI was not in accordance with NUREG 0661 (Reference 2). An alternate method of calculating drag volume was used in this load

calculation. It produced drag volumes for the ring girder of about half of those that the NUREG 0661 procedure would have produced. A discussion of this is included in Appendix 3. The FSI drag calculation was based on local pool accelerations at the ring girder due to the response of the entire shell. The post chug and FSI analysis considered frequencies to 31 Hz, which were combined by adding the values of the five maximum components to the SRSS sum of the others.

5.3.3 Loads Due to Attached Structure

Loads applied to the ring girder by structures attached to it were evaluated by equivalent static analysis, using the 1/16 model (Figure 5-2). The important loads are applied in the area of the support saddle and columns which make the ring girder very stiff and minimizes dynamic interaction. Because of this, dynamic amplification of the static ring girder stresses was not done (DLF = 1.0). The load input to the ring girder was a result of a dynamic analysis of the attached system (or had an appropriate DLF applied) and, therefore, included the effects of dynamic amplification on load.

The following loads are applied to the ring girder and were considered:

- Tee-quencher support beam thrust due to SRV discharge.

- Tee-quencher and support drag loads.

- Vent header support column reaction loads during pool swell.

- Vent header support column drag loads.

- Catwalk support column reactions and drag.

**TELEDYNE
ENGINEERING SERVICES**

As stated in Section 5.1, stresses resulting from attached structure have been included in the following results.

5.4 Results & Evaluations

5.4.1 Ring Girder Web & Flange

The controlling load combination for the ring girder web and flange is load case 16 of Table 1; this includes:

Pool Swell ($0\triangle P$) + Internal Pressure + Weight

The controlling stress is:

LOCATION	LOAD DIRECTION	STRESS TYPE	ACTUAL STRESS	ALLOWABLE STRESS
Web	Down	Membrane + Bending	16.6 ksi	28.95 ksi
Flange	Down	Membrane	15.0 ksi	19.3 ksi

5.4.2 Weld to Torus Shell

The controlling load combinations for the shell weld are load cases 21 and 25 as indicated below. These cases include:

Load Case 21
   DBA.CO + Seismic (SSE) + Pressure + Weight

Load Case 25
   Pool Swell (full$\triangle P$) + Seismic (SSE) + Pressure + Weight

For these cases, the controlling loads are:

RING GIRDER/SHELL WELD LOADS

LOCATION	LOAD CASE	STRESS TYPE	ACTUAL LOAD	ALLOWABLE LOAD
Inner Column Region	21	Shear	7.46 K/in	8.53 K/in
Outer Column Region	21	Shear	8.34 K/in	8.53 K/in
Saddle Region	25	Shear	8.29 K/in	8.53 K/in

TELEDYNE
ENGINEERING SERVICES
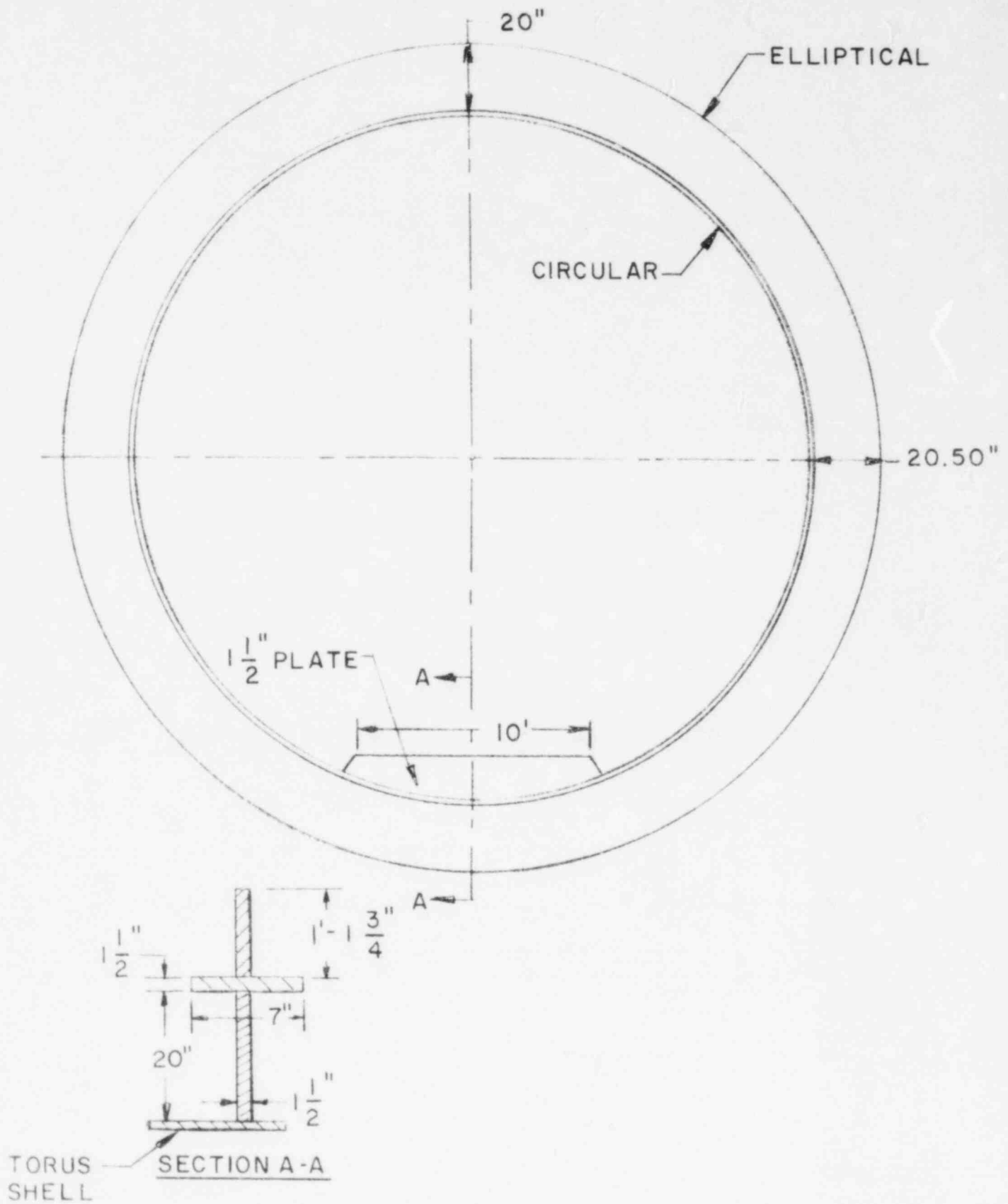
FIG. 5-1
RING GIRDER - PILGRIM
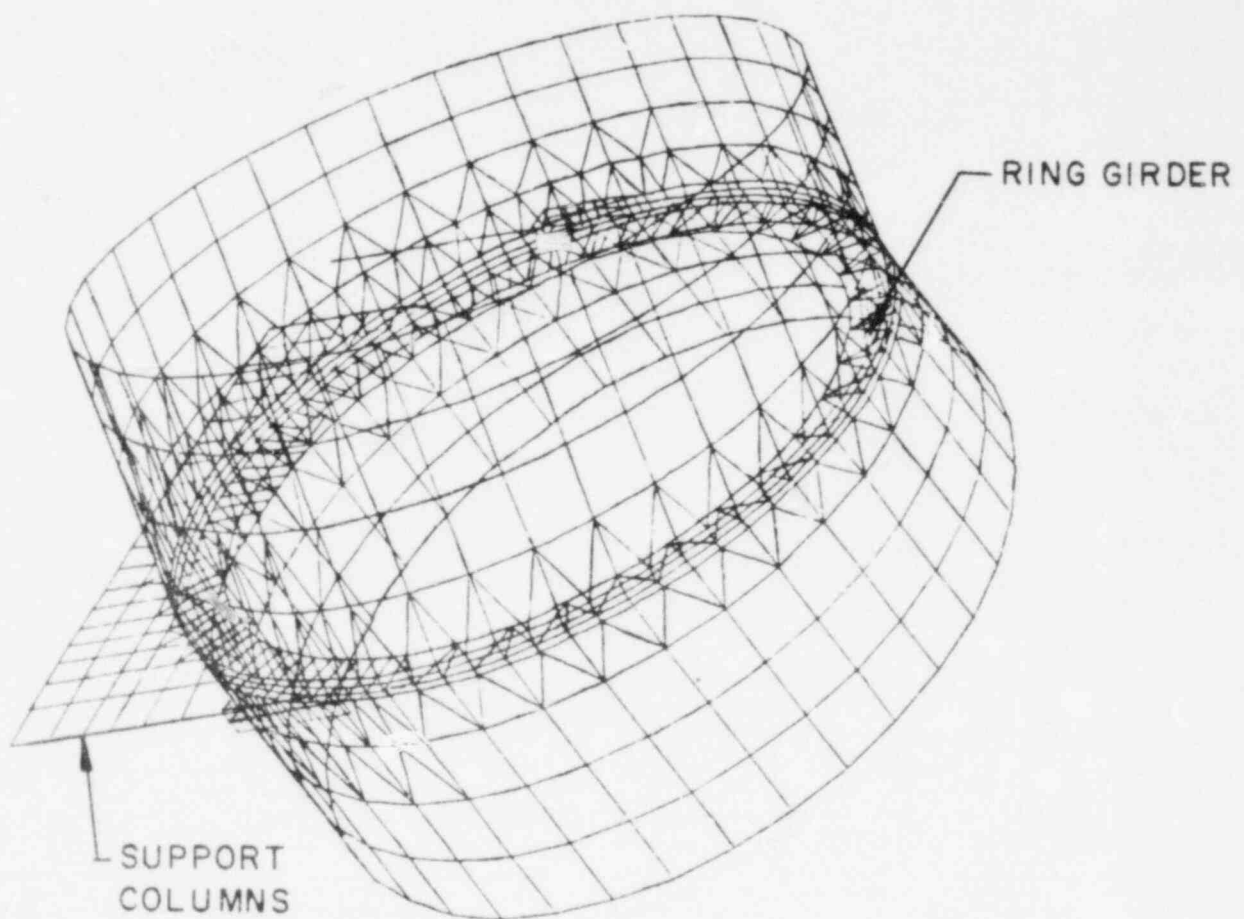
**TELEDYNE
ENGINEERING SERVICES**

RING GIRDER

SUPPORT
COLUMNS

FIG. 5-2

DETAILED RING GIRDER - SHELL MODEL

MITRE JOINT OFFSET —————|—————— RING GIRDER

FIG. 5-3

DETAILED RING GIRDER - SHELL MODEL

QUENCHER & VENT HEADER
ATTACHMENT AREA
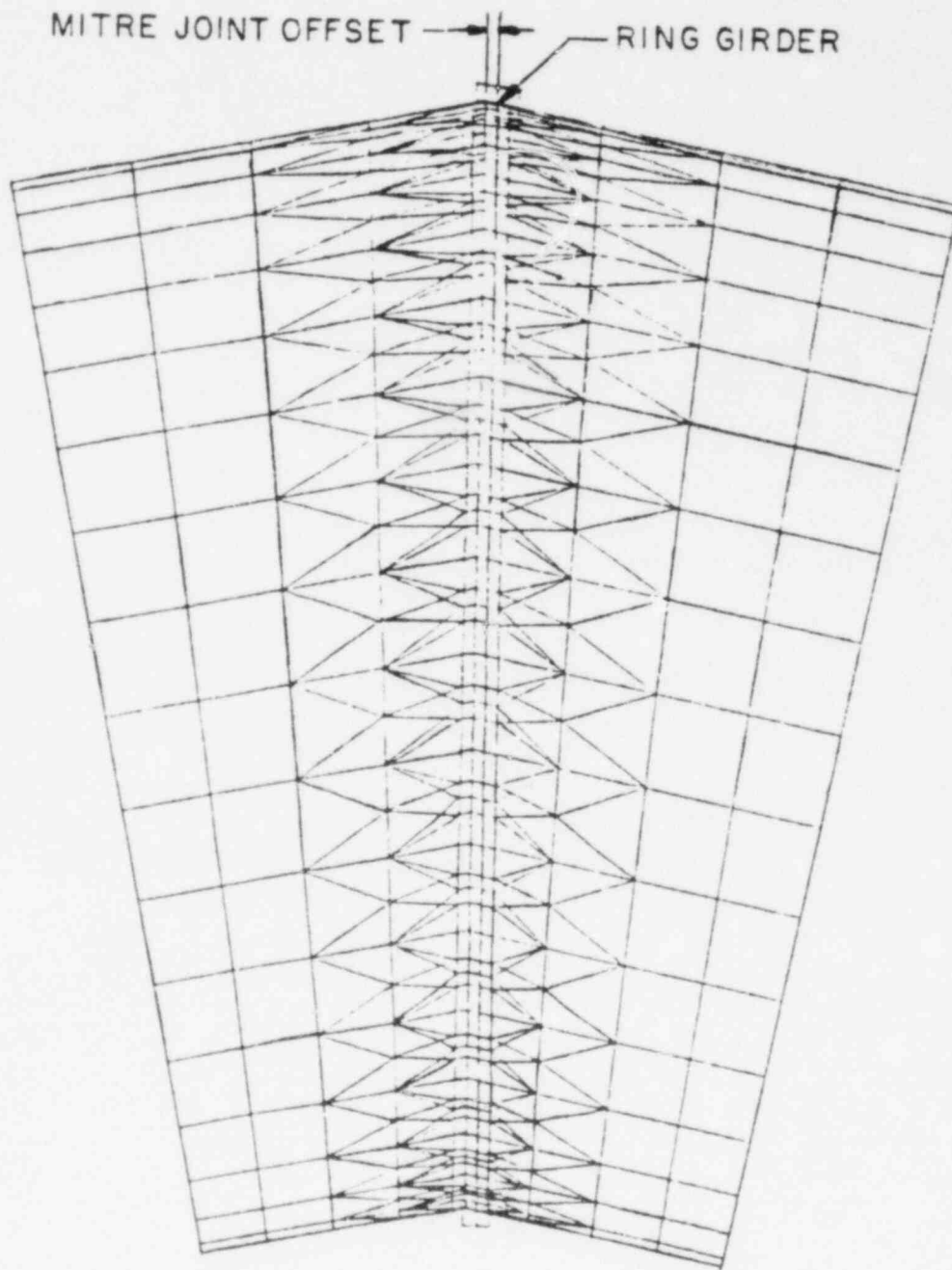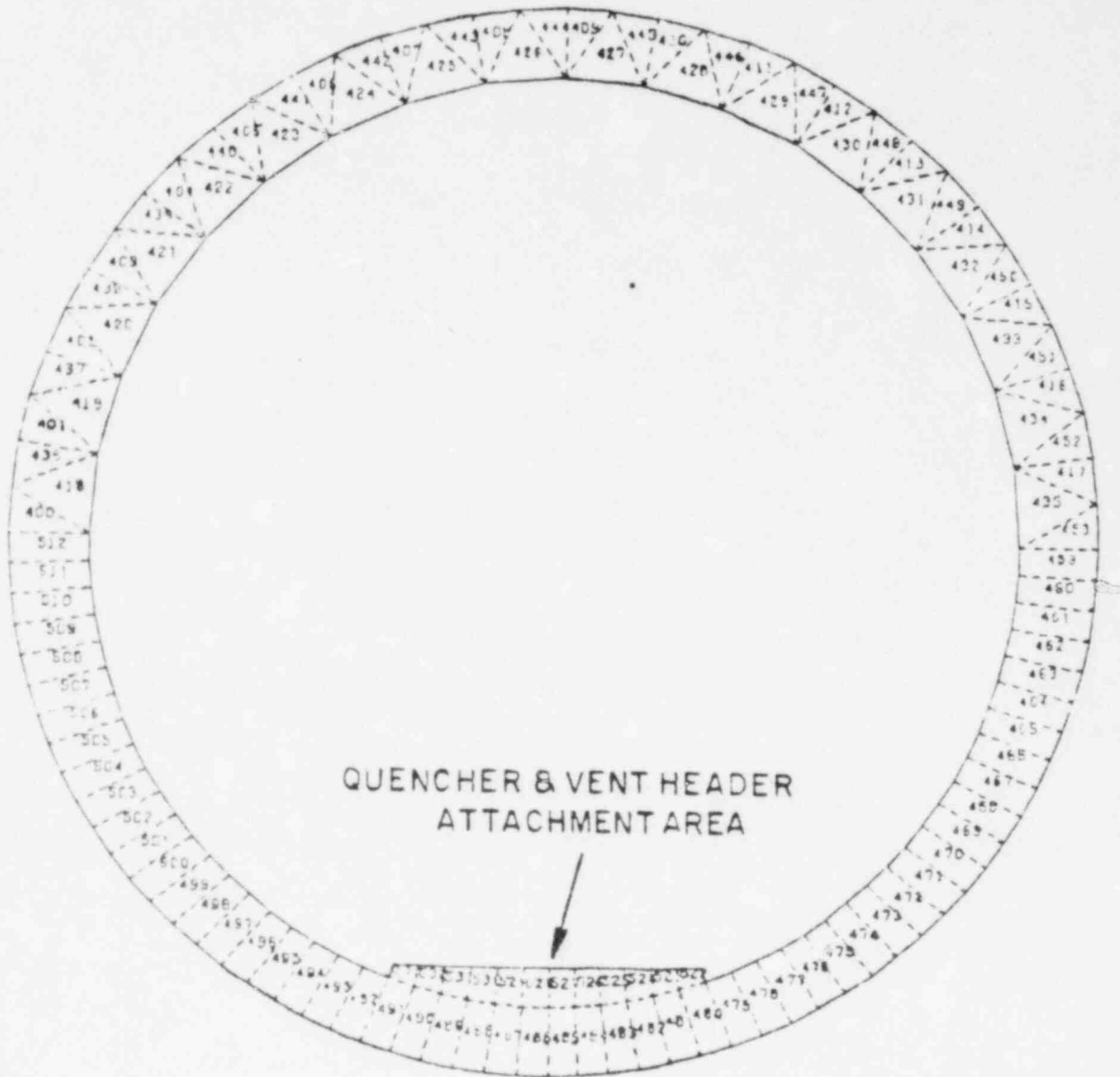
FIG. 5-4
DETAILED RING GIRDER - SHELL MODEL
RING GIRDER ELEMENTS

**TELEDYNE
ENGINEERING SERVICES**

6.0 TEE-QUENCHER AND SUPPORT

The following results for the tee-quencher and support are conservative due to the combined effect of several factors, three of which are:

- The calculational methods to determine applied loads improved after this analysis was complete, and would provide reduced stresses. Computer program RVFOR-04 was used to calculate SRV blowdown loads. RVFOR-05 is now available and gives less conservative loads.

- Some loads were intentionally bounded by conservative values from other plants so a single calculation could be used for more than one plant.

- For submerged drag loads, individual frequency components were added to produce maximum stress without regard to load direction.

The effect of these conservatisms vary among stresses, but can be significant in some cases.

6.1 Structural Elements Considered

The configuration of the quencher and support is shown in Figure 2-8. Pilgrim has four discharge lines, each enters the pool at a 20° angle.

The structural elements considered in this section include:

- The quencher.

- The submerged portion of the SRV line.

- The quencher support beam and attachments.

6.2 Computer Models

The computer model used in this analysis is shown in Figure 6-1.

This is a STARDYNE beam model which represents all piping and structure between the drywell jet deflector and the ring girder. For these analyses, the ring girder was assumed rigid and the vent pipe penetration was represented by a stiffness matrix which was developed from a finite element model of the penetration. Releases were modeled between the quencher and support plates to allow for free rotation of the quencher arms in the supports.

This model was used for both static and dynamic analysis.

6.3 Loads Analysis

6.3.1 SRV - Load

The calculation of stress due to SRV blowdown was done by applying the dynamic loads to the computer model and calculating the time-history response of the system. The applied loads included both the blowdown forces on the piping and the water clearing loads at the quencher. The controlling condition was for a second, multiple valve actuation after an IBA/SBA break, with steam in the drywell (SRV case C3.3). This case produces a high reflood level at the time of the second actuation and produces maximum load on the support system. Loads for this analysis were developed using G.E. computer program RVFOR-05.

6.3.2 Pool Swell Loads

The effects of pool swell jet and bubble loads on the quencher and support system were conservatively estimated by static analysis and a dynamic load factor of 2. It was clear from this analysis that combined pool swell events would not control stresses - no further analysis was done.

6.3.3 Chugging Loads

Dynamic analysis of the quencher and support system was done for drag loads due to pre-chug, post chug and chugging FSI. All these analyses were based on a set of harmonic analysis which provided results for all steady-state frequency excitations from 1-31 Hz. Results for individual load conditions were determined by scaling individual frequency results of the computer analysis by the appropriate pressure amplitude.

The mass of the structure used in the computer analysis was adjusted to account for the "added mass" effect of the surrounding water. For FSI and post-chugging analyses, individual frequency components were combined ng the five maximum frequency contributors to the SRSS sum of the others (see Reference 12 for discussion). The maximum value of each frequency component was used in the combination, regardless of vector direction or time of instantaneous response. FSI loads were calculated by considering the calculated local accelerations in the pool due to response of the entire shell.

6.3.4 Condensation Oscillation Loads

The quencher and support system are subjected to condensation oscillation drag and CO-FSI drag. Analysis for these loads was based on the same harmonic analysis discussed in paragraph 6.3.3, scaled to the CO amplitudes. Each of the three CO spectra shown in Figure 4.4.1-1 of Reference 1 were considered.

All other discussion from paragraph 6.3.3 for chugging applies to the condensation oscillation analysis, except that the final load was determined by adding the four maximum frequency contributors to the SRSS sum of the others.

**TELEDYNE
ENGINEERING SERVICES**

6.3.5 Other Loads

Calculations of stress due to weight, thermal and seismic loads was done by using the computer model in Figure 6-1 and static analysis. Pressure stresses for the piping and quencher were calculated by hand.

6.4 Results and Evaluation

The results reported in this section may be conservative depending on the effect of factors discussed in Sections 1.0 and 6.0 of this report.

6.4.1 Tee-Quencher

The controlling stress in the tee-quencher itself occurs in the ramshead between the quencher arms. It is the result of a second SRV actuation after an SBA accident - load case 15 of Table 1. It includes:

SRV blowdown (case C3.3) + Chugging Drag + Weight + Seismic + Internal Pressure + Thermal

The controlling stress is:

STRESS LOCATION	STRESS TYPE	ACTUAL STRESS	ALLOWABLE STRESS
Bifurcated Elbow	Bending	18,671 psi	24,705 psi

6.4.2 Submerged SRV Line

The controlling stress for the submerged portion of the SRV line occurs in the inclined lines and is a result of load case 15 in Table 1. This case includes:

SRV Blowdown (case C3.3) + Chugging Drag + Weight + Seismic + Internal Pressure + Thermal

The controlling stress is:

STRESS LOCATION	STRESS TYPE	ACTUAL STRESS	ALLOWABLE STRESS
Vertical Section Above First Elbow	Bending	9,094 psi	27,000 psi

6.4.3 Tee-Quencher Support

The controlling stress that was calculated for the tee-quencher support is the result of load case 15 of Table 1. This case includes:

SRV Blowdown (case C3.3) + Chugging Drag + Weight + Seismic + Thermal

The controlling stress for the beam is:

STRESS LOCATION	STRESS TYPE	ACTUAL STRESS	ALLOWABLE STRESS
At the Brace Connection	Bending	17,361 psi	27,000 psi

6.4.4 Tee-Quencher Support Brace

The controlling stress that was calculated for the tee-quencher support diagonal brace is the result of load case 15 of Table 1. This case includes:

SRV Blowdown (case C3.3) + Chugging Drag + Weight + Seismic + Thermal

The controlling stress is:

STRESS LOCATION	STRESS TYPE	ACTUAL STRESS	ALLOWABLE STRESS
In Brace	Bending	12,719 psi	27,000 psi

TELEDYNE
ENGINEERING SERVICES

VENT PIPE PENETRATION

QUENCHER SUPPORT

TEE QUENCHER
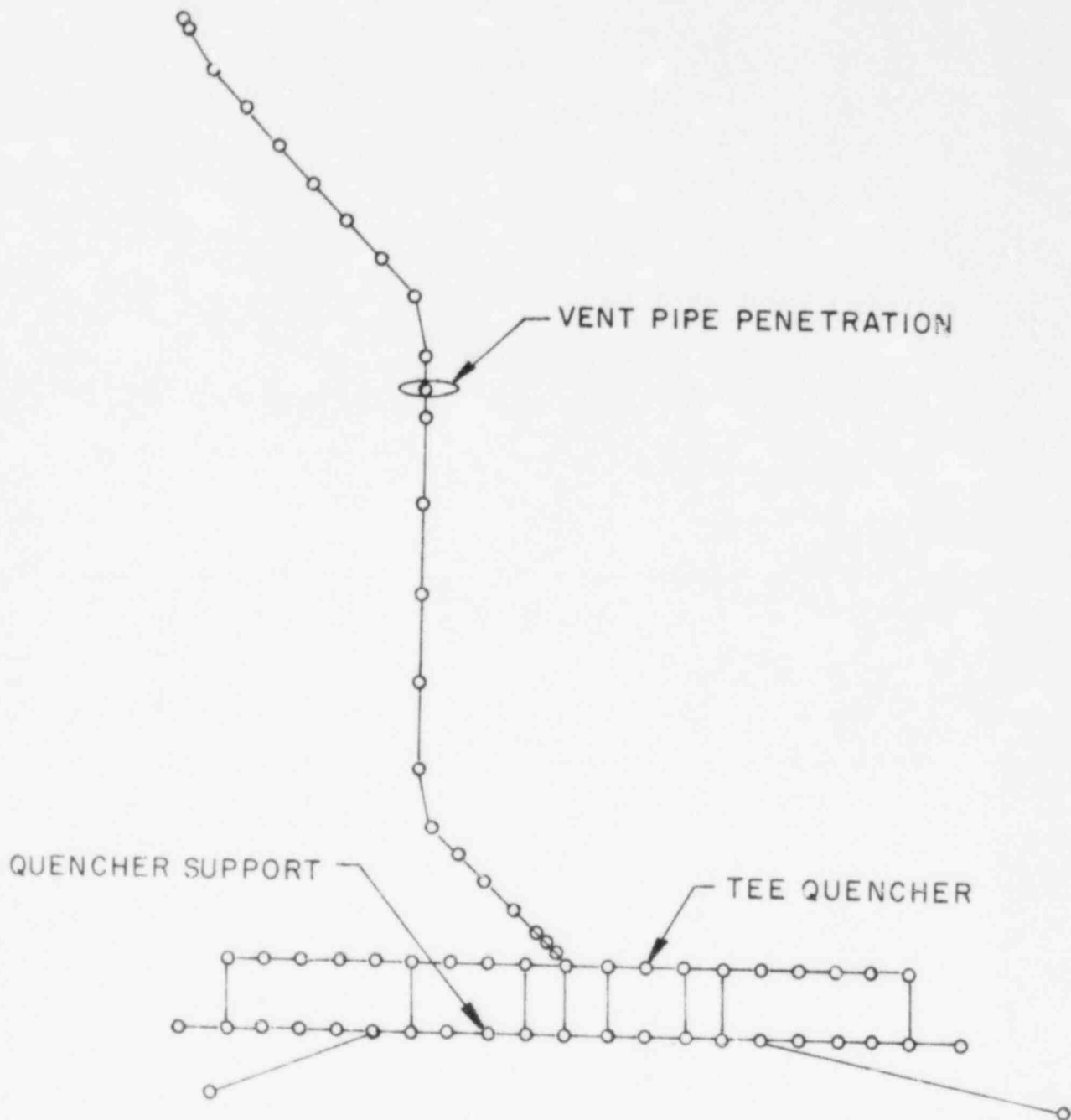
FIG. 6-1
PILGRIM ANALYTIC MODEL

7.0 OTHER STRUCTURES

7.1 Catwalk

The catwalk structure is attached to the ring girders and provides 360^0 access to the inside of the torus. It consists of a horizontal frame structure which supports sections of open grating. At each ring girder, one side of the frame is attached directly to the ring girder by a short horizontal member; the far side of the catwalk is supported by vertical columns which connect to the ring girder below the water line. Additional pipe column supports were added and the hand rail is wire rope as shown on Figures 2-14 and 2-15.

7.1.1 Computer Model

The computer models of the catwalk are shown in Figures 7-1 and 7-2 for the original and modified catwalk. It represents the structure for one full bay, beginning at mid-bay. They include all of the load carrying structural members, but do not include the grating or handrails. Loads from these elements are calculated and applied to the frame as forces at the points of attachment.

All catwalk analysis was performed on these linear models. All analysis used static application of loads, increased to account for dynamic amplification, where appropriate.

7.1.2 Loads Analysis

Loads analysis for the catwalk was performed for the direct effects of the following loads. Indirect effects due to motion of the ring girder at the attachments points were considered, but judged to be negligible.

7.1.2.1 Pool Swell Drag (4.3.4)

Pool swell drag loads are produced as the rising pool envelops the main frame, grating and handrails. Loads on the frame were

🦅 TELEDYNE
ENGINEERING SERVICES

calculated based on velocities taken from plant unique QSTF movies and the methods in Reference 1. These were multiplied by two to account for the dynamic effect. Loads on the grating were taken from Section 4.3.4 of Reference 1; these loads already include a dynamic factor, since they are based on test data.

7.1.2.2 Pool Swell Fallback (4.3.6)

Pool fallback loads were calculated and applied in accordance with Reference 1, except in unusual cases where fallback loads exceeded upward loads. In these cases, the maximum values of upward load were used for fallback also. Fallback affects the main frame and grating as well as the handrails.

7.1.2.3 Froth Load (4.3.5)

Froth loads have their major effect on the catwalk handrails; and, when applied horizontally, can produce high bending stresses in the vertical handrail members. Froth loads were calculated in accordance with Reference 1, except that the froth 1 influence region was redefined using plant-unique QSTF movies. These movies show clearly that froth 1 loads do not reach the catwalk railing; the analysis was therefore performed with froth 2 loads only.

Except for the handrails, the entire catwalk is submerged before froth loads reach this part of the torus; because of this, froth was only considered on the handrails.

7.1.2.4 Drag Loads (Support Columns)

The submerged portion of the catwalk support columns are subject to loading from drag forces from the following sources:

(a)   Pool Swell
(b)   SRV Discharge

      (c)   Condensation Oscillation

      (d)   Chugging

        Loads from these sources were calculated and applied to the support columns as static loads. The natural frequency of the support was calculated using hand calculations and compared to the frequency(s) of each source. The statically determined stress was then multiplied by a dynamic amplification factor, developed by considering the worst case frequency ratio and the fact that this is a harmonic loading.

7.1.2.5 Weight and Seismic Loads

        Stresses due to weight loads were analyzed using static analysis and the computer model shown in Figure 7-2. Seismic loads are small and were considered using hand analysis and scaling static stresses.

7.1.3 Results and Evaluation

        Table 1 allows stresses in the catwalk structure (excluding attachments) to exceed yield; and, in certain cases, to exceed ultimate. Our analysis was based on a linear model and all stresses were maintained below the stress at which a plastic hinge would form. Controlling stress and load combination for various catwalk elements are listed here.

7.1.3.1 Main Frame

        The controlling stress in the catwalk frame occurs in the inboard supporting channel, Point A in Figure 7-2. It is a result of the combined condition that includes:

      Pool Swell + SRV + Seismic + Weight (case 25)

      The maximum stress value is:

TYPE OF STRESS	ACTUAL STRESS	ALLOWABLE STRESS
Bending + Axial	24,700 psi	40,600 psi

7.1.3.2 Support Columns, Support Diagonal Braces & End Joints

The controlling load case for the support system and end joints includes:

SRV + Seismic + Weight (case 3)

Resulting stresses are:

TYPE OF STRESS	STRESS LOCATION	ACTUAL STRESS	ALLOWABLE STRESS
Axial + Bending	Column to Ring Girder	8,415 psi	12,600 psi

7.1.3.3 Welds to Ring Girder

The controlling load combination for this stress is also case 25:

Pool Swell + SRV + Seismic + Weight

For this condition, stresses are:

TYPE OF STRESS	ACTUAL STRESS	ALLOWABLE STRESS
Shear	8,007 psi	42,000 psi

7.2 Internal Spray Header

The internal spray header is attached to the ring girders and to a penetration on the shell. It is located at the top of the torus, above the vent header (Figure 2-3).

7.2.1 Computer Model

The computer model used to analyze the spray header is shown in Figure 7-3. It was constructed to allow determination of stresses in a typical multi-span area as well as at branch connections. This is part of a piping system and piping elements were used in the model. All results were obtained through the use of static analysis, with factors applied to account for dynamic response.

7.2.2 Loads Analysis

The spray header is high enough in the torus so it does not experience direct water impact-froth in the only pool swell related load that is applied.

The motion of the ring girder that results from pool swell loads on the shell was considered but judged to be a negligible input to the spray header. Shell displacement at the nozzle connections was input to the computer analysis.

7.2.2.1 Froth Load (4.3.5)

Froth loads on the spray header were calculated as outlined in Reference 1. The worst stress condition existed for a vertically applied load. The loads were applied statically to the system (DLF = 1.3).

7.2.2.2 Weight, Seismic & Ring Girder Displacement

The effects of weight, seismic and shell displacement were all considered by using the model shown in Figure 7-3 and applying loads and displacments statically.

7.2.3 Results and Evaluation

The controlling stress for the spray header piping is a result of load case 19 in Table 1.

This case includes:

Froth, Weight, Seismic and Shell Motion

The controlling stress is:

SPRAY HEADER PIPING

STRESS LOCATION	STRESS TYPE	ACTUAL STRESS	ALLOWABLE STRESS
Mid-bay	Bending	22,784 psi	32,880 psi

ATTACHMENTS TO RING GIRDER

STRESS LOCATION	STRESS TYPE	ACTUAL STRESS	ALLOWABLE STRESS
Support Hold Down Plate	Bearing	17,298 psi	34,200 psi

WELDS TO RING GIRDER

STRESS LOCATION	STRESS TYPE	ACTUAL STRESS	ALLOWABLE STRESS
At Ring Girder	Tension + Shear	1,868 psi	18,000 psi

**TELEDYNE
ENGINEERING SERVICES**

7.3 Vent Pipe Bellows

The vent pipe bellows forms the pressure seal between the vent pipe and torus and allows for relative motion between these parts. It is illustrated in Figure 7-4.

7.3.1 Analysis Method

The bellows are rated by the manufacturer for differential motion both axially and radially. These ratings are intended to define static differences which occur over a long enough time so that dynamic response of the bellows itself can be ignored.

In the present analysis, both ends of the bellows are experiencing dynamic motion; one end is controlled by the vent pipe, the other by the torus shell. We expect that the dynamic characteristics of the convoluted bellows should increase stresses over their static equivalents. We also expect that the convolutions will produce complex modes and stress patterns that will not couple efficiently with specific input frequencies; i.e., high dynamic reponse is not expected. Further, the "pogo" and "rolling" modes of the convolutions are non-linear, highly cross-coupled modes that would not be predicted by ordinary structural codes.

Our approach to the bellows evaluation is to compare the maximum calculated difference in dynamic response (displacement) across the bellows to the manufacturers' allowable. We accept the bellows as adequate for all cases where a large margin exists between predicted input motion and the static capacity, as stated by the manufacturer.

7.3.2 Loads Analysis

Calculation of vent pipe motion and torus shell motion was done as a part of the analysis work discussed in Sections 3.0 and 4.0 of this report. The analysis of the torus shell in Section 3.0 was based on a

computer model of the non-vent bay and therefore did not account for the presence of the vent pipe hole, or the heavy shell reenforcement in that area.

7.3.3 Results and Evaluation

The maximum differential motion across the bellows occurs as a result of case 25 in Table 1; this case includes:

> Pool Swell Pressure on Shell + Water Impact on the Vent System + Vent System Thrust + Pressure + Weight + SRV + Seismic

For this case, the following deflections occurred:

	MAXIMUM DIFFERENTIAL MOTION	MANUFACTURERS' STATIC ALLOWABLE
Axial Compression (in.)	.038	.875
Axial Extension (in.)	.038	.375
Lateral Motion (in.)	.062	.625

All calculated values are less than 11% of the manufacturer's allowables. We consider that this large difference demonstrates the acceptability of the bellows, especially if we consider that much of the load is either static or a single-pulse transient (maximum amplification of 2).

7.4 Vacuum Breaker Penetration Reinforcement

The vent header penetration for the drywell-to-wetwell vacuum breakers required modification as a result of load case 19 of Table 1.

This case includes:

Pool Swell + Seismic + Weight

PENETRATION STRESS

STRESS TYPE	ACTUAL STRESS	ALLOWABLE STRESS
Primary + Secondary	46,013 psi	57,900 psi

The modification was to add three stiffener plates to each penetration as shown in Figure 2-18.

7.5 Electrical Juntion Canister

The electrical canisters (2) near the top of the wetwell required modification as a result of load case 19 of Table 1. The canisters are subject to Level D service limits which allows for yielding of the material. The stress reported is compared to yield.

This case includes:

Pool Swell (froth) + Seismic + Weight

MAXIMUM CANISTER STRESS

LOCATION	STRESS TYPE	ACTUAL STRESS	ALLOWABLE STRESS
Canister Support Arm	Bending	46,000 psi	46,000 psi (yield)

The modification support arm and ring to each penetration is shown in Figure 2-19.

TELEDYNE
ENGINEERING SERVICES
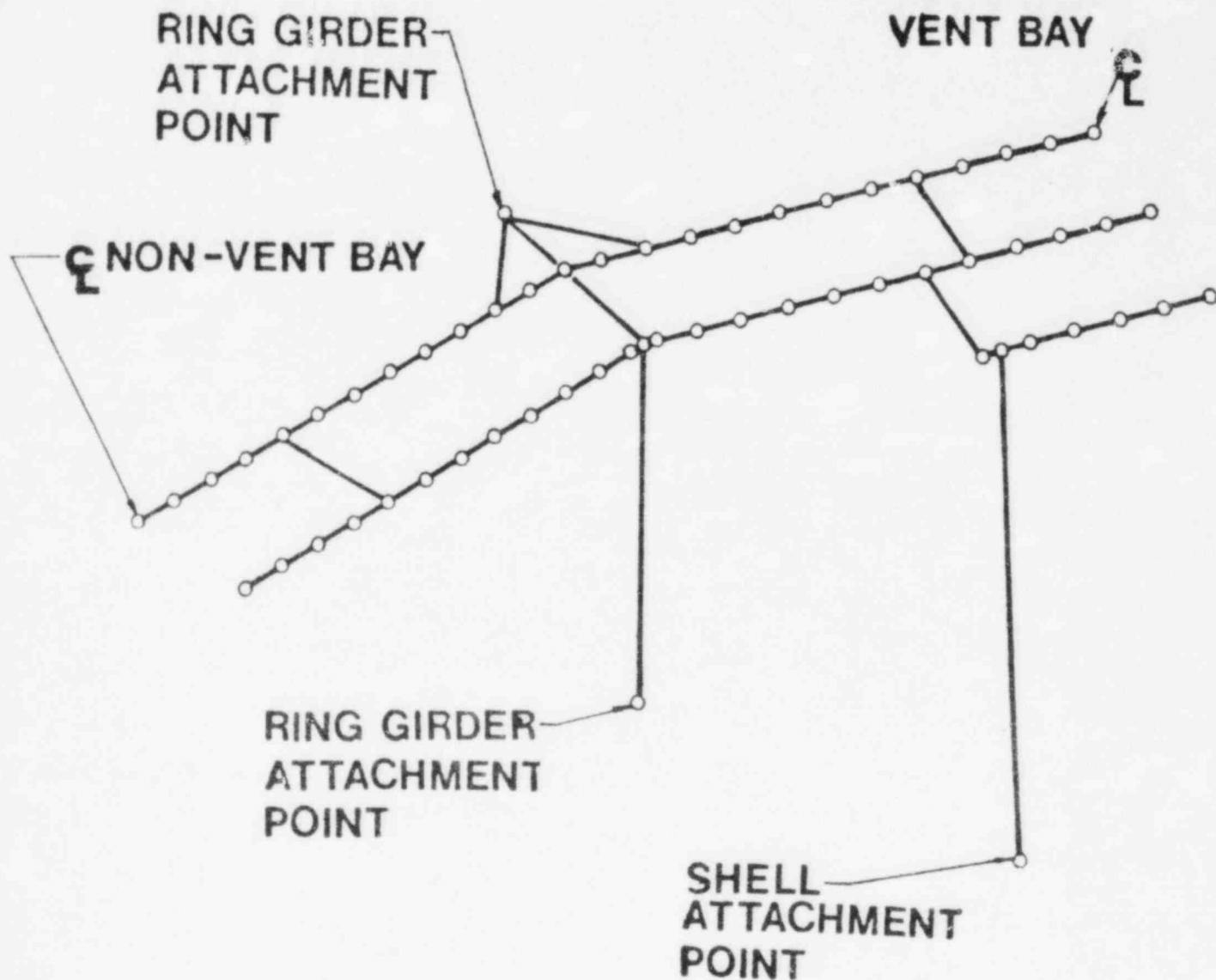
FIG. 7-1

UNMODIFIED CATWALK COMPUTER MODEL-PILGRIM

TELEDYNE
ENGINEERING SERVICES

VENT BAY

RING GIRDER
ATTACHMENT
POINT

NON-VENT BAY

RING GIRDER
ATTACHMENT
POINTS

SHELL
ATTACHMENT
POINT

FIG. 7-2
MODIFIED CATWALK COMPUTER MODEL - PILGRIM

TELEDYNE
ENGINEERING SERVICES

SHELL
PENETRATION
X211B

SHELL
PENETRATION
X211A

REACTOR
℄
0°   90°
270° ✳ 180°

7⁵/₈"
1¹/₂"   4⁵/₈"   1¹/₂"

RING GIRDER FLANGE
typ.

7¹/₂"

1¹/₂"   2⁵/₁₆"

1/4
3/16
3/16

SUPPORT (TYP, at 16 PLACES)

FIG. 7-3

INTERNAL SPRAY HEADER 360° COMPUTER MODEL - PILGRIM

**TELEDYNE
ENGINEERING SERVICES**

CALCULATED
BELLOWS ⟶
MOTION

.062

.038

.038

.062

22.18°

FIG. 7-4

MAXIMUM VENT PIPE - TORUS SHELL RELATIVE MOTION

ZERO - ΔP POOL SWELL - PILGRIM

8.0 SUPPRESSION POOL TEMPERATURE EVALUATION

The Mark 1 modification which added tee-quenchers at the discharge end of the SRV lines required that we consider the high temperature performance characteristics of these devices. Several meetings took place where the high temperature effectiveness and condensation stability of the devices was discussed. An important consideration in high temperature performance is the mixing characteristics of the device and the attendent local-to-bulk temperature difference (Δt).

In response to these concerns and to assure reliable operation of these devices, the NRC has set limits on maximum pool temperatures for tee-quencher operation, as well as guidelines for a temperature monitoring system for the suppression pool. These requirements are stated in NUREG 0661 (Reference 2) and NUREG 0783.

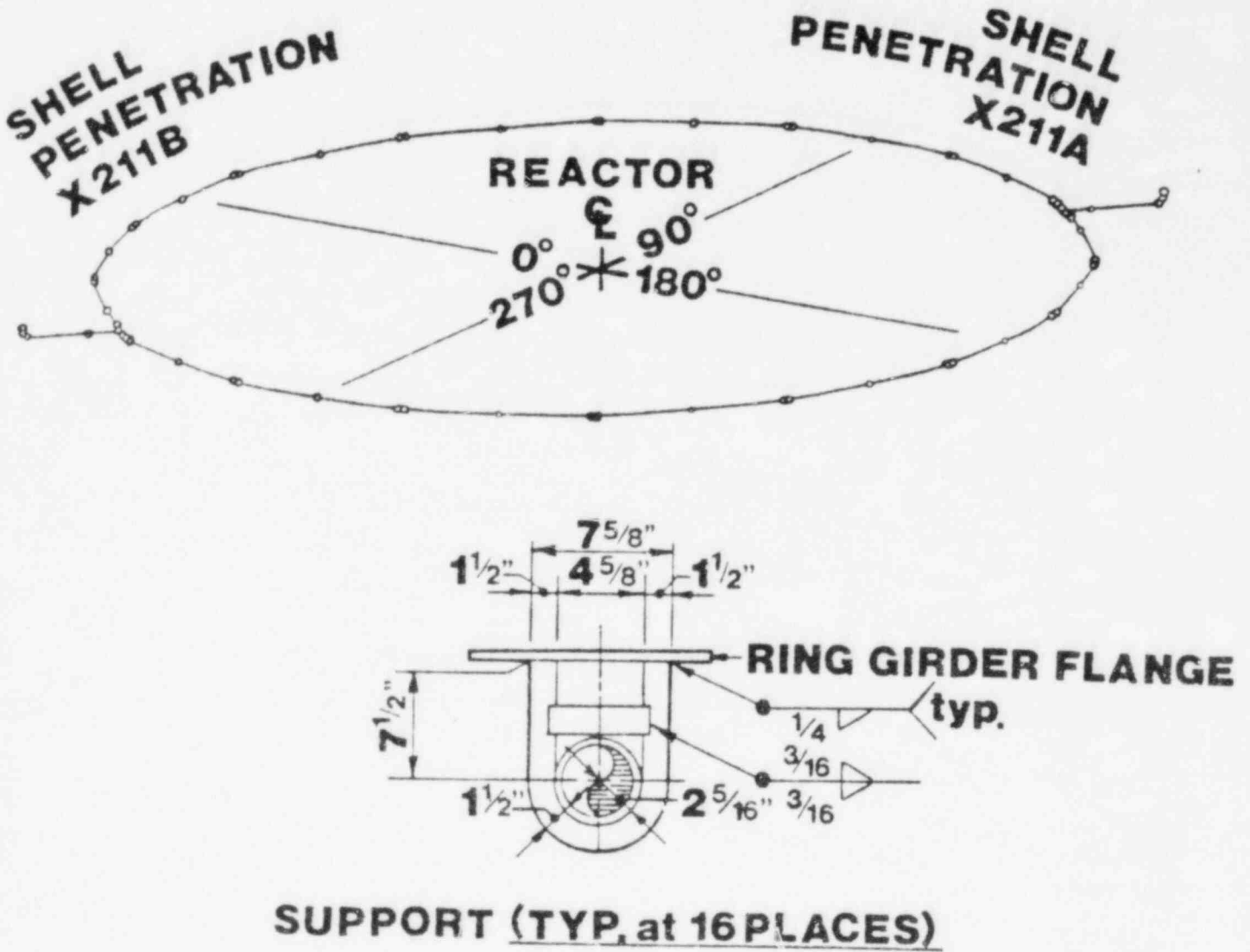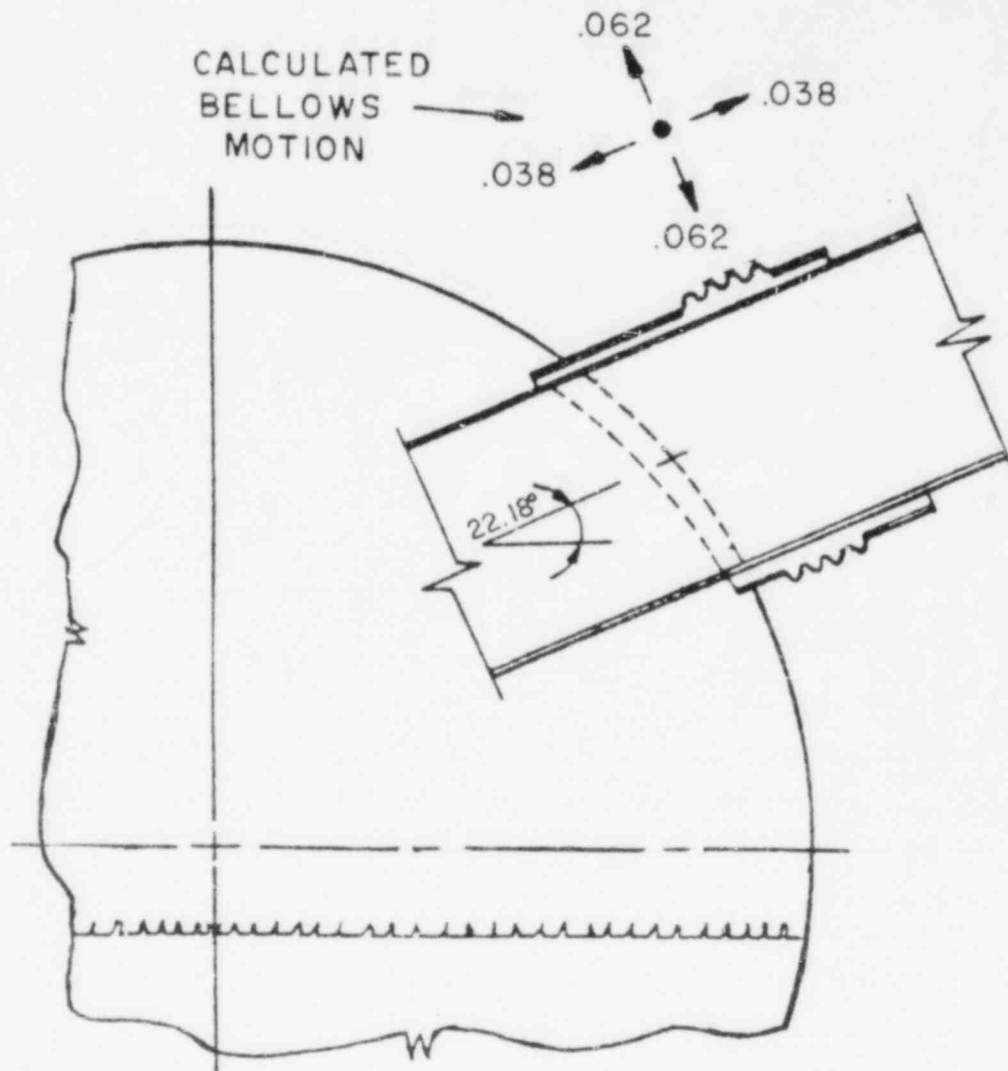### 8.1 Maximum Suppression Pool Temperature

NUREG 0783 presents maximum pool temperature limits for tee-quencher operation at different flow rates, and for several different plant conditions. Evaluation of the Pilgrim Plant for these conditions was done by General Electric Company under contract to Boston Edison. The results of that work are reported here.

The local pool temperature limits for the Pilgrim Plant and in accordance with NUREG 0783 are given in Figure 8-1. These correspond to a minimum quencher submergence of 7.0 feet.

General Electric evaluated the Pilgrim Plant for the following seven conditions that bound those specified in NUREG 0783. This analysis was performed using an initial pool temperature of $90^{\circ}F$.

**TELEDYNE
ENGINEERING SERVICES**

1A   Stuck-open SRV during power operation with one RHR loop available.

1B   Stuck-open SRV during power operation assuming reactor isolation due to MSIV closure.

2A   Isolation/scram and manual depressurization with one RHR loop available.

2B   Isolation/scram and manual depressurization with the failure of an SRV to reclose (SORV).

2C   Isolation/scram and manual depressurization with two RHR loops available. This case demonstrates the pool temperature responses when an isolation/scram event occurs under normal power operation, i.e., when all systems are operating in normal mode.

3A   Small-break accident (SBA) with manual depressurization; accident mode with one RHR loop available.

3B   Small-break accident (SBA) with manual depressurization and failure of the shutdown cooling system.

The result of the G.E. analysis showed that the pool temperature remained below the limiting values shown in Figure 8-1 for all seven cases and is therefore acceptable. The results of the analysis for the seven cases are listed in Table 8-1.

8.2 Pool Temperature Monitoring System

The NRC criteria also presents guidelines for a monitoring system to constantly monitor pool temperature. A monitoring system will be installed at Pilgrim which uses a network of RTDs set in thermowells in the torus wall, hard wired to a display console in the control room. The system is described more fully in Section 2.2.1 of this report and is illustrated in Figures 2-9, 2-17 and 2-20.
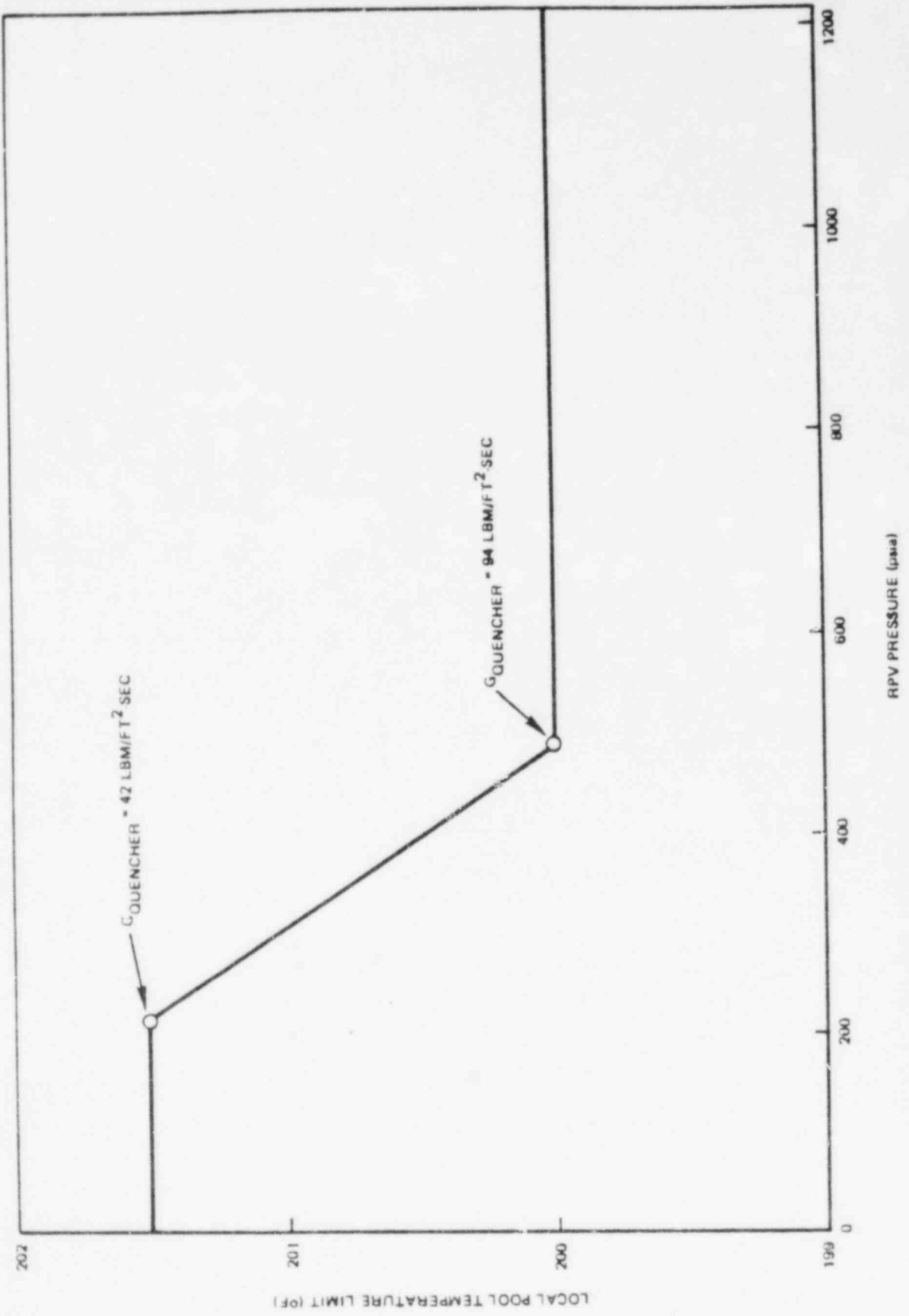
Figure 8-1 NRC Specified Local Pool Temperature Limit Based on NUREG-0783 for Pilgrim

TABLE 8-1

RESULT SUMMARY OF PILGRIM POOL TEMPERATURE RESPONSES

Case No.	Event	Number of SRVs Manually Opened	Maximum Cooldown Rate (^{o}F/hr)	Maximum Bulk Pool Temperature (^{o}F)	Maximum Local Pool Temperature (^{o}F)
1A	SORV at Power, 1 RHR Loop	0	880*	148	182
1B	SORV at Power, Spurious Isolation, 2 RHR Loops	0	710	152	195
2A	Rapid Depressurization at Isolated Hot Shutdown, 1 RHR Loop	4	1000	157	196
2B	SORV at Isolated Hot Shutdown, 2 RHR Loops	0	710	140	182
2C	Normal Depressurization at Isolated Hot Shutdown, 2 RHR Loops	4	100	147	176
3A	SBA-Accident Mode, 1 RHR Loop	4 (ADS)**	4400	156	190
3B	SBA-Failure of Shutdown Cooling Mode, 2 RHR Loops	4	100	148	174

*When the main condenser becomes available.
**ADS = Automatic Depressurization System

TELEDYNE
ENGINEERING SERVICES

REFERENCES

1. G.E. Report NEDO-21888, Rev. 2, "Mark 1 Containment Program Load Definition Report", dated November 1981.

2. NRC "Safety Evaluation Report, Mark 1 Containment Long-Term Program", NUREG 0661, dated July 1980.

3. G.E. Report NEDO-24583-1 "Mark 1 Containment Program Structural Acceptance Criteria Plant Unique Analysis Application Guide" dated October 1979.

4. G.E Report NEDO-21944 "...¼ Scale 2-D Plant Unique Pool Swell Test Report" dated August 1979.

5. G.E. Report NEDO-24615 "....¼ Scale Suppression Pool Swell Test Program: Supplemental Plant Unique Test", dated June 1980.

6. G.E. Report NEDE-24840 "Mark 1 Containment Program - Evaluation of Harmonic Phasing for Mark 1 Torus Shell Condensation Oscillation Loads" October 1980.

7. G.E. Report NEDE-24519-P "Mark 1 Torus Program Seismic Slosh Evaluation" dated March 1978.

8. G.E. Report NEDE-21968 "Analysis of Vent Pipe - Ring Header Intersection" dated April 1979.

9. G.E. Report NEDE-24555P "Mark 1 Containment Program - Application Guides 1-6, 9, 10 - Vol. 6 and 10, Rev. 3, others are Rev. 2".

10. G.E. Report NEDO-24565, Rev. 2, "Mark 1 Containment Program - Plant Unique Load Definition - Pilgrim Station: Unit 1," dated May 1982.

**TELEDYNE
ENGINEERING SERVICES**

REFERENCES (CONTINUED)

11. ASME B&PV Code, Section III, Division 1, through Summer 1977.

12. Structural Mechanics Report SMA-12101.05-R001, "Design Approach for
     FSTF Data for Combining Harmonic Amplitudes for Mark 1 Post Chug
     Response Calculations," dated May 1982.

13. Mark 1 Containment Program Report WE8109.31 "Buckling Evaluation of
     a Mark 1 Torus", dated January, 1982.

14. Structural Mechanics Assoc. Report SMA-12101.04-R003D, "Response
     Factors Appropriate for Use with CO Harmonic Response Combination
     Design Rules", dated March, 1982, pg. 3.

15. Intentionally Blank

16. Welding Research Council Bulletin No. 107, "Local Stresses in
     Spherical & Cylindrical Shells due to External Loadings", dated
     August 1965 with March 1979 revision.

17. Welding Research Supplement, "Local Stresses in Spherical Shells
     from Radial and Moment Loadings", P.P. Bijlaard, dated May 1957.

18. "On the Effects of Tangential Loads on Cylindrical & Spherical
     Shells", P.P. Bijlaard, Unpublished, Available from PVRC, Welding
     Research Council.

CLASS MC COMPONENTS AND INTERNAL STRUCTURES

TABLE I

**TELEDYNE
ENGINEERING SERVICES**

TABLE 2

PLANT PHYSICAL DIMENSIONS

PILGRIM

TORUS

Inner Diameter	29'6"
Number of Sections	16
Shell Plate Thickness	
Vent Pipe Penetration	1.125"
Top Half	.568"
Bottom Half	.629"

SUPPORT COLUMNS

	Quantity	Size
Outer	16	I-Beam (12.5" x 1.25" Flange & 10" x 1.125 Web)
Inner	16	I-Beam (12.5" x 1.25" Flange & 10" x 1.125 Web)
Base Assembly	Sliding	

RING GIRDER

Quantity	16
Size	T-Beam (7" x 1.5" Flange, 1.5" x 20" (Average) Web)

EARTHQUAKE RESTRAINT SYSTEM

Quantity	4
Type	Support Saddles

DRYWELL VENT SYSTEM

	Quantity	Size
Vent Pipe	8	6'9" I.D.
Vacuum Breakers (Internal)	10	18" I.D.
Vent Header Support Columns	16 pairs	6" Sch. 80
Downcomers	96	24"
Minimum Submergence	3'0"	

**TELEDYNE
ENGINEERING SERVICES**

TABLE 3

PLANT ANALYSIS INFORMATION

PILGRIM

Seismic Acceleration Values (G's)

	OBE	SSE
Vertical	.06	.10
Horizontal	.08	.15

Effective Water Mass for Horizontal Seismic Load (Reference 7)

25.3%

Effective Water Mass during Pool Swell Uplift (Reference 4)

Full $\triangle$ P - 50%

Zero $\triangle$ P - 30%

Plant Unique C.O. Multiplier (Reference 1)

.917

APPENDIX 1

Use of SRV In-Plant Test Data for Analysis

Test Data

The in-plant SRV tests used to support structural analysis were run at Pilgrim in August, 1980. The data was collected in a series of four tests, each consisting of one actuation with a cold line and a second about one minute later (hot line). The test sets were about three hours apart to allow for SRV line cool down.

The torus shell was instrumented with a combination of strain and pressure transducers as shown in Figure A1-1. Strain gages were mounted in pairs on both sides of the shell to allow separation of bending and membrane stresses. Additional gages were located on the columns (Figure A1-2), the SRV quencher (Figure A1-3) and an attached piping system (Figure A1-4).

Two independent data collection systems were used to provide a check on system accuracy. The major system was a multiplexed FM tape system on which all data was collected. The second system was a hard wired oscillograph to produce direct, quick-look readout on several channels.

In all, 84 transducers were used during the testing. Some difficulty was experienced with the shell pressure gages and some gages did not work properly; however, the remaining gages provided sufficient data to fulfill test objectives.

Use of Data - Applications

The SRV test data was used to calibrate computer analysis of the shell and support systems and also to establish actual numbers for SRV drag loads on submerged structures.

Use of Data - Shell & Support System Analysis

Evaluation of shell stress and support system loads due to SRV actuation
was done with a large detailed computer model as discussed in para. 3.2.4 of
the report. Data collected from the in-plant tests was used to define the
actual shell pressures and decay time for a benchmark (test) condition and to
develop correction factors between these measured results and values pre-
dicted by generic analytical methods. The steps involved are these:

1. Determine maximum average shell pressure, average frequency and
    waveform for the four cold tests.

2. Calculate these same quantities for the test conditions using the
    generic computer programs (QBUBS 02).

3. Calculate calibration factors relating predicted-to-actual pres-
    sure and predicted-to-actual frequency.

4. Calculate predicted pressures and frequencies using the generic
    computer program, for other SRV conditions.

5. Apply the calibration factors calculated in step (3) to all other
    predictions for pressure and frequency. The duration of the pres-
    sure transient, as measured in the test, is affected proportionally
    by the frequency correction and used as the basis for all computer
    model loading.

Verification of Computer Model

The test data was also used to verify the accuracy of the computer model.
This was done by the following method:

1. The computer model was loaded with the measured shell pressures.

2. The model was run and stresses at all strain gage locations were calculated.

3. Comparisons were made between computer predicted shell stress and measured shell stress at the same points.

Correlations for shell stress were excellent - generally within 5%. Correlations to column loads were not so good - generally off by about 50%. This difference in computer results for test conditions was handled by developing a second calibration factor for supports only, and combining it with the previous pressure calibration factor. The results were two different calibration factors to be applied to final analysis - one for the shell and one for the columns. The factors developed and used are:

Shell pressure = .62 x predicted

Support load = .4 x predicted

Multiple Valve Contributions

For cases where more than one valve actuates, the contributions from other valves were added directly (same signs). The maximum value used was 1.65 x the pressure from a single valve (Reference 2).

SRV Test Data for Drag Loads

In the period after the Pilgrim SRV test and May, 1982, TES ran in-plant SRV tests in four plants, and collected SRV drag information on submerged structures in accordance with the following table:

	Catwalk Supports	Vent Column	Downcomer	Ring Girder
Millstone	X	X	X	
Nine Mile Point		X	X	
Vermont Yankee	X	X		
Fitzpatrick	X	X	X	X

Data collected in these tests was evaluated, analyzed and used to develop loads for SRV drag on submerged structures for these four plants, as well as for Pilgrim. (The Pilgrim in-plant SRV test pre-dated this period, at a time when the very conservative nature of calculated SRV drag loads had not been established).

During these tests, strains were measured on the structures indicated (except for the ring girder, which was a pressure measurement). The strain gages were positioned to show bending stress due to the combined effect of SRV jet and bubble drag. Figures A1-5 and A1-6 show typical test instrumentation on these structures.

Evaluation of the test data for the four plants showed these important results:

1. Structural response occurred at the natural frequency of the structure only.

2. Responses were much less than would be predicted by program analysis methods - generally less than one-tenth of predicted loads.

An important consideration in the application of this data was the possibility that resonant structural response might occur at some other SRV condition. This was considered and dismissed based on two separate arguments; they are:

1. If a major frequency component existed in the drag force, it would be detectable on each of the structural responses for a given test. This did not occur.

2. The response frequencies of the structures tested (structural natural frequencies) ranged from 8.1 to 38 Hz.* If any single strong frequency existed in the drag load, one of the structural responses should have demonstrated some degree of resonant response - none did.

We conclude from this that the structures involved are responding to a fairly uniform random field and that the test data represents useable data for all SRV conditions.

The next step in the process was to calculate an equivalent static load for each structure. This is the static load that produces the same bending stresses measured in the test, when applied uniformly to the submerged area. These static pressure values were plotted against distance from the quencher and Figure A1-7 was developed. This curve represents the equivalent static drag pressures, including quencher jet loads. It is scaled upward from test conditions to more severe SRV cases by the ratio of the calculated shell pressures for the two cases, for application to structures under different loading conditions.

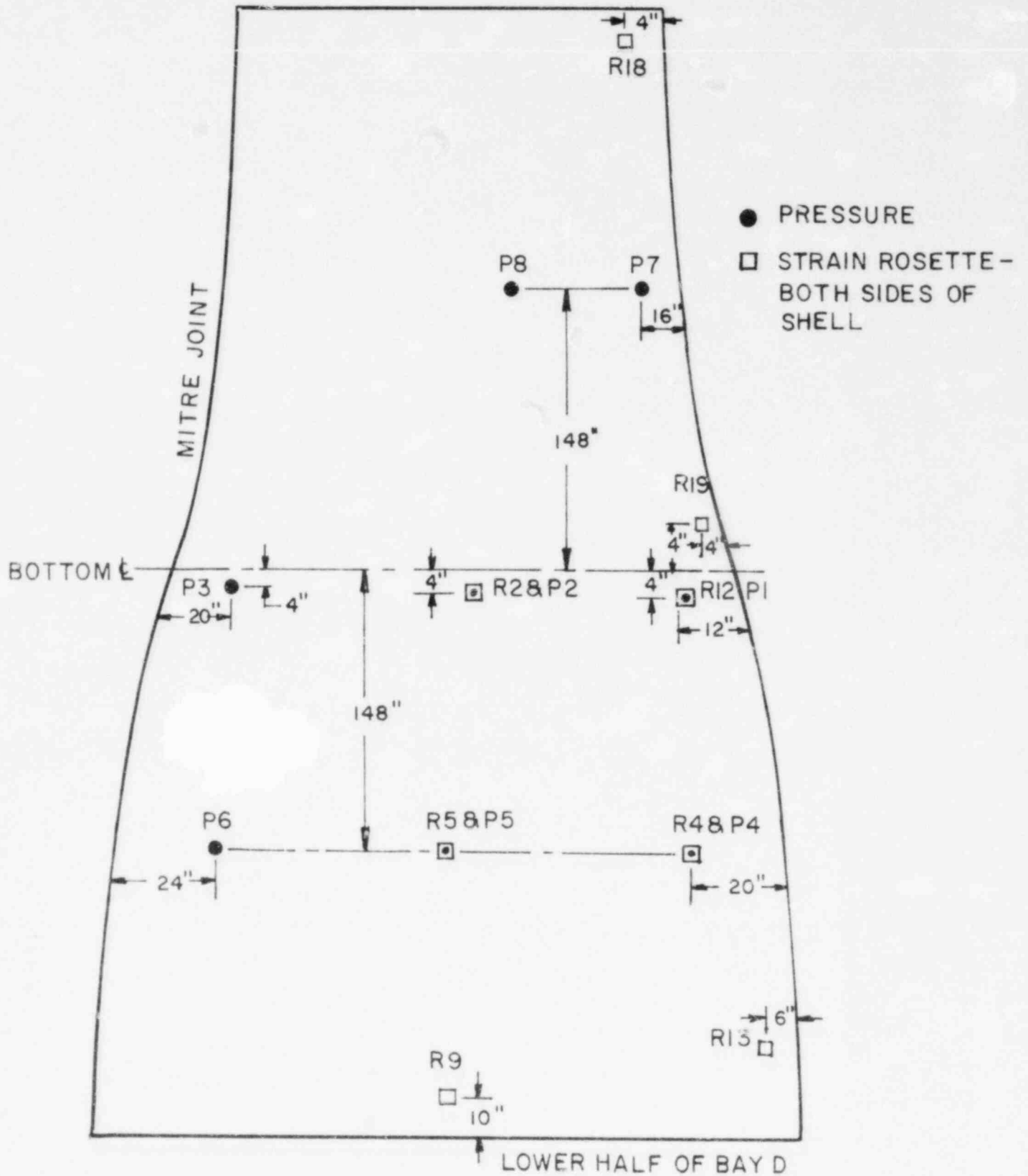*Actual values were 8.1, 8.2, 14.5, 15, 21, 23, 24, 25, 29, 30, 34 and 38 Hz.

TELEDYNE
ENGINEERING SERVICES

● PRESSURE

□ STRAIN ROSETTE-
BOTH SIDES OF
SHELL

FIG. A1-1

SRV TEST INSTRUMENTATION - PILGRIM
SHELL GAGES

TELEDYNE
ENGINEERING SERVICES

RING GIRDER   RING GIRDER

TEST BAY

DCDT
MIDBAY

A
B
C D E

C3 INNER

F E   D C
G   B
H A

C3 OUTER

SADDLES NOT COMPLETE
TO GROUND
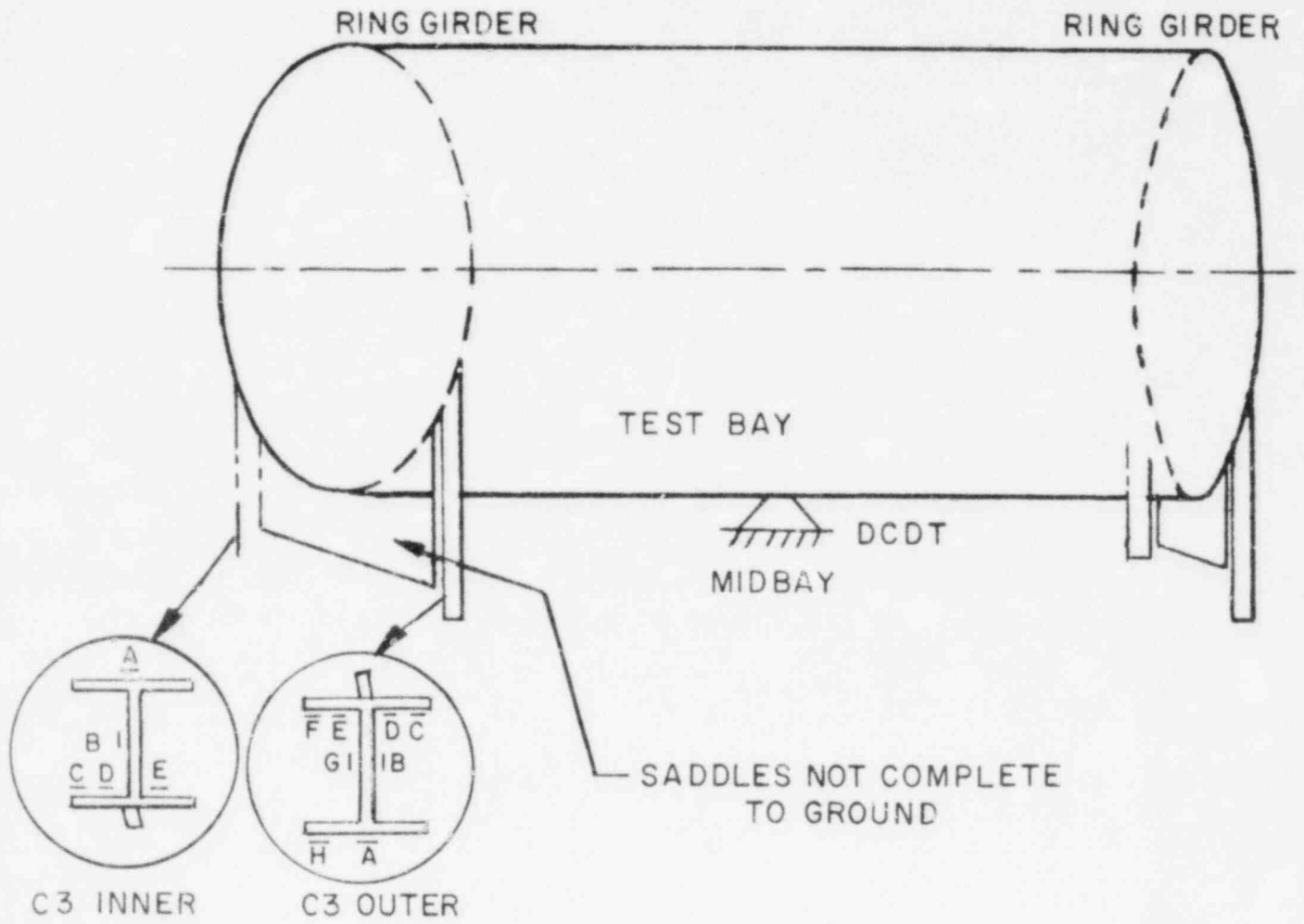
FIG. A1-2

SRV TEST INSTRUMENTATION-PILGRIM
COLUMN GAGES

SRV LINE
4 GAGES
AT 90°

4 GAGES AT 90°

$51\frac{1}{2}'$

QUENCHER SUPPORT
4 GAGES AT 90°
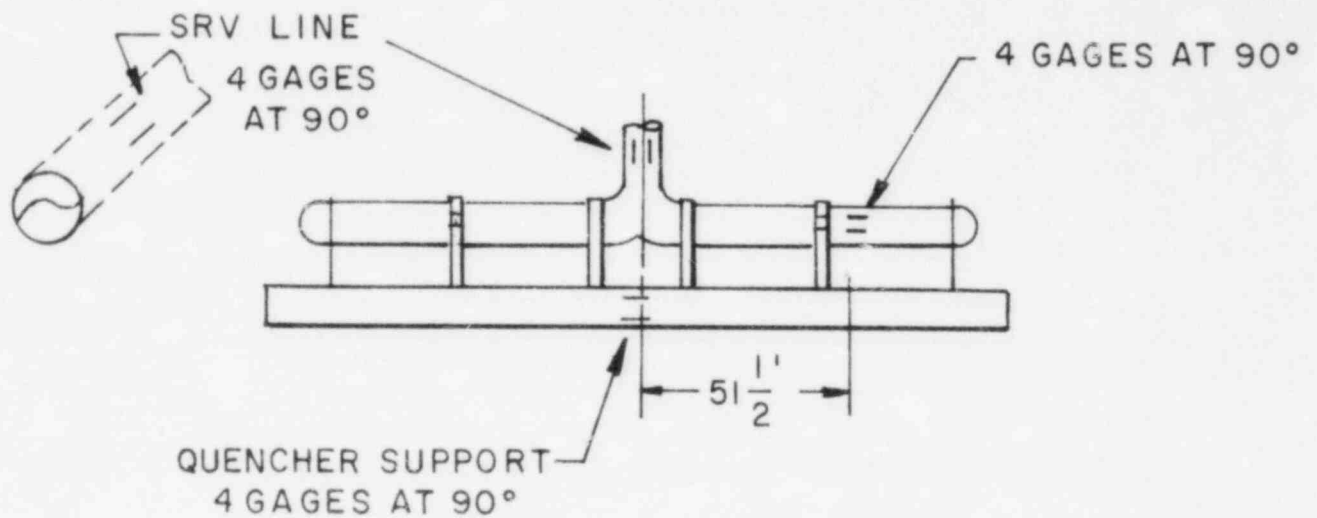
I STRAIN GAGES

FIG. A1-3
SRV TEST INSTRUMENTATION — PILGRIM
SRV QUENCHER & SUPPORT

SHELL

ACCELEROMETER
WITHIN 1" OF WEL

C B A

A

B

C

TORUS SHELL
BAY BETWEEN D&A

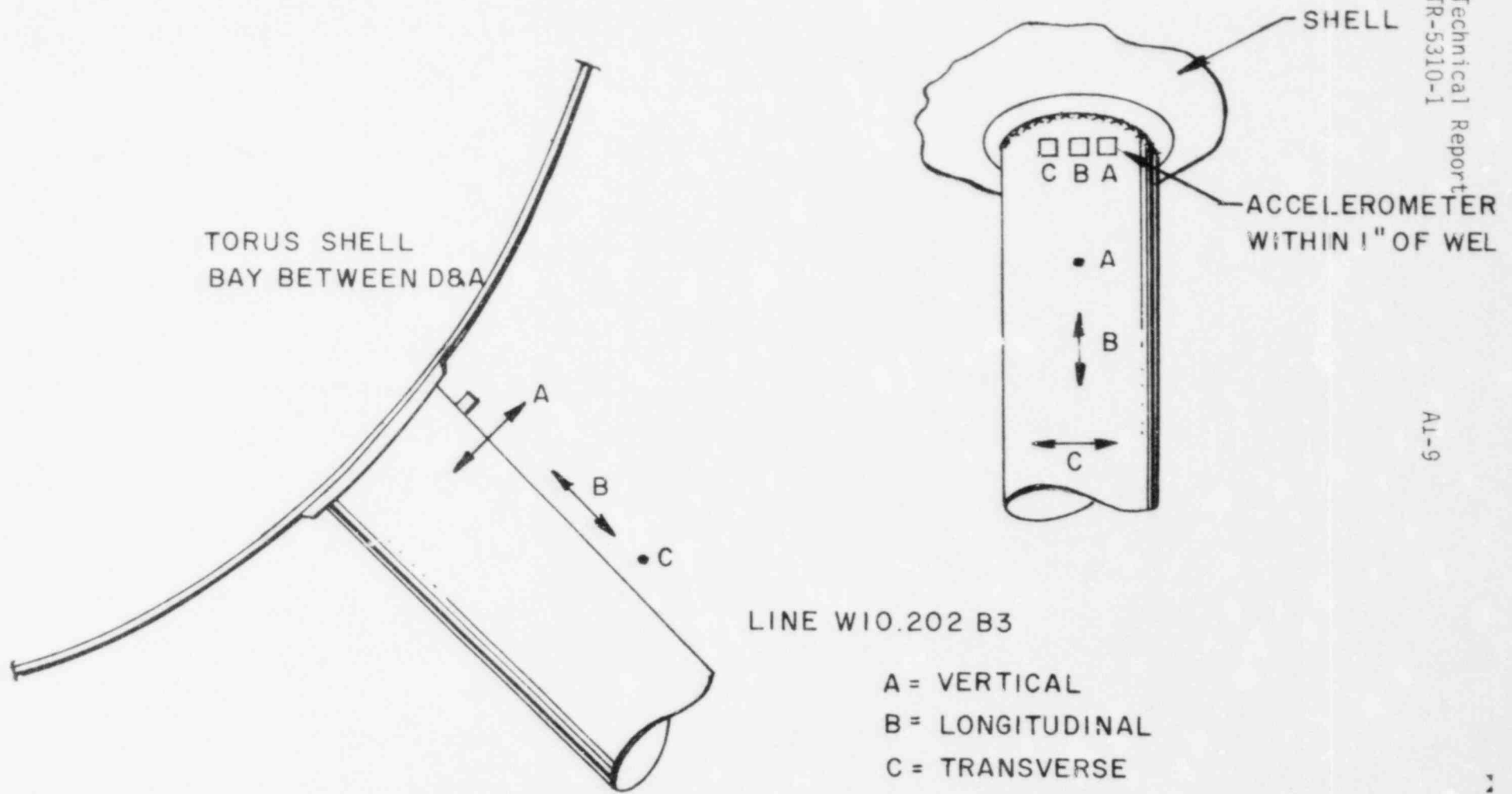A

B

• C

LINE W10.202 B3

A = VERTICAL

B = LONGITUDINAL

C = TRANSVERSE

FIG. A1-4

SRV TEST INSTRUMENTATION - PILGRIM
ATTACHED PIPING

TELEDYNE
ENGINEERING SERVICES

VENT HEADER
SUPPORT COL.

CATWALK SUPPORT
COLUMN

I STRAIN GAGE

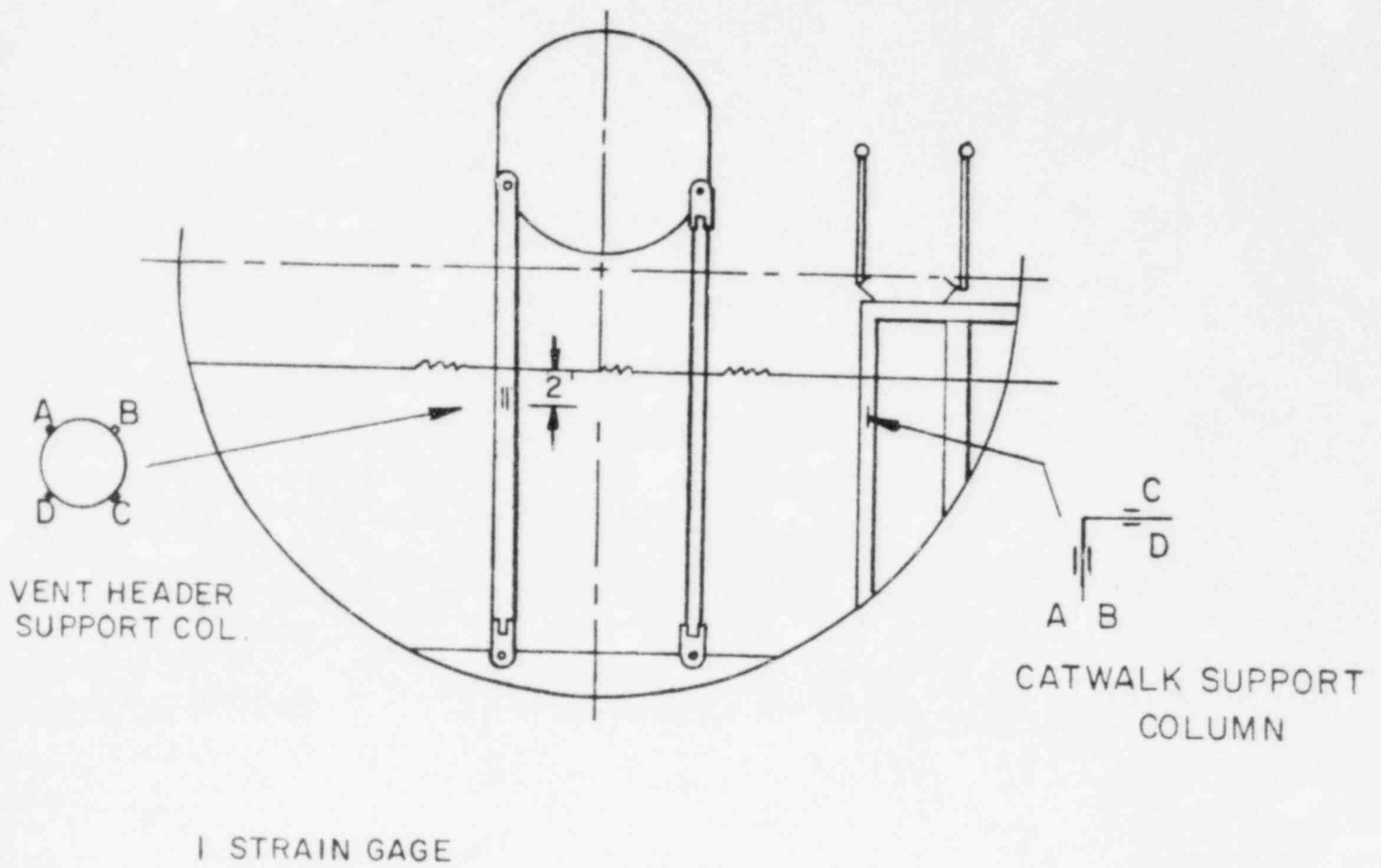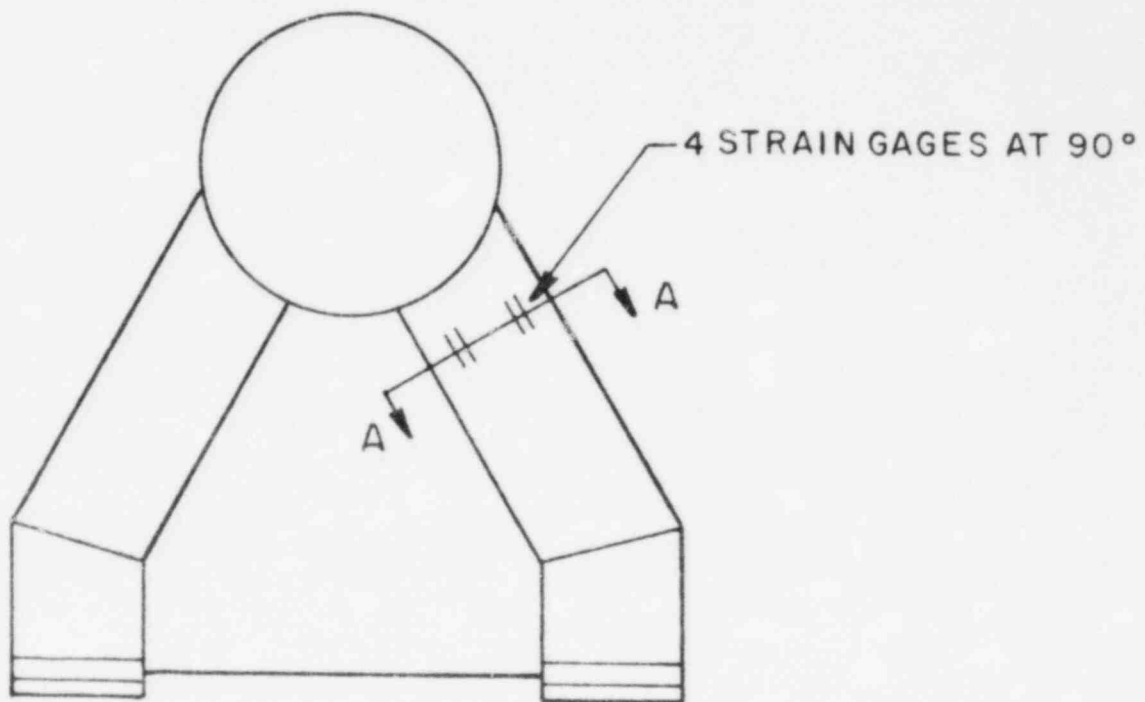FIG. A1-5

SRV TEST INSTRUMENTATION-TYPICAL
INTERNAL STRUCTURES

**TELEDYNE
ENGINEERING SERVICES**

-4 STRAIN GAGES AT 90°

A

A

SECTION A-A
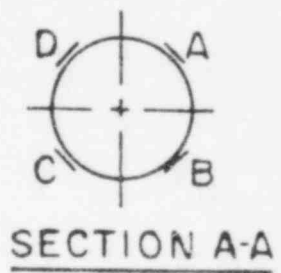
SRV TEST INSTRUMENTATION-TYPICAL DOWNCOMER
FIG. A1-6

SRV CASE A1.1
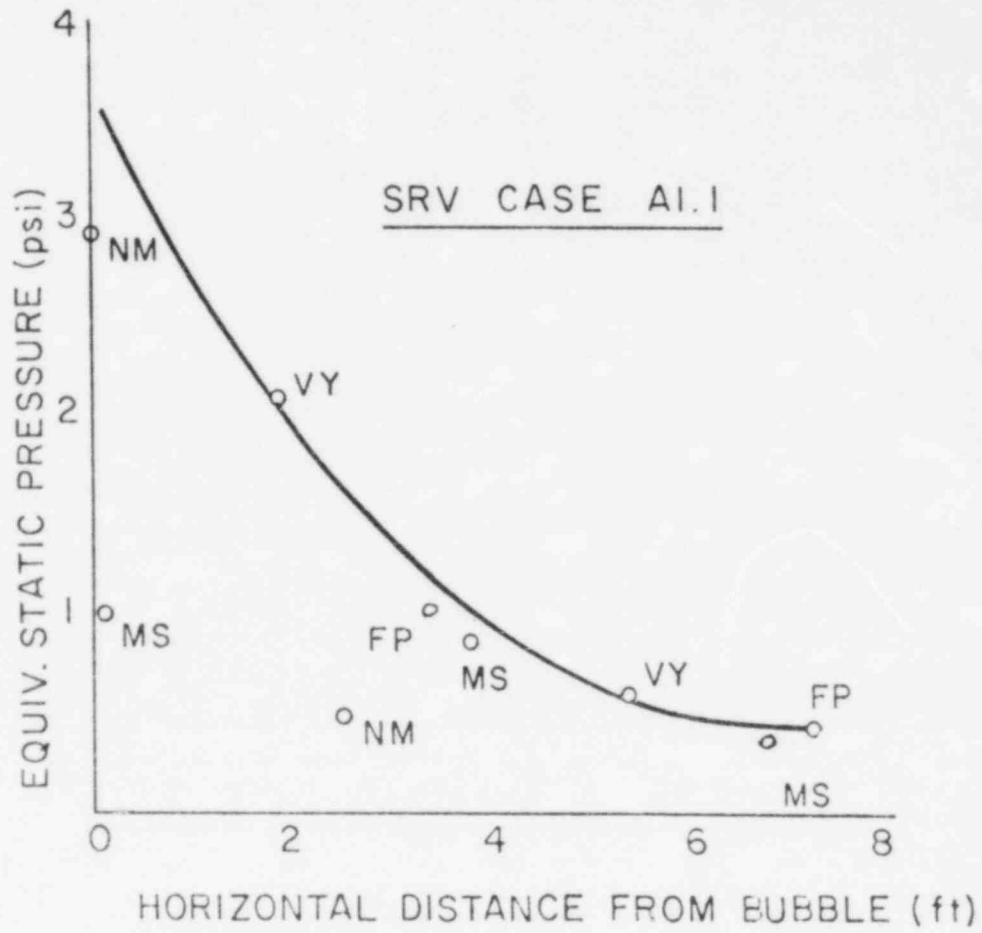
EQUIVALENT SRV DRAG FROM IN PLANT TESTING

FIG A1-7

APPENDIX 2

Discussion of 32 Hz Frequency Cut-off for
Condensation Oscillation and Post Chug Analysis

TES made the decision to limit CO and Post Chug response analysis to frequencies below 32 Hz early in the program. The decision was the result of several considerations that led to the conclusion that the 32 Hz cut-off would produce realistic results.

The basis for use of a 32 Hz cut-off involved strong fundamental arguments, both in the loads used for the analysis, and in the stress analysis itself. The primary arguments are different for CO, and for Post Chug, and are given here:

For condensation analysis.

1. Load Definition - A PSD study of the CO pressure data showed that frequencies above 25 Hz accounted f only 10% of total power (Reference 1, page 4.4.1-10). This means that a system with flat frequency response to 50 Hz would suffer a 10% unconservative stress error if a 25 Hz cut-off was used. Since we are using a 32 Hz cut-off and our system is highly responsive at low frequencies (not flat), we should expect a much smaller error.

2. Structural Response Analysis - The relative importance of loads below and above 32 Hz can be judged based on examination of the modal frequencies and generalized coordinates of the structure in both frequency ranges. If we consider the characteristics of a typical torus model in these ranges, we find:

	Number of Frequencies	Number of* $GX\phi^2$ > 1000	Number of $CX\phi^2$ > 2000	Max. Value $GX\phi^2$
Below 32 Hz	44	25	14	167,858
32-50 Hz	34	5	1	4,594

*Product of generalized weight and the square of the participation factor - used as an indicator of modal response strength.

These figures show that for condensation oscillation, frequencies below 32 Hz clearly dominate the response and frequencies above 32 Hz are relatively insignificant. They provide a strong indication that the 10% worst-case unconservatism discussed above will be greatly reduced by the selective nature of the structural response. We should logically expect the structural response characteristics, and the fact that we are using a 32 Hz cut-off, instead of 25, to reduce the 10% maximum error to less than 5%. An error of this magnitude is consistent with other assumptions which must be made in the analysis and is considered acceptable.

A further statement regarding the validity of this approach may be found in References 11 and 14.

For the post chug load, the second consideration of structural response is also valid, but the load definition is not as heavily skewed toward the low frequency end as is CO The decision for handling post chug was heavily influenced by the fact that it produced very low stress and, in fact, that shell membrane stresses would be bounded by pre-chug. This is discussed further in Section 3.2.3.2 of this report.

APPENDIX 3

CO/CH Drag Loads for Ring Girder Analysis

TES did not follow the calculational methods of NUREG 0661 (Reference 2) for calculation of CO/CH drag loads on the ring girder. This appendix describes the method that was used, the differences with the NUREG method and the basis for the change.

The NUREG analysis method specifies that acceleration drag forces (and effective hydrodynamic mass) for flat plates be based on an equivalent cylinder with radius equal to $\sqrt{2}$ times the radius of the circumscribed circle. It also specifies that the drag forces be increased by an additional factor of 2 for structures attached to the torus shell, to account for wall interference.

Application of the NUREG criteria produces a factor of 4 multiplier for drag force for flat plate structures in the fluid; and a factor of 8 multiplier for flat plate structures in the fluid and attached to the shell. These values are referenced to a drag force equal to 1.0 for flat plate calculations based on potential flow theory and neglecting interference effects.

These increases in loads are supported by data available in Reference A3-1 and A3-2. Keolegan and Carpenter show in Reference A3-1 that the drag forces on a plate in an oscillating flow may be a factor of 4 higher than the theoretical force based on potential flow. Sarpkaya shows in Reference A3-2 that forces on a cylinder near a boundary, may be twice as high as forces away from the boundary.

Both References 1 and 2 present results as a function of the VT/D ratio where:

> V = maximum velocity
>
> T = period of flow oscillation
>
> D = diameter

Keolegan and Carpenter show the effective hydrodynamic mass coefficient for a plate varies from a maximum of 4 at $\frac{VT}{D}$ = 125 to 1 at VT/D = 0. (pure potential flow). Sarpkaya shows an increase in the hydrodynamic mass coefficient for a cylinder near a boundary that varies from a maximum factor of 2 at $\frac{VT}{D}$ = 15 to a minimum of 1.65 at VT/D = 0.

NUREG 0661 appears to use the bounding values from both of these references to formulate its' analysis method. It implies by this that large values of $\frac{VT}{D}$ will exist in the torus. In fact, this is not true for CO and CH drag loads on the ring girder. For this structure, under this load, $\frac{VT}{D}$ ratios are near zero and the use of maximum multipliers should not be necessary. It is on this basis that we have used an alternate method to calculate CO and CH drag loads on the ring girder.

The TES method to calculate these drag loads on the ring girder used the same references as above (A3-1 and A3-2), but accounted for calculated values of $\frac{VT}{D}$, rather than the values corresponding to the maximum increases. Consideration of the actual $\frac{VT}{D}$ ratio for wall interference led to an interference factor of 1.65 (instead of 2).

Low values of $\frac{VT}{D}$ suggest that the theoretical hydrodynamic mass coefficient for the ring girder is appropriate. The theoretical coefficient for this structure is estimated by an equivalent cylinder with a radius equal to the circumscribing radius. Use of this cylinder results in a hydrodynamic mass coefficient equal to two. The total factor used was related to the NUREG multiplier by:

$$\frac{2.0}{4.0} \times \frac{1.65}{2.0} = .41$$

The factor   ed by TES was .41 x the NUREG 0661 factor.

REFERENCES

A3-1 Keolegan and Carpenter, "Forces on Cylinders and Plates in a Oscillating Fluid," National Bureau of Standards, Vol. 60, No. 5, May 1959.

A3-2 Sarpkaya, "Forces on Cylinders near a Plane Boundary in a Sinusoidally Oscillating Fluid", Journal of Fluids Engineering, September 1976.